



universität
wien

MASTERARBEIT / MASTER'S THESIS

Titel der Masterarbeit / Title of the Master's Thesis

„Isolation and Characterization of TGR-5/ROR_{yt} –
Modulators from Chaga (*Inonotus obliquus*)“

verfasst von / submitted by

Tobias Valentin Bäumer, BSc

angestrebter akademischer Grad / in partial fulfilment of the requirements for the degree of
Magister pharmaciae (Mag.pharm.)

Wien, 2022 / Vienna 2022

Studienkennzahl lt. Studienblatt /
degree programme code as it appears on
the student record sheet:

UA 066 605

Studienrichtung lt. Studienblatt /
degree programme as it appears on
the student record sheet:

Masterstudium Pharmazie

Betreut von / Supervisor:

Univ.-Prof. Dr. Judith M. Rollinger

Acknowledgements

First of all, I want to thank Univ.-Prof. Dr. Judith M. Rollinger for the great opportunity to research at the wonderful "Phytochemistry & Biodiscovery" group, Division of Pharmacognosy in the Department of Pharmaceutical Sciences. Her excellent guidance, overview, expertise, and help were of great value and have brought me and my work to where it is now.

Further I would like to thank my co-supervisor Benjamin Kirchweger, who accompanied me throughout the entire work. From preparing the first experiments, to writing this Thesis, I could contact him with any question, and I was always helped.

An important part in my work, the activity measurements, was done by Alexander Perhal, Patrik Schwarz and their group in the laboratory of Prof. Dr. Verena Dirsch (Molecular targets, Division of Pharmacognosy, University of Vienna). I would like to express my gratitude to them.

I also gratefully acknowledge ao. Univ.-Prof. Mag. Dr. Ernst Urban for recording NMR data, and Dr. Ammar Tahir for recording mass-spectra for me.

Special Thanks to the whole Pharmacognosy Division and everyone who worked with me. You have always enriched my work motivation and made this an enjoyable time, full of interesting discussions, great conversations, and good music.

Finally, I need to thank my family, friends, and girlfriend, for the big support. You helped me calm down in stressed times, supported me financially or emotionally and helped me managing my life. Without you, all this would not have worked as good as it did.

Big thank you to all of you!

Table of Contents

1. Abstract	9
2. Aim of this master thesis	10
3. Introduction	11
3.1 Natural product drug discovery	11
3.2 <i>Inonotus obliquus</i>	13
3.3 Bioactive properties of <i>Inonotus obliquus</i>	17
3.4 Metabolic and immunological targets	19
3.4.1 TGR-5/GPBAR-1	19
3.4.2 ROR_{yt} receptor	21
4. Results and Discussion	24
4.1 Description of starting materials	24
4.2 UPC² chromatograms and analysis	25
4.3 Fractionation and analysis of IO#2_PE	28
4.4 Analysis of IO#4-7_DCM	46
4.5 Analysis of IO#3_DCM	56
4.6 Analysis of IO#2_DCM	61
5. Material and Methods	66
5.1 Chromatography	66
5.1.1 Thin-layer chromatography	66
5.1.2 Gel permeation chromatography	67
5.1.3 Supercritical fluid chromatography	68
5.1.4 Ultra-performance liquid chromatography	72
5.2 Mass spectrometry	74
5.3 Nuclear magnetic resonance spectroscopy (NMR)	75
5.4 <i>In vitro</i> testing	77
5.5 Material	78
6 References	78
7 Appendix	82
7.1 Zusammenfassung	82
7.2 NMR spectra of pure substances	83

List of Abbreviations

APT	attached proton test
<i>C. elegans</i>	<i>Caenorhabditis elegans</i>
CD ₃ OD	deuterated methanol
CDCl ₃	deuterated chloroform
CO ₂	carbon dioxide
DCM	dichlormethane
DMSO	dimethylsulfoxid
ELSD	evaporative light scattering detector
et al.	et alii (lat.)
EtOH	ethanol
GPBAR1	G protein coupled bile acid receptor
GPCR	G protein-coupled receptor
HEK	human embryonic kidney
HMBC	heteronuclear multiple bond correlation
HSQC	heteronuclear single quantum coherence
LC	liquid chromatography
LCA	lithocholic acid
m/z	mass-to-charge ratio
MeOH	methanol
MS	mass spectrometry
MW	molecular weight
NF-κB	nuclear factor Kappa-Light-Chain-Enhancer of activated B cells
NMEs	new molecular entities
NMR	nuclear magnetic resonance
NP	natural product
PDA	photo diode array
R _t	retention time
ROR _γ	retinoic acid receptor-related orphan receptor-gamma
SFC	supercritical fluid chromatography
TGR5	Takeda G-protein-coupled receptor 5
TLC	thin layer chromatography
UPLC	ultra performance liquid chromatography
UV	ultra violet
Vis	visible light
WHO	world health organization

1. Abstract

Inonotus obliquus is a parasitic fungus from the class Hymenochaetaceae. Its sclerotia, commonly called chaga, are used in the traditional medicine of many Nordic countries. Claimed health effects comprise the improvement of heart function, anticancer, anti-inflammatory and antidiabetic properties.

However, the mode of action of *I. obliquus* is not sufficiently understood. Some receptors are promising molecular targets e.g. modulators of the Takeda G-protein-coupled receptor 5 (TGR-5) and retinoic acid receptor-related orphan receptor-gamma (ROR_{γt}) mediate similar effects as claimed for chaga. Moreover, both receptors are targeted by natural products (NPs) like lupan type triterpenes. Related metabolites i.e. lanostane triterpenes are known from the mushroom. It was therefore tempting to speculate that *I. obliquus* constituents modulate these receptors and thus mediate the therapeutic effect. In fact, three *I. obliquus* fractions showed modulatory activity in a previous bioactivity screening.

The aim of this thesis was to isolate and identify the responsible constituents of the TGR-5/ROR_{γt} activity in the fractions of the fungus. Pure substances obtained by various chromatographic methods were characterized by mass-spectrometry (MS) and nuclear-magnetic-resonance spectroscopy (NMR).

Eleven constituents were isolated and identified: These are: Inotodiol, 3β-hydroxy-lanosta-8,24-dien-21-al, trametenolic acid, betulinol, inonotsutriol A/B, osmundacetone, syringic acid, inonotsudriol D/E and lanosta-8,25-diene-3,22,24-triol as well as two not fully characterized diacetylated congeners of inonotsutriol A/B.

Bioactivity measurements showed a strong ROR_{γt} inhibition of three isolated compounds and a significant TGR-5 activation of one isolated chaga compound.

In summary, further studies are needed to better understand the ROR_{γt}/TGR-5 activity of *Inonotus obliquus* e.g., synergistic effects.

2. Aim of this master thesis

Extracts and preparations from the medicinal mushroom *Inonotus obliquus* (Ach. ex Persoon:Fr.) Pilát are traditionally used against many diseases; among others, against diabetes, various inflammatory diseases and cancer. However, the fungus has not been sufficiently investigated to explain its traditional use. Mycochemical investigation and *in vitro* experiments are important pillars to achieve this.

The aim of this work therefore deals with the isolation and characterization of constituents of the fungus, which, when elucidated, may explain the traditional use and thus various medicinal effects.

The focus was set on four fractions derived from a chaga sclerotia extract. The fractions, which have different polarities, have been tested for two different effects, on two different receptors - TGR-5 activation and ROR_{γt} inhibition. Three of these fractions showed promising activities. Thus, they were separated into sub-fractions using various preparative chromatographic separation techniques. These were then further separated to obtain pure compounds. Purity was evaluated by UPLC and 1D/2D nuclear magnetic resonance spectroscopy (NMR). Isolated pure compounds were characterized by structure elucidation methods including mass spectrometry (MS) and NMR. Pure substances and generated fractions were forwarded for testing at the two receptors. In this way, it was aimed to identify the active principles.

3. Introduction

3.1 Natural product drug discovery

Everywhere, where people live, a diversity of plants, microorganisms and fungi exists. And like humans, plants and higher fungi had to evolve over a long time to protect themselves from environmental stresses and predators. They have, presumably to protect themselves, developed a biosynthetic machinery that produces various metabolites such as odours, colours, toxins, or decomposing mucilage (carnivorous plants). These different compounds have always been tried to use and find a wide application especially in traditional medicine (Thomford et al. 2018).

For thousands of years, herbs, plants and mushrooms, have played a major role as remedies for medicinal treatments. They enabled their recipients a longer or less painful life. For a long time, the knowledge on healing or poisonous effects of plants was passed down orally, until it could be written down with the advent of writing. For a very long time, those NPs were the only drugs, which could be used by the humankind, against all sort of diseases. There are still peoples which are mostly using traditional, natural, plant-based medicine (Redvers et al., 2020).

At the beginning of the 19th century, the chemical sciences emerged. This made it possible to examine plant materials more closely and to identify and understand biological components, ingredients and mechanisms of action. In 1804, morphine was purified from opium poppy by Sertürner, which mostly reproduced the sedative and analgesic effects of opium (Lockemann, 1951). After this success, many scientists searched for other active substances in various medicinal plants (J. A. Beutler, 2019).

Although modern medicine has largely replaced traditional medicine, the use of medicinal plants still plays a big role in pharmaceutical therapy. Approximately one-fourth of FDA-approved new molecular entities (NMEs) are derived from NPs. Even one-third of FDA-approved drugs in the last 20 years are NPs or their derivatives (Patridge et al., 2016). Prominent examples are paclitaxel and morphine, as well as penicillin. The aforementioned discovery of penicillin, for example, led to increased screening of microorganisms for potential antibiotics. Tetracycline and cyclosporine, for example, have been found as a result.

Modern medicine and its current drug discovery strategies are oriented towards the use of single active compounds, not complex plant/fungal extracts. Synergistic effects in extracts, however, often lead to better therapeutic effects than single isolated compounds (Smeriglio, 2021). In order to better understand the molecular basis of these additive and synergistic effect(s), whole plant extracts must be studied in more detail (Caesar et al., 2019). For example, there is an herbal medicine for asthma consisting of extracts of *Ganoderma lucidum*, *Glycyrrhiza uralensis*, and *Sophora flavescens*. In animal models, it alleviates bronchoconstriction and restores cytokine balance. Those effects contribute to a long-lasting asthma relieving benefit. It results only from the synergistic actions of the three extracts (Wen M.C., 2005).

It is a great challenge to find drug candidates that treat various diseases and have little side effects. Innovative drug discovery strategies that differ from the “Blockbuster” pharmaceutical R&D strategy continue to be sought. One promising approach is to go back to nature. After all, this has already worked before as can be seen with cancer drugs such as taxol, or antimalarials such as quinine. They were discovered from NPs and are highly effective. The research and development of NPs could therefore take on a more central role in the discovery of innovative drugs. Also, in response to growing challenges in the public health sector.

However, the use of NPs and the acceptance of their therapeutic effect is still challenging. This is due, among other things, to a lack of standardization procedures, a lack of clarification of the biological mechanisms, a lack of controlled clinical trials and a lack of isolations of pure substances (Thomford et al., 2018). This work should contribute to this field.

3.2 *Inonotus obliquus*

Mushrooms have long been used by humans and animals not only as source of protein, minerals, and vitamins but also because of their secondary metabolites and efficacy in treating different diseases. Mushrooms contain different classes of bioactive molecules like phenols, terpenes and steroids, which are able to modulate pathologic processes in the human (and animal) body (Duru et al., 2019).

Inonotus obliquus (Fr.) Pilát (Hymenochaetaceae), commonly also referred to as chaga, is a medicinal mushroom which has a long tradition as folk medicine in Russia, Poland, and the Baltic states (Cui Y., 2005). It is distributed in forests around the northern hemisphere in Europe, Asia and North America.

It is a parasite mainly attached to birch trees, but it can also be found on oak, alder, beech, maple, rowan, hornbeam, ash, willow, planetree, chestnut, walnut or poplar trees. The parasite infects trees through wounds in the bark and causes decomposition of live trunks. The age of its targets is approximately 30-50 years, and it can grow another 30-80 years on the trunk (Manka K., 2005; Szczepkowski A., 2013). Some years after the invasion, the fungus starts to produce its characteristic sclerotia. A sclerotium (vegetative or asexual fruiting bodies) is a hardened fungal mycelium mass, to survive environmental extremes. Its cracked-up surface and the black-brown color let the mushroom look like coal (Figure 1). This is due to a high melanin pigment concentration. The orange-brown, yellow-veined mycelium normally lies underneath the bark (Szychowski, K. A., 2020).



Figure 1: The outside (left) and the inside view (right) of the chaga sclerotium

Since the sclerotia grow very slowly, *I. obliquus* needs about 10-15 years to reach diameters of over 10 cm. However, on old trees its diameter can reach over 50 cm. When the host tree dies after many years, annual fruiting bodies of the sexual stage appear. They grow when it gets warm due to the advanced decay of the wood and only very rarely if the tree is still alive. The fruiting bodies, which grow up to 4 m long and 50 cm width, provide a food base for many insects, which in turn act as spore distributors. After their one year long fruiting body life cycle, the mushroom dies (Szczepkowski A., 2013).

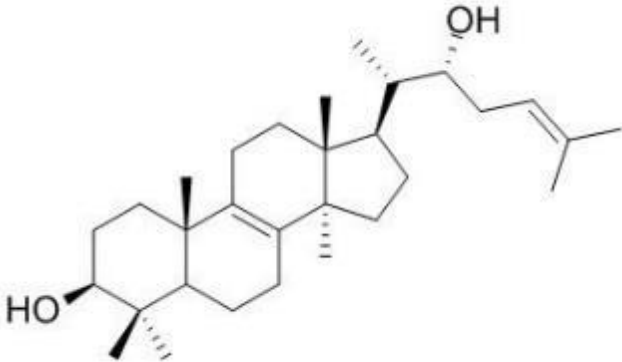
Inonotus obliquus was traditionally prepared and used in different ways: (1) as an infusion of the mushroom e.g., to wash wounds externally, (2) as aqueous macerates, (3) as tea substitution, (4) for inhalation or as (5) part of antiseptic soaps (Saar M., 1991).

There are several therapeutic areas in which beneficial effects have been reported. In a lot of countries, the mushroom was used due to its beneficial effects on the

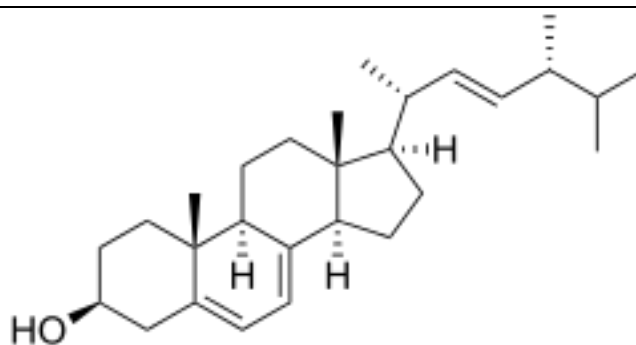
heart function and on the plasma lipid system. Also, the anti-cancer, antibacterial, antioxidant and anti-inflammatory activities gave reason to use the fungus. It was for example used against cardiovascular diseases, gastrointestinal cancer, diabetes mellitus, and viral infections (Shashkina M.Y., 2006).

The chemical composition of *I. obliquus* is very complex. Due to the cold climate with high temperature fluctuations, freezing, high UV exposure as well as bacterial and viral infections, the fungus has developed a sophisticated arsenal of defensive compounds. This includes more than 200 different bioactive molecules. Among them are antioxidants, triterpenes, phenolic compounds, melanin, ergosterol and its peroxides, sesquiterpenes, benzoic acid derivatives, hispidin analogues and one of the most important classes, polysaccharides (Szychowski K.A., 2020). In Table 1, various, already described, bioactive molecules from different substance classes of Chaga are shown.

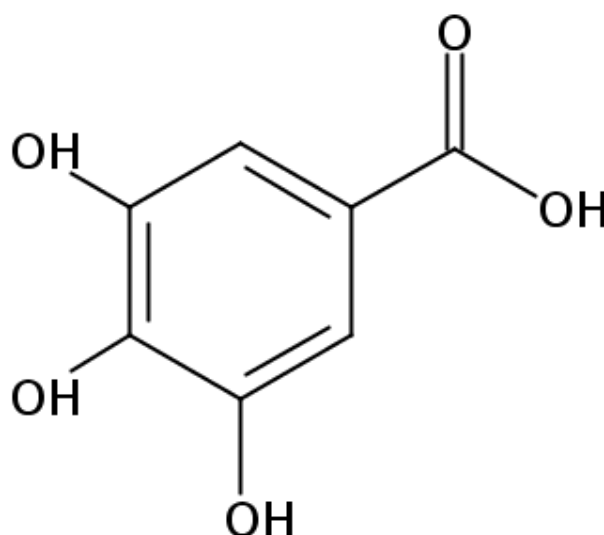
Table 1: Example of exemplary bioactive chaga constituents from different substance classes including name and structure.

Substance class, name	structure
Triterpene, inotodiol	

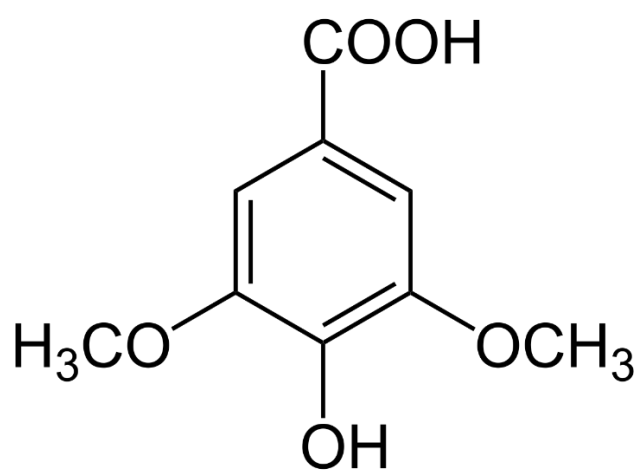
ergosterol



Phenolic compound,
gallic acid



Antioxidant, syringic acid



3.3 Bioactive properties of *Inonotus obliquus*

An *I. obliquus* sclerotia-extract was found to be tested in a previous work using the *Caenorhabditis elegans* (*C. elegans*) worm model (Figure 2). It was found that the extract made the worms live longer and lowered fat accumulation (Zwirschmayr et al., 2020).

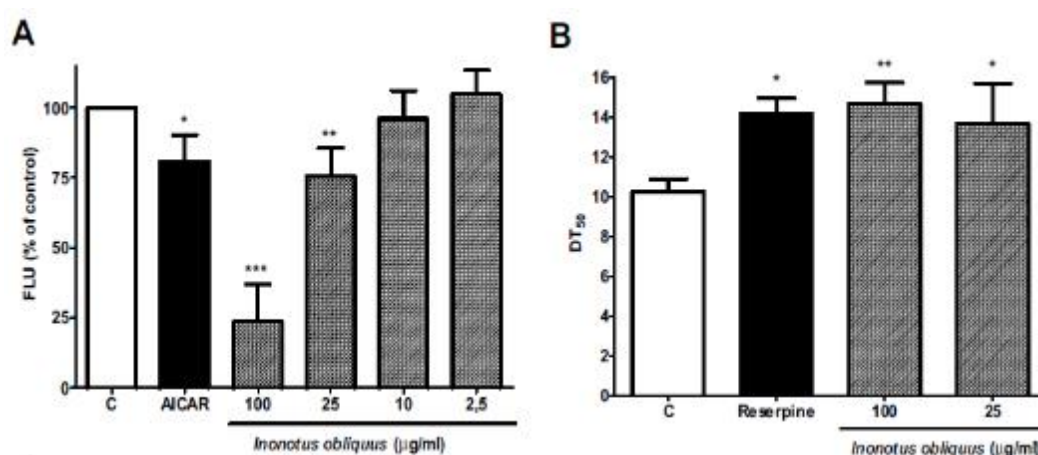


Figure 2: Fat accumulation (A) and survival(B) of *C. elegans* treated with different concentrations of *Inonotus obliquus* extract. Fat accumulation is assessed as lipid-stained Nile red fluorescence (FLU), survival as timepoint when 50% of worms are dead (DT₅₀). Charts include bars for vehicle-control group (C), and positive controls. AICAR lowers the fat accumulation significantly and Reserpine is known to prolong the life of *C. elegans*. Image from Zwirschmayr et al., 2020.

Three fractions (IO#4-7_DCM, IO#3_DCM and IO#2_PE) described in Figure 6 were tested *in vitro* for TGR-5 activation and ROR_{γt} inhibition and in Figure 3 the results are shown.

As can be seen in Figure 3, the bile acid lithocholic acid (LCA) was used as the positive control for TGR-5 activation. The chemical structures of both positive controls are shown in Figure 4. At a concentration of 10 μM LCA showed a significant activation of about six (±) fold compared to the vehicle control (containing 0,1% DMSO). The highest activation of the TGR-5 receptor was achieved with the fraction IO#4-7_DCM at 30 μg/ml (9 (±) times fold compared to the control). The IO#3_DCM extract at 30 μg/ml was significantly active as well, although not as strong with a 5 (±) time fold activation. There was no significant activation in response to 30 μg/ml of IO#2_PE (1,5 (±) times fold activation).

At the ROR_{yt} receptor, SR2211 was used as positive control for the receptor inhibition. At a concentration of 1 μ M it showed a significant inhibition with 0,35 (\pm) receptor activity compared to the vehicle control (containing 0,1% DMSO). All three extracts (10 μ g/ml) exerted a significant fold inhibition with IO#2_PE being the most potent extract with 0,6 (\pm) and IO#3_DCM being the least potent extract with 0,75 (\pm) fold receptor activity.

It can be concluded that the tested fractions are significantly active at the two tested receptors, whereby IO#2_PE seems to be the strongest inhibitor of ROR_{yt} while not being significantly active at TGR-5. IO#4-7_DCM seems to be the strongest activator of TGR-5 and active at ROR_{yt}. Additive and synergistic effects of different compounds of the extracts are likely.

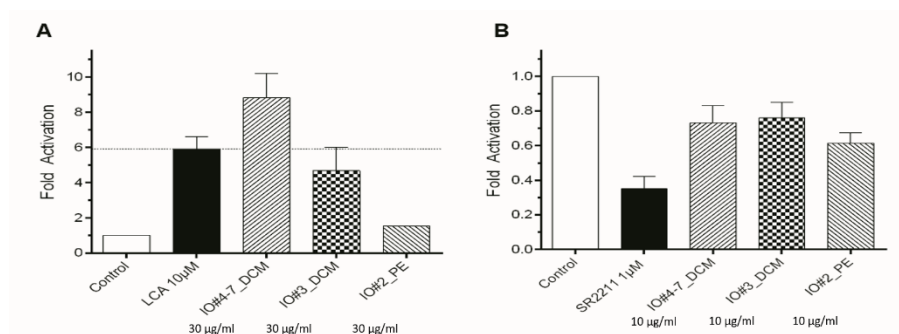


Figure 3: Bioactivity of three different *Inonotus obliquus* fractions on two different receptors. **A** TGR-5 receptor activation in comparison to the positive control LCA (10 μ M). **B** Fold activation of the ROR_{yt} with the positive control SR2211 (1 μ M). Data are shown as means \pm SEM of (at least) three biological replicates measured in technical quadruplicates. The experimental setup is described in 6.4.

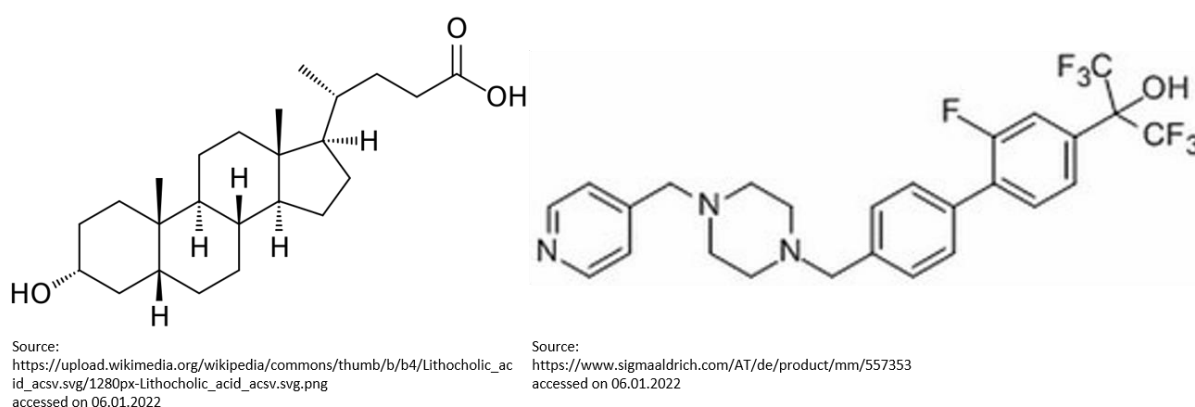


Figure 4: Structural formula of the positive control molecules on both receptor assays. On the left lithocholic acid is shown, an activator of the TGR-5 receptor. On the right SR2211 is shown, a synthetic inhibitor of the ROR_{yt} receptor.

3.4 Metabolic and immunological targets

Over the last 50 years, the prevalence of overweight and obesity has tripled. In 2016, the world health organization (WHO) reported that 39% of adults were overweight and 13% obese (WHO, 2016). There are estimations, that by 2035, 4 billion people will be either overweight or obese (Revels et al. 2017). This has a big impact on our society and economy. Interventions already existing, such as a sugar tax in the UK, a food traffic light system in France, and impending advertising bans, are not enough to eliminate this problem (Nestle et al., 2000; Schwendicke et al., 2017; Day et al., 2013). In addition to these measures, a better understanding of the causes of obesity-related diseases is needed so that pharmaceutical companies can provide pharmacological agents to control it (Nolan et al., 2019).

Several regulatory proteins of lipid-, glucose- and energy homeostasis were reported in the last years. The identification of modulators of these targets proteins is a promising approach for drug discovery. Two identified promising targets to combat overweight and obesity are the TGR-5 and the ROR_{yt}.

3.4.1 TGR-5/GPBAR-1

G-protein coupled receptors (GPCRs) are a large family of membrane-bound proteins and play an important role in many cellular pathways. They consist of seven transmembrane domains and, after binding ligands in the extracellular space, transmit these signals intracellularly by triggering a downstream cascade (Figure 5) which includes guanine nucleotide-binding proteins (G-proteins). They are vital to many physiological and pathological process (e.g. tasting, seeing, immune system, brain function) and therefore have great importance for the treatment of many diseases (Guo C., et al., 2016). They are the largest therapeutic target class in medicine. Approximately one-third of the drug genome and 40% of marketed drugs, including 25% of the 100 top-selling drugs, interact with GPCRs. The global profit is over \$100 billion. This results in a continuing large focus of pharmaceutical research on GPCR-based ligands (Cvijic, M., 2015).

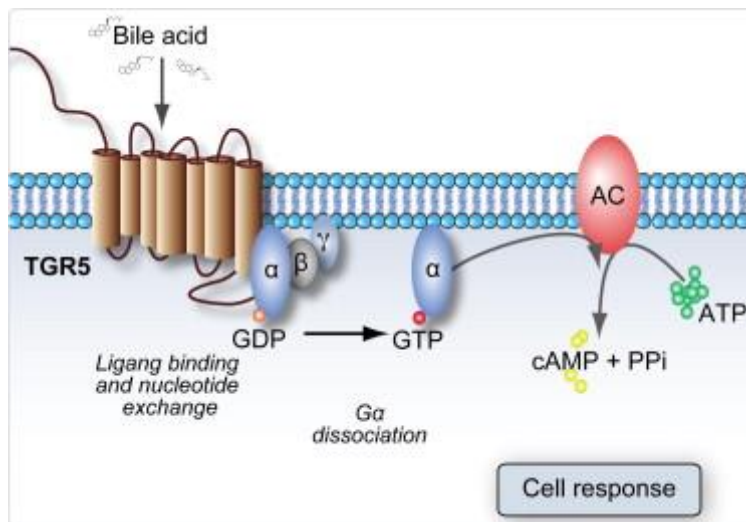


Figure 5: Simplified overview of the TGR5-signaling pathway leading to downstream signalling via cAMP induction. Source: Pals et al. 2010 J Hepatol. 54(6):1263-72

The TGR-5 or G protein-coupled bile acid receptor 1 (GPBAR-1) receptor is a member of the GPCR family. It was discovered in 2002 (Maruyama et al., 2002).

The TGR-5 gene can be found in humans at chromosome position 2q35. It has 993 base pairs, which code for 330 amino acids. The mRNA is found in increased concentrations in various organs such as stomach, liver, lung, small intestine, placenta and spleen (Tiwari et al., 2009). The receptor is activated by bile acid binding which induces cAMP production via $G_{\alpha s}$ (Maruyama et al., 2002).

The natural, endogenous agonists of the TGR-5 receptor are therefore bile acids. The secretion, synthesis and cycling of bile acids is closely related to the timing and content of food intake. The primary function of bile acids are their emulsification and solubilisation properties on luminal lipids. Additionally, they can act as signalling molecules at different receptors, with downstream effects on metabolism. Due to the obesity pandemic (Popkin et al., 2012) and the resulting health problems, the interest in the biology of bile acids increased strongly in recent years (McGlone et al., 2018).

There are several bile acids which can induce the cAMP production in human TGR-5-transfected CHO cells. They can be ordered by potency: Taurolithocholic acid (TLCA) > LCA > deoxycholic acid (DCA) > chenodeoxycholic acid (CDCA) > cholic acid (CA) (Guo C. et al., 2016).

TGR-5 plays an important role in cell signalling pathways. It inhibits the pro-inflammatory nuclear factor Kappa-Light-Chain-Enhancer of activated B cells

(NF- κ B) via phosphorylation of c-Fos to regulate NF- κ B p65 activation. Further Protein kinase B (ATK) and extracellular signal-regulated kinases (ERK), which are playing an important role in diverse cell processes like proliferation, differentiation, survival, and metabolism, are also regulated by TGR-5 activation. It is also suggested that TGR5 activation induces GLP-1 secretion via intracellular cAMP production, as well as improve glucose tolerance, decrease fasting blood glucose and the glycosylated hemoglobin A1c, which could help with type 2 diabetes (T2D) therapy (Katsuma et al., 2005, Zheng et al., 2015). Another promising cellular mechanism is the increase of energy expenditure in brown adipose tissue (BAT) through an increase of cAMP-dependent thyroid hormone-activating enzymes, after TGR5 activation (Watanabe et al., 2006). This effect may help fighting obesity.

Results from rodent models or *in vitro*-studies suggest that the TGR-5 is a potential target for the treatment of metabolic, inflammatory, and digestive disorders (Broeders et al., 2015; Kumar et al., 2012). It shows promising effects for the treatment of T2D and obesity. Also, it has a crucial role in liver protection, and it shows novel effects on inflammation and cancer in various organs (Guo C. et al., 2016).

Interestingly, the ethnopharmacological use of Chaga is very similar to the potential application fields of TGR-5 agonists. Both should have the ability to help against T2D, inflammatory diseases, gastrointestinal cancer, and cardiovascular diseases. Moreover, plant triterpenes, for example from clove and allspice were already described as TGR5 agonists (Ladurner et al., 2017). Triterpenes were also reported from Chaga (Szychowski et al., 2020). It was therefore tempting to speculate that TGR-5 might be a potential target receptor of Chaga constituents.

3.4.2 ROR γ t receptor

The ROR γ is the most recently discovered receptor of the ROR subfamily of nuclear receptors (NR). Nuclear receptors are a family of 48 intracellular proteins whose function is to convert an external signal in form of a ligand into a transcriptional output. They also act as sensors for their ligands (Flanagan et al., 2019). Those NRs typically consist of a conserved structure and a significant sequence

homology. Four major functional domains are identified. Those four domains are the N-Terminus where the ligand-independent activation function 1 (AF1) is located at, a DNA-binding domain (DBD), a hinge region and a ligand binding domain (LBD) (Jetten, 2009; Ladurner et al., 2020). NRs can bind DNA as monomers (like RORs do). However, with other members of the RXR subfamily as partners, they can also bind DNA as homodimers or heterodimers. The LBD consists of 12 α helices, which form a cavity for the binding of hydrophobic ligands. Without ligands, NRs are bound to co-repressor proteins and act as transcriptional repressors. Binding of agonists leads to repression of co-repressors and recruitment of co-activators, resulting in expression of target genes (Ladurner et al., 2020).

Since NRs play a central role in signal transduction, and small molecules are able to block or activate the LBD of NRs, they are strongly represented among the classical drug targets (Moore et al., 2010).

The ROR subfamily consists of ROR $_{\alpha}$, ROR $_{\beta}$ and ROR $_{\gamma}$. Four isoforms of ROR $_{\alpha}$ have been identified in humans (ROR $_{\alpha 1-4}$). ROR $_{\beta}$ only has one isoform, and ROR $_{\gamma}$ has two (ROR $_{\gamma 1}$ or ROR $_{\gamma}$ and ROR $_{\gamma 2}$ or ROR $_{\gamma t}$) (Jetten, 2009).

It is now known that RORs influence various physiological and pathological processes. Examples would be the circadian rhythm, the development of neuronal cells, the differentiation of immune cells, but also autoimmune-, inflammatory-, or metabolic diseases. In this context, ROR $_{\alpha}$ is mainly found in many peripheral tissues (liver, lung, skin, etc.). ROR $_{\beta}$ is only expressed in the brain, retina, bone and in the pineal gland. ROR $_{\gamma}$, as mentioned, occurs in two isoforms, which are different. They differ only by the first 100 nucleotides at the N-terminus. While ROR $_{\gamma}$ is expressed in muscle tissue, prostate, pancreas, heart, testicles, and liver, ROR $_{\gamma t}$ is found only in lymphoid tissue. It is mainly expressed in the thymus where it mediates for the proliferation of T helper cells 17 (Th-17) and the production of pro-inflammatory interleukin 17 (IL-17). The specific expression of ROR $_{\gamma t}$ in the thymus shows a special role in the development of the immune system. ROR $_{\gamma t}$ is an important regulator of immune homeostasis. Due to this role, ROR $_{\gamma t}$ ligands have become of interest as a therapeutic target for inflammatory diseases (Ladurner et al., 2020; Sun N., 2019).

The main endogenous ligands for ROR $_{\gamma t}$ seem to be steroids like cholesterol sulfate, desmosterol and oxysterols. Structurally, terpenes in various plants are close

orthologues to steroids in humans. Various terpenes such as ursolic acid or betulinaldehyde and other substances such as polyketides or cardiac glycosides showed activity at the ROR_{yt}. This suggests that there are still some undiscovered plant substances that could be active at the ROR_{yt} (Ladurner et al., 2020).

The chaga fungus, has a broad terpene profile and other interesting constituents that have not yet been fully explored. Since it is traditionally used against inflammatory and metabolic diseases, as well as against cancer, properties that could be associated with inhibition at the ROR_{yt}, it is assumed that the mushroom produces some substances that show activity at the ROR_{yt}.

4. Results and Discussion

4.1 Description of starting materials

The *I. obliquus* sclerotia used in this study were derived from wild collection in Finland above the Arctic circle. Previously, 500 g of dried and ground sclerotia had been extracted with an MV-10 ASFE system (Waters, 2012). The extraction was performed five times with 100 g of material. Each extraction was performed successively in cycles of 20 minutes at a flow rate of 10 ml/min supercritical fluid. Firstly, it was extracted with pure supercritical carbon dioxide (CO₂) in two cycles at 100 bar – combined to extract **IO#1**; secondly with 10% EtOH in a single cycle at 100 bar – combined to extract **IO#2**; thirdly with 20% EtOH in a single cycle at 200 bar – combined to extract **IO#3**; fourthly, with 20% EtOH in four cycles at 300 bar at the same conditions - **IO#4-7**. Each of the three extracts (**IO#2**, **IO#3**, and **IO#4-7**) were subsequently fractionated by liquid-liquid partition between water, petrol ether (PE), dichloromethane (DCM) and ethylacetate (EA). The fractionation tree is shown in Figure 6. Highlighted in orange are the three fractions worked with, and which were tested for bioactivity (**3.3**). Those fractions were IO#2_PE, IO#3_DCM and IO#4-7_DCM.

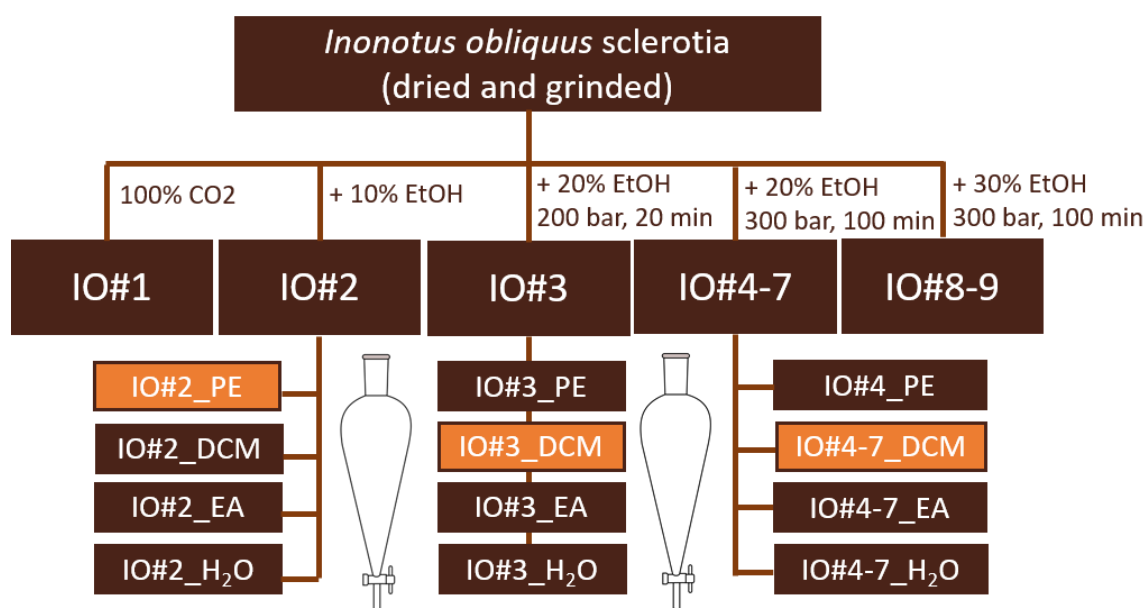


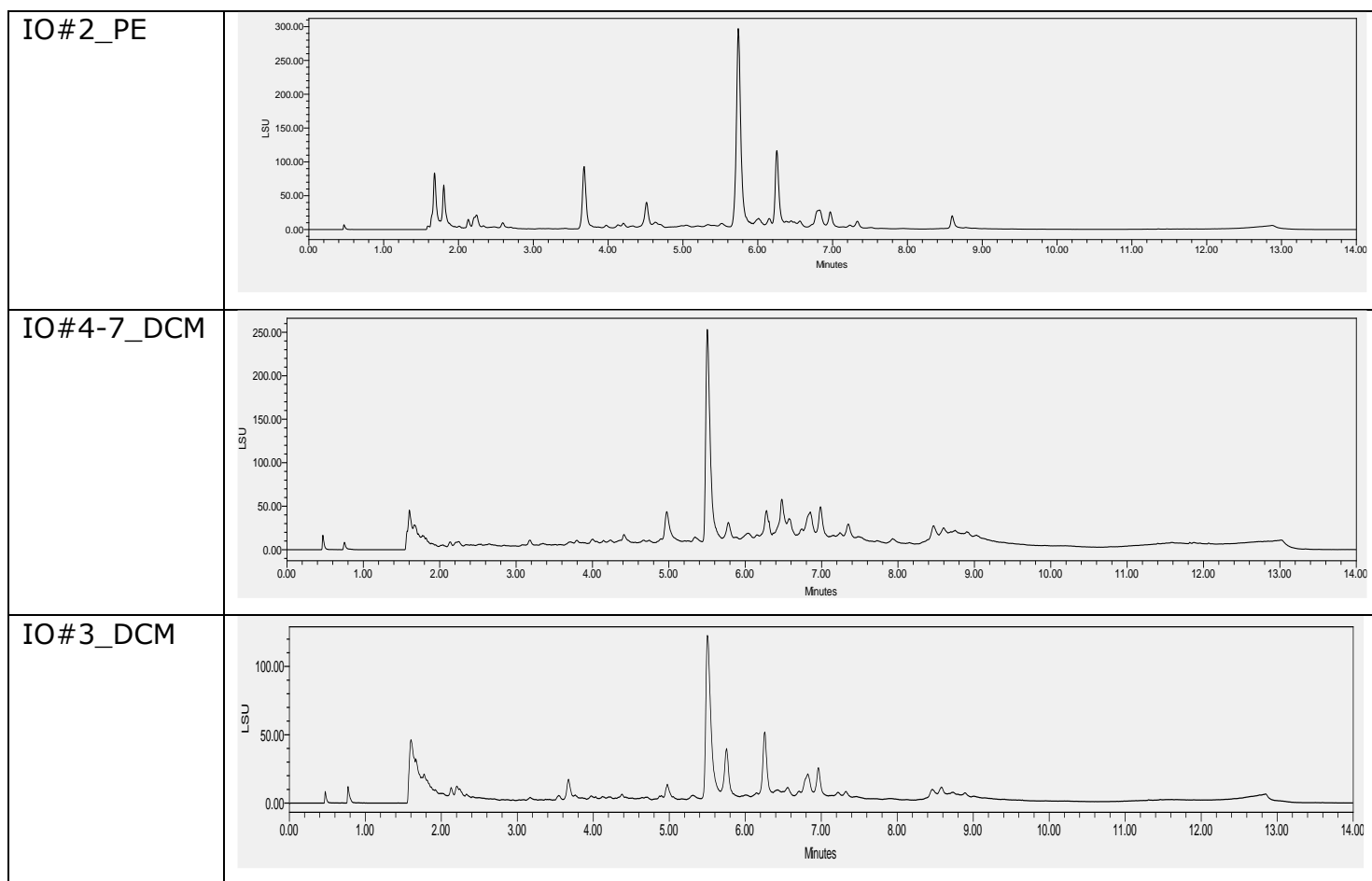
Figure 6: Extraction and fractionation of *I. obliquus* sclerotia; PE = petrolether, DCM = dichloromethane, EA = ethylacetate, in orange = bioactivity measured fractions

4.2 UPC² chromatograms and analysis

The tested fractions were analyzed with ultrahigh-performance supercritical fluid chromatography (UPC²) (**5.1.3**) paired with a photo diode array (PDA) and an evaporative light scattering detector (ELSD). Aim of this first analysis was to efficiently separate constituents and to get a first insight into the fraction's composition. In Table 2, the ELSD-chromatograms of fractions IO#2_PE, IO#2_DCM, IO#3_DCM, and IO#4-7_DCM are shown.

The gradient optimization is described in Material and Methods – Supercritical fluid chromatography (5.1.3) in Table 20.

Table 2: UPC² analysis of fractions. Chromatograms of IO#2_PE, IO#4-7_DCM, IO#3_DCM and IO#2_DCM (ELSD detection, Waters UPC², Torus 1-AA column, 40°C, co-solvent B = methanol, gradient start with 0% B non-linear up to 50% at minute 12 (Table 20), washed for 1,5 minutes at the end of every run with CO₂).



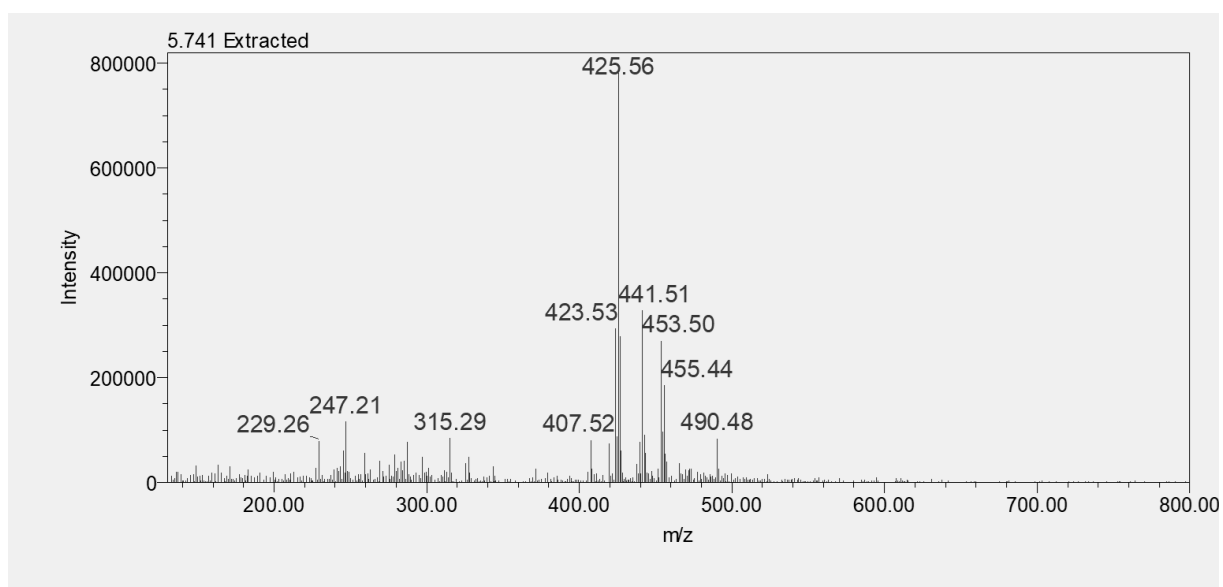
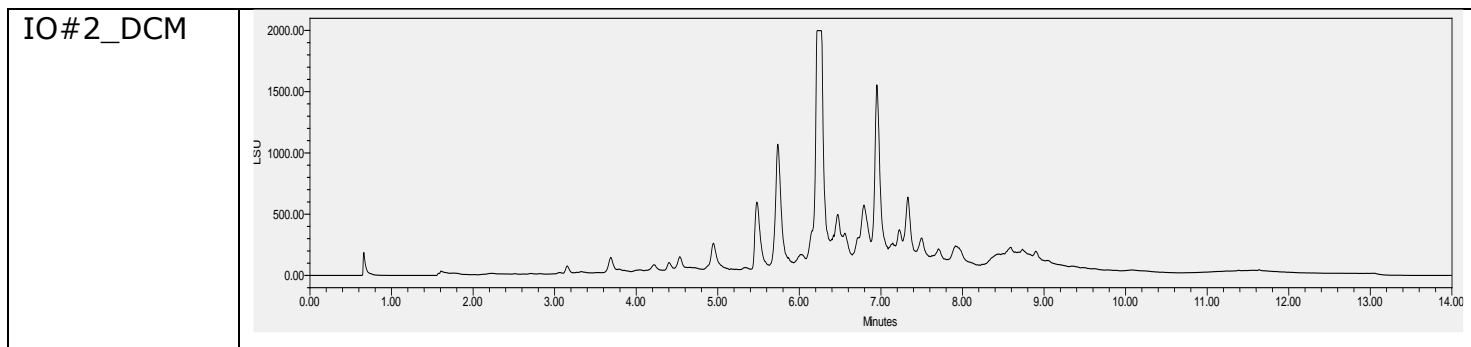


Figure 7: Extracted QDa $[m/z]^+$ spectrum of main peak in IO#2_PE at 5.74 min

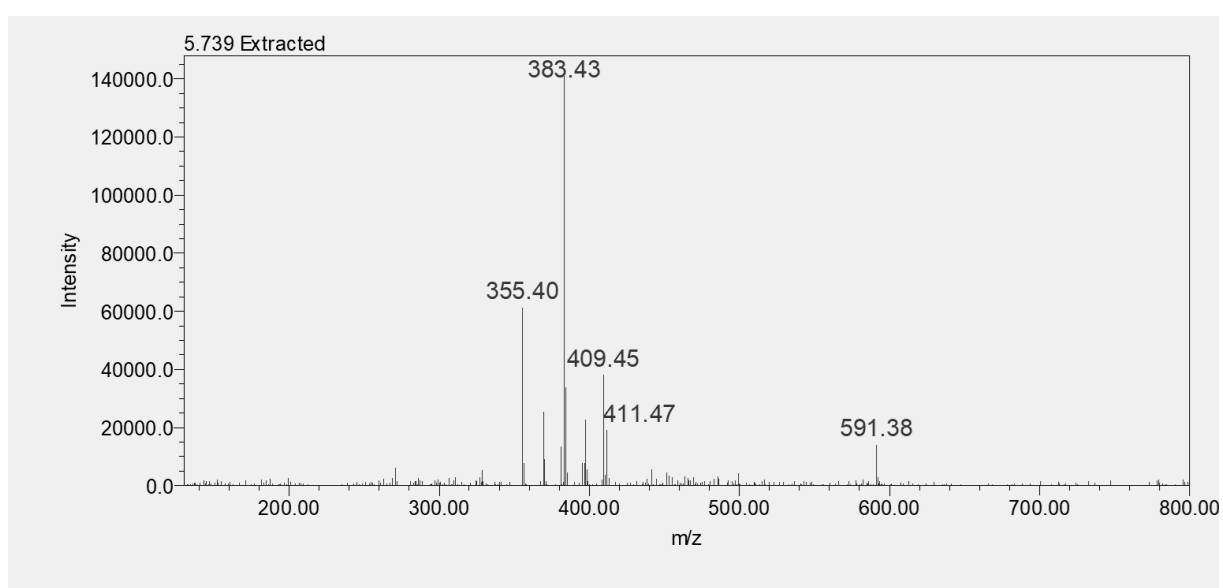


Figure 8: Extracted QDa $[m/z]^-$ spectrum of main peak in IO#2_PE at 5.74 min

The SFC separation of IO#2_PE seemed to be very proficient and the fraction not very complex. A major peak at $R_t = 5.75$ min showed the suspected main constituent. The MS showed that it most likely consists of a triterpene, but a clear assignment to a known compound was not possible (Figure 7+8). The peaks between minute three and seven, were suspected to be other triterpenes as well. The last peak seemed like a small, more hydrophile molecule. The first couple of peaks were suspected to be fatty acids. The different peaks were in general well separated from each other. That led to the decision, to start with the separation of this fraction.

The fractions IO#4-7_DCM and IO#3_DCM appeared more complex than IO#2_PE. More, and more asymmetric peaks were observed. Many peaks were insufficiently separated. One major peak at $R_t = 5.5$ min was observed. The PDA and QDa spectra (Figure 9) suggested a small molecule with a molecular weight (MW) of 183 or 384 Dalton. A clear assignment to a known molecule was not possible. The peaks at $R_t = 5.7 - 8$ min were expected to be a complex mix of triterpenes, because of extracted mass spectra with $(m/z) > 400$ (Figure 10) and PDA absorption were observed. Chaga is known to contain a variety of different triterpenes.

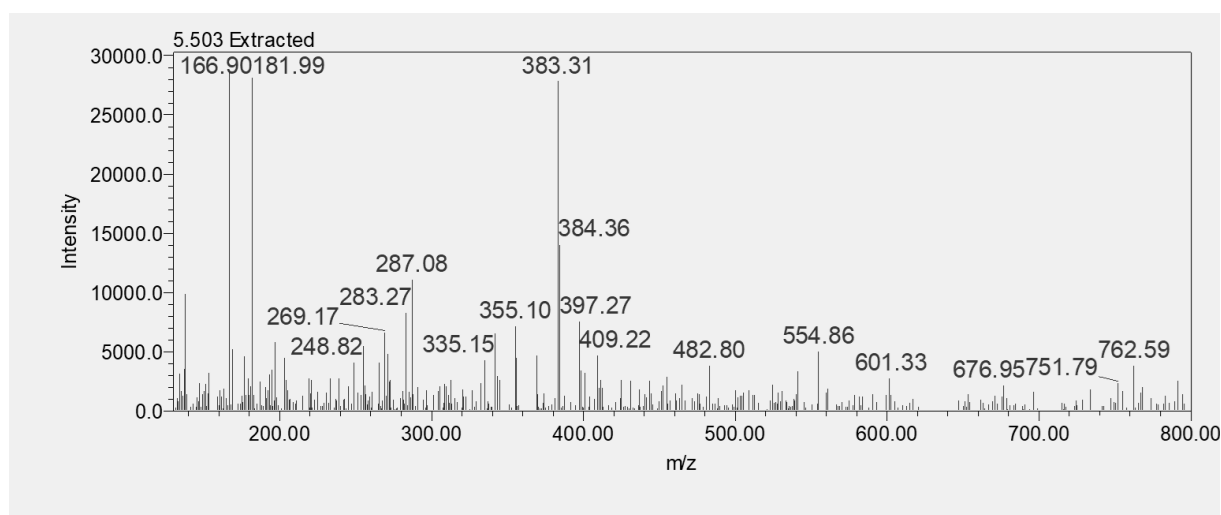


Figure 9: Extracted QDa [m/z]- spectrum of main peak in IO#4-7_DCM and IO#3_DCM at 5.5 min

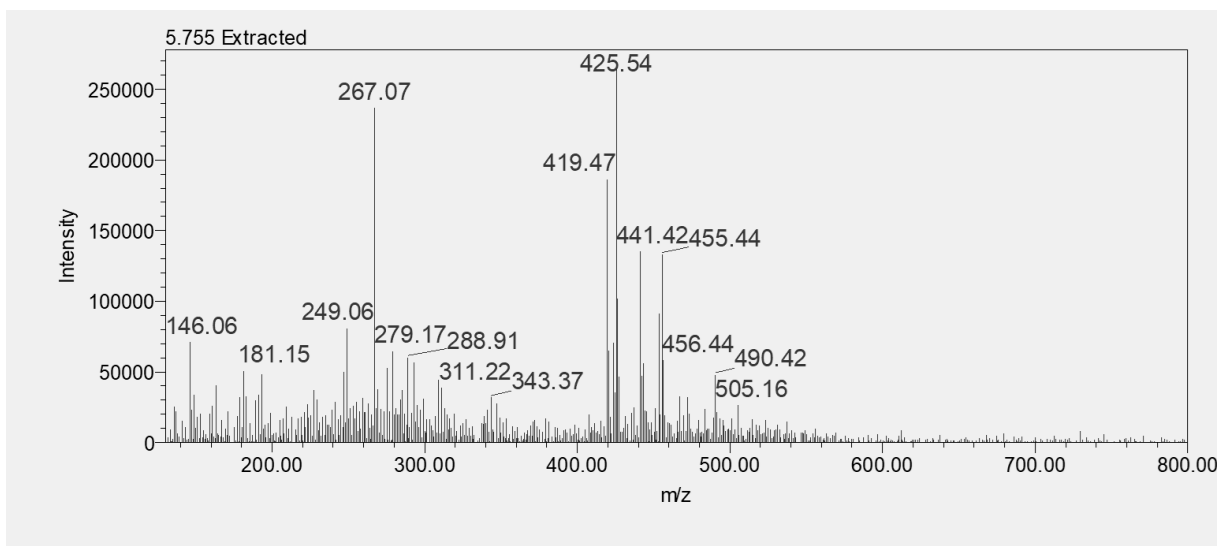


Figure 10: Extracted $[m/z]^+$ QDa spectrum of a constituent from IO#3_DCM and IO#4-7_DCM at 5.75 min

The last chromatogram, IO#2_DCM was not tested for activity. However, it was decided to also fractionate it, as it seemed to contain many constituents of the other three active fractions. As there was only little extract available (e.g. from IO#4-7_DCM), it was questionable if purified substances in sufficient quantity for NMR and bioactivity analysis could be yielded. Hereby, fractions from IO#2_DCM could contribute to the yields, e.g. by combining orthologous fractions with similar constituents.

4.3 Fractionation and analysis of IO#2_PE

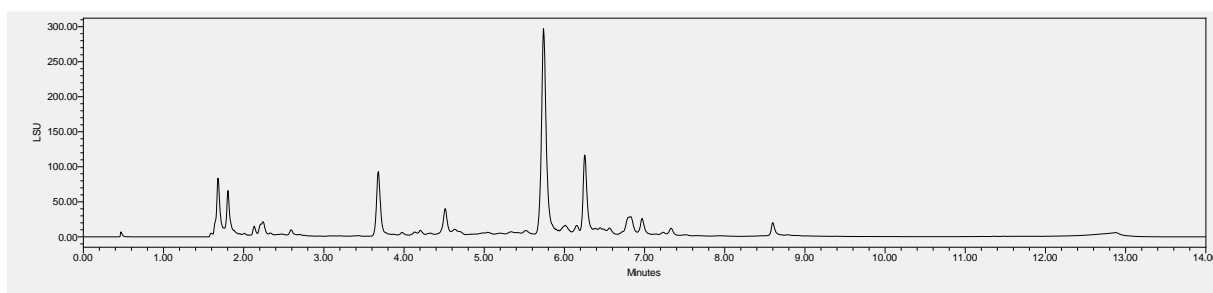


Figure 11: IO#2_PE SFC chromatogram (ELSD detection, Waters UPC², Torus 1-AA column, 40°C, co-solvent B = Methanol, 14 minute method (Table 19))

The peak-separation on the UPC² was already good and only few well-separated peaks were detectable.

Thus, preparative SFC (Prep-15, Waters), seemed to be a reasonable choice for further fractionation. For the scale-up of the UPC² method to the preparative scale,

small adaptations to the gradient were made. This was necessary because of an increased flowrate, other column dimensions but also because of a mandatory initial concentration of 5% co-solvent. The reason for the latter is the modifier-stream injection of the Prep-15 device which introduces the sample (up to 100 μ l) into the co-solvent stream before it is mixed with CO₂. Therefore, the original UPC² gradient was adapted accordingly. The optimized SFC-15 MeOH co-solvent gradient is shown in Table 21 and the chromatogram with the isolation cuts in Figure 12. 496.51 mg of IO#2_PE were dissolved in hexane:isopropanol (1:1) and fractionated. 106 fractionation runs with 100 μ l per injection were executed. 16 sub-fractions (IO#2_PE_1 – IO#2_PE_16) were collected. IO#2_PE_16 was the combined wash solvent.

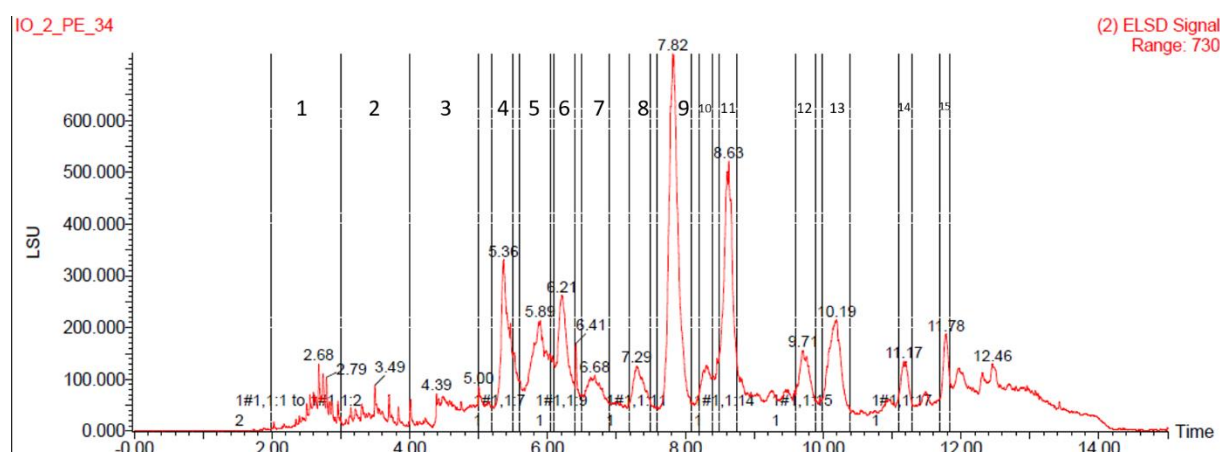


Figure 12: ELSD chromatogram of IO#2_PE at the Prep-15, with the adjusted method (Figure 11), including the isolation cuts for each sub-fraction

After fractionation with the Prep-15, every fraction was analyzed for purity and identity, with UPC²-PDA-ELSD and UPC²-PDA-QDa with the analytical method described in chapter 5.1.3. Table 3 shows the chromatograms of the sub-fraction of the Prep-SFC fractionation, monitored by UPC²-PDA-ELSD. Also, a thin layer chromatography (TLC) (5.1.1) was performed for every sub-fraction (Figure 13).

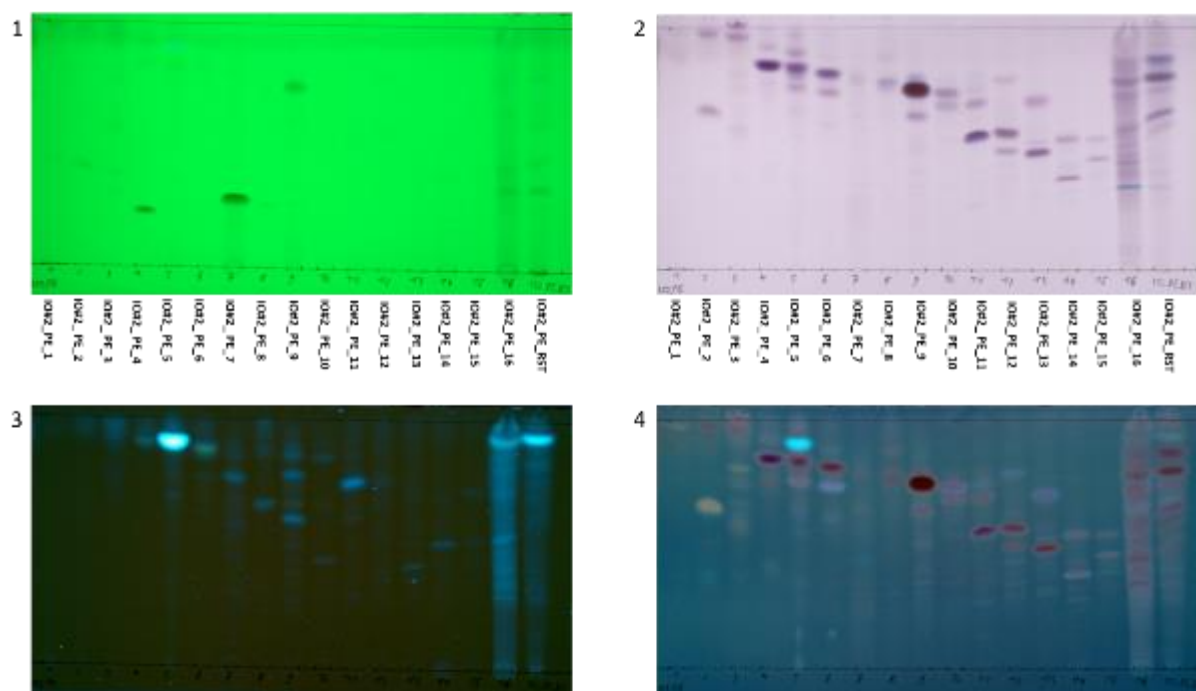
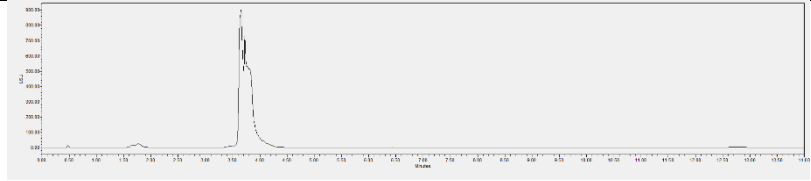
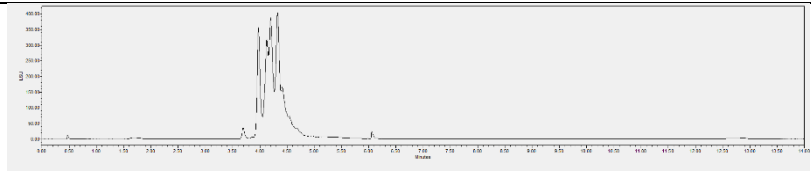
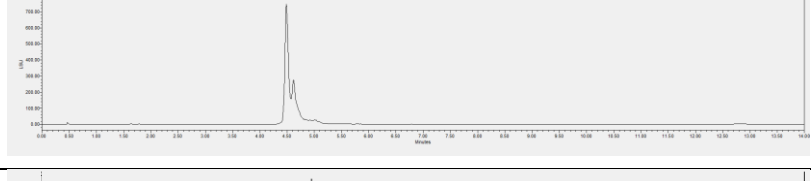
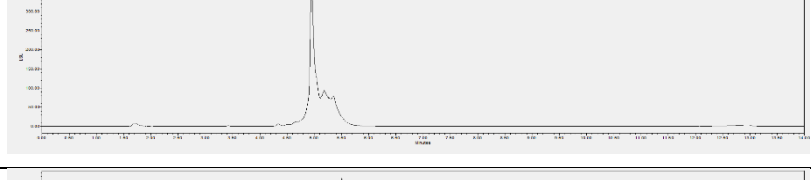
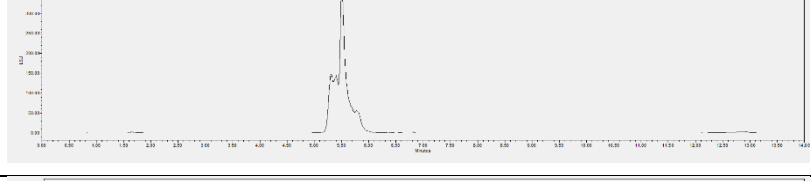
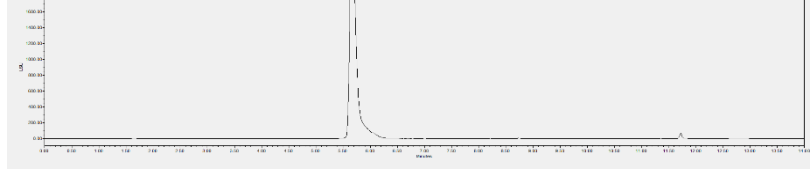
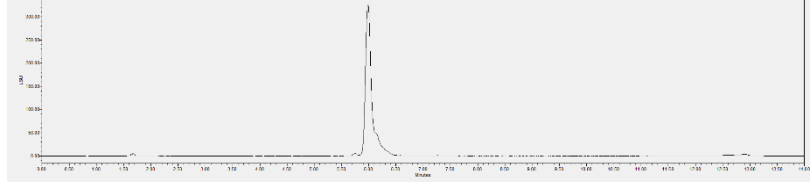
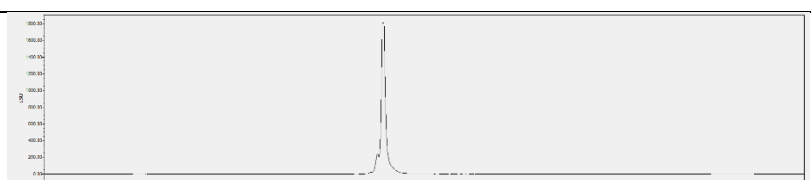
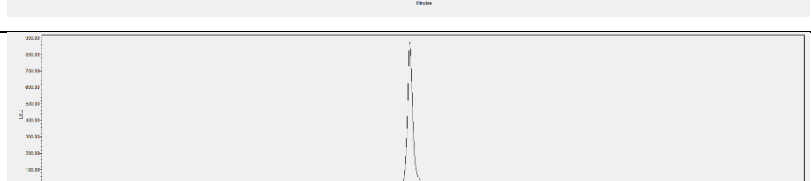
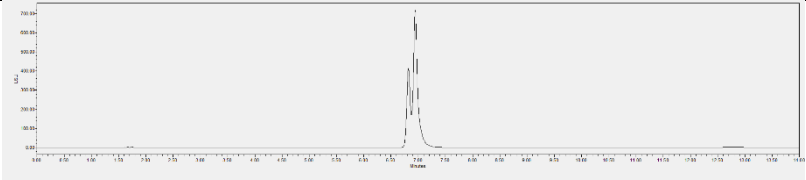
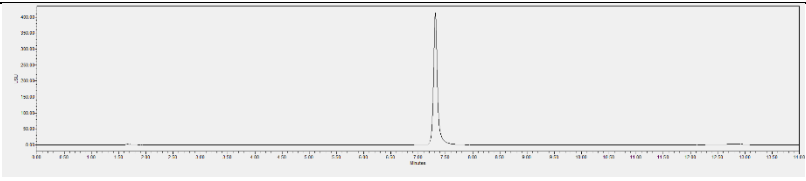
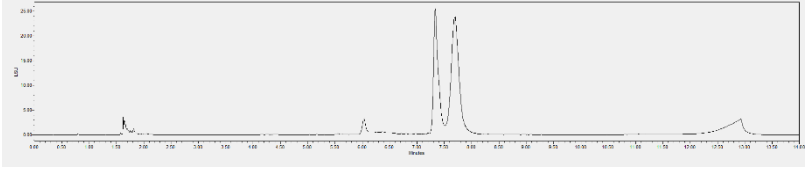
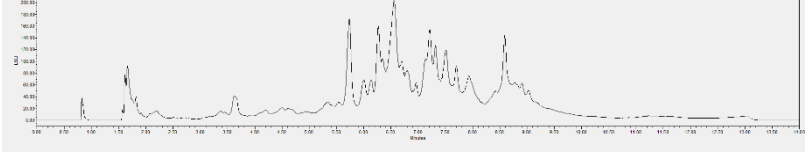


Figure 13: TLC (5.1.1) of IO#2_PE sub-fractions, 1 254 nm before derivatization with Vanillin/sulphuric acid, 2 Vis after derivatization, 3: 366nm before derivatization, 4: 366 nm after derivatization.

Table 3: Chromatograms of the sub-fractions from IO#2_PE, including yield and if determined mass and substance-prediction.

Name	ELSD - chromatograms	[m/z] of peak	Predicted substance	Yield [mg]
IO#2_PE_1		n.d. (not determined)	n.d.	14,54
IO#2_PE_2		n.d.	n.d.	6,84
IO#2_PE_3		n.d.	n.d.	8,32

IO#2_PE_4		n.d.	n.d.	11
IO#2_PE_5		n.d.	n.d.	38,79
IO#2_PE_6		n.d.	n.d.	13,11
IO#2_PE_7		n.d.	n.d.	7,95
IO#2_PE_8		n.d.	n.d.	6,71
IO#2_PE_9		$[M+Na]^+$ = 465.1 $[M-OH]^+$ = 425.5	Inotodiol MW = 442.71	29,51
IO#2_PE_10		n.d.	n.d.	4,32
IO#2_PE_11		$[M-H]^-$ = 455.5	Tramete- nolic acid MW = 456.71	16,72
IO#2_PE_12		n.d.	n.d.	6,41

IO#2_PE_13		n.d.	n.d.	11,77
IO#2_PE_14		n.d.	n.d.	4,45
IO#2_PE_15		n.d.	n.d.	5,79
IO#2_PE_16		n.d.	n.d.	71,35

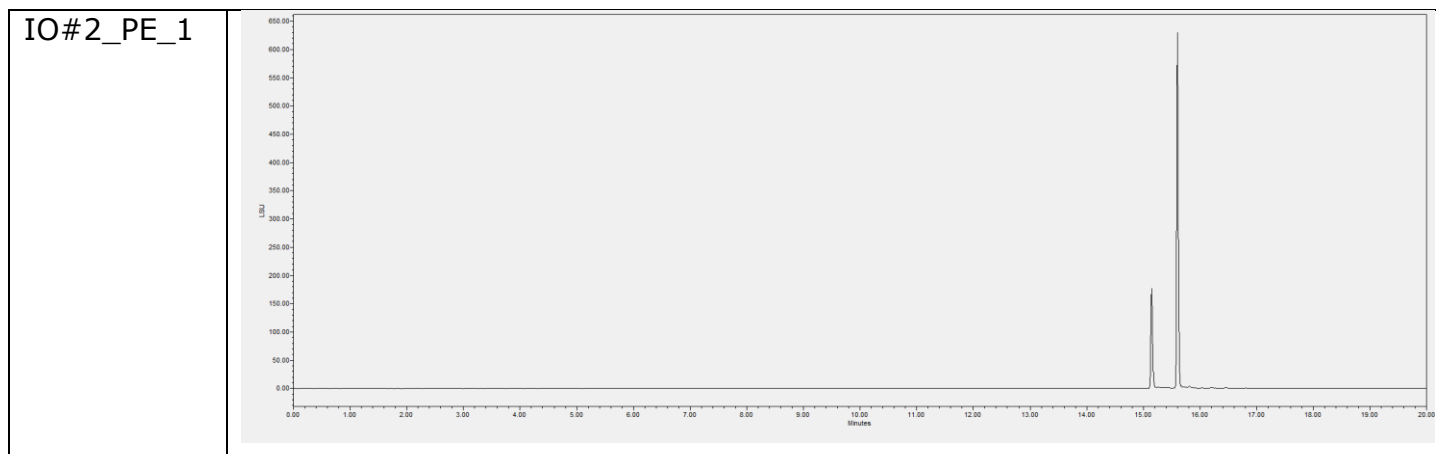
In total, 98,64 mg (19,9%) could not be recovered after this fractionation step. The reason for this might be attributed to (1) absorption of pigments to the stationary phase. IO#2_PE fraction was observed to be yellow while all yielded sub-fractions were colourless. (2) Washing processes, (3) an incorrect setting of the delay time at the first 39 runs. After those 39 fractionation runs, the delay time was adjusted. (4) Loss of volatile compounds upon drying.

However, two pure compounds could be isolated. Those were the main compound, IO#2_PE_9, which was identified as inotodiol and IO#2_PE_11, which was identified as trametenolic acid (TA). They were identified with the help of available reference substances by means of m/z values, R_t and ^1H NMR chemical shifts. The NMR spectra can be found in the appendix. Further 3 more sub-fractions showed single peaks in the analytical UPC². Those sub-fractions were IO#2_PE_10, IO#2_PE_12 and IO#2_PE_14. Their identity could not be determined by MS dereplication. The NMR measurements that were carried out later showed that these putative pure compounds were still mixtures (**Appendix**). This can also be seen clearly in the TLC (Figure 13).

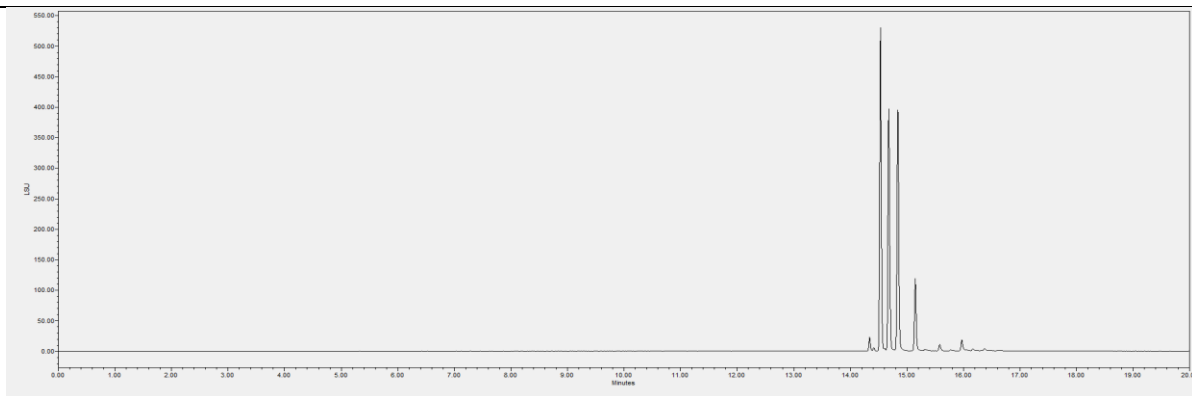
IO#2_PE_4 and IO#2_PE_6 seemed like a mixture of two compounds. Those were aimed to separate by sephadex column chromatography. Two sub-fractions with single pure TLC bands could be separated from IO#2_PE_4 (IO#2_PE_4_2,

IO#2_PE_4_4) and one out of IO#2_PE_6 (IO#2_PE_6_2). IO#2_PE_6_2 was later confirmed to be an isolated compound, and identified as 3 β -hydroxy-lanosta-8,24-dien-21-al by means of MS, 1D and 2D NMR, and comparison of spectroscopic data with reference spectra and literature (Shin, 2000). IO#2_PE_13 was a mixture of two main compounds which were later separated by Ruzica Colic with sephadex column chromatography. The constituents were characterized as inonotsutriol A/B and betulinol. IO#2_PE_15 was a mixture of three compounds, of which two could be separated by UPLC separation. NMR measurements helped characterizing these isolates as inonotsutriol D/E and lanosta-8,25-diene-3,22,24-triol. The fact that single peaks were displayed in the UPC² chromatograms of IO#2_PE_10, IO#2_PE_12 and IO#2_PE_14, although NMR showed us that the peaks consisted of more than one substance, is probably due to the fact, that the structures of the triterpenes forming the peak, are very similar and plateaus in the gradient led to co-elution. Because successful separation on UPC² could not be achieved for every sub-fraction, the semi pure substances were tried to get separated on the UPLC BEH C18 column (1.7 μ m) equipped with ELSD and PDA detector (5.1.4). The gradients can be found in 5.1.4. The UPLC-Chromatograms of the sub-fractions with a putatively pure compound are shown in Table 4.

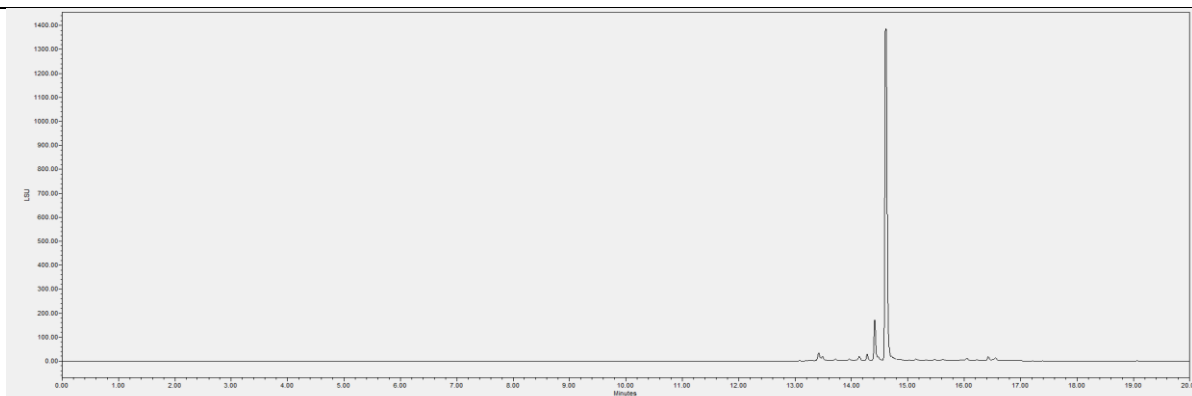
Table 4: ELSD - chromatograms of IO#2_PE sub fractions measured with the UPLC



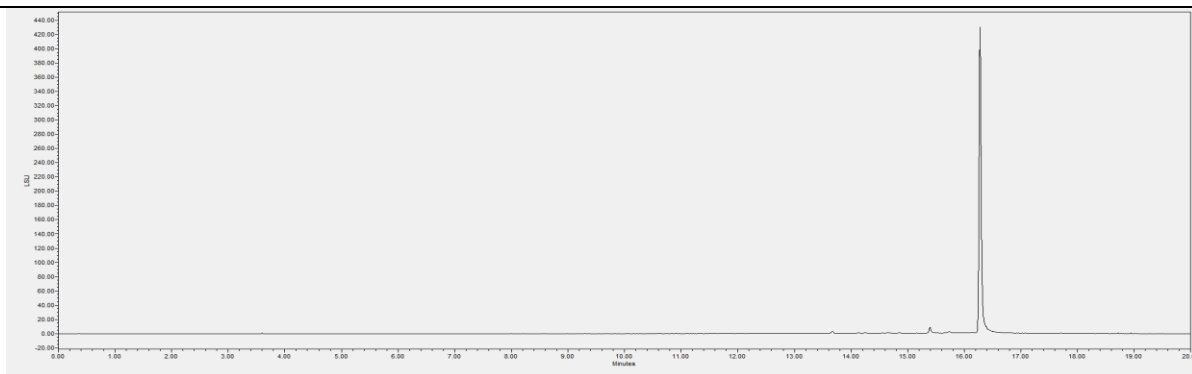
IO#2_PE_2



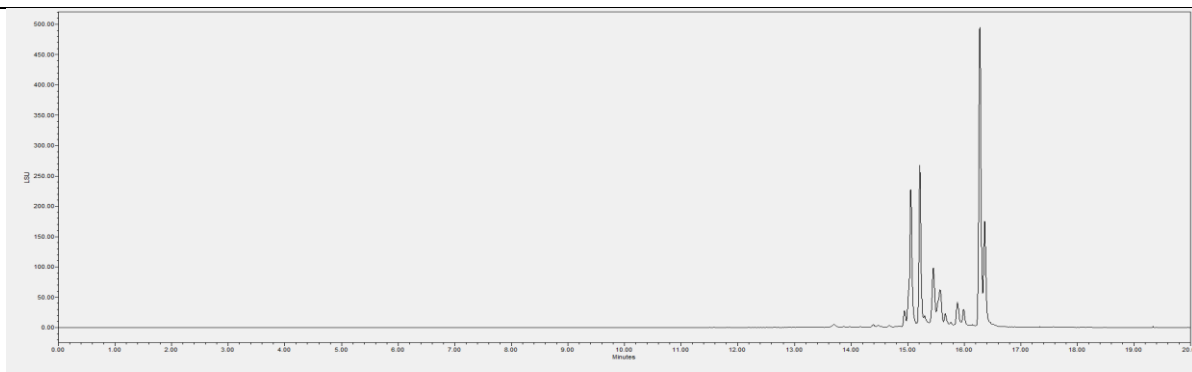
IO#2_PE_3



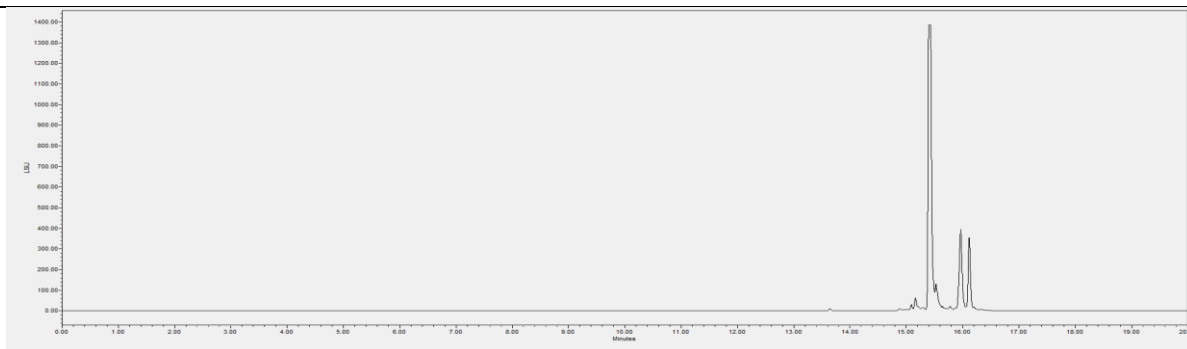
IO#2_PE_4



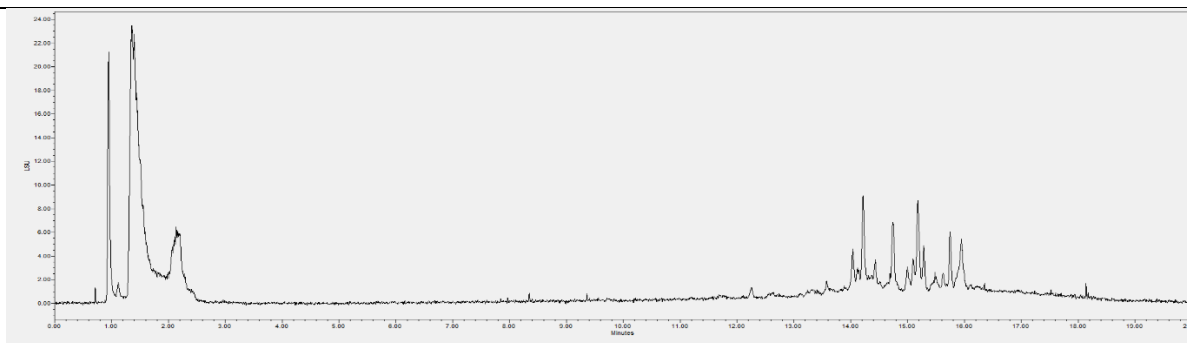
IO#2_PE_5



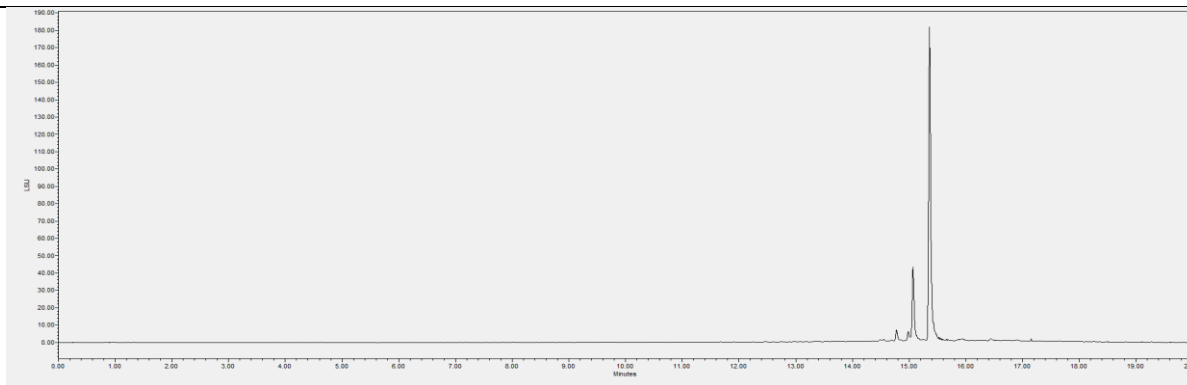
IO#2_PE_6



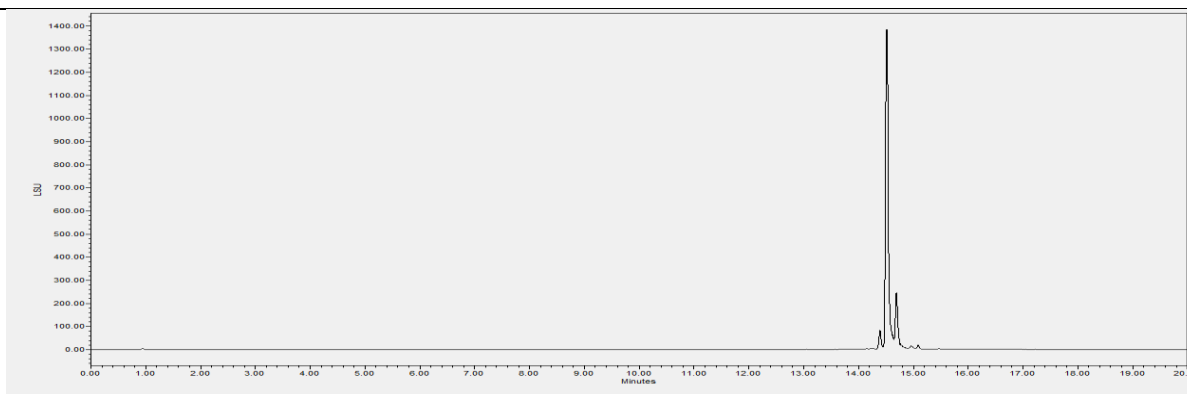
IO#2_PE_7



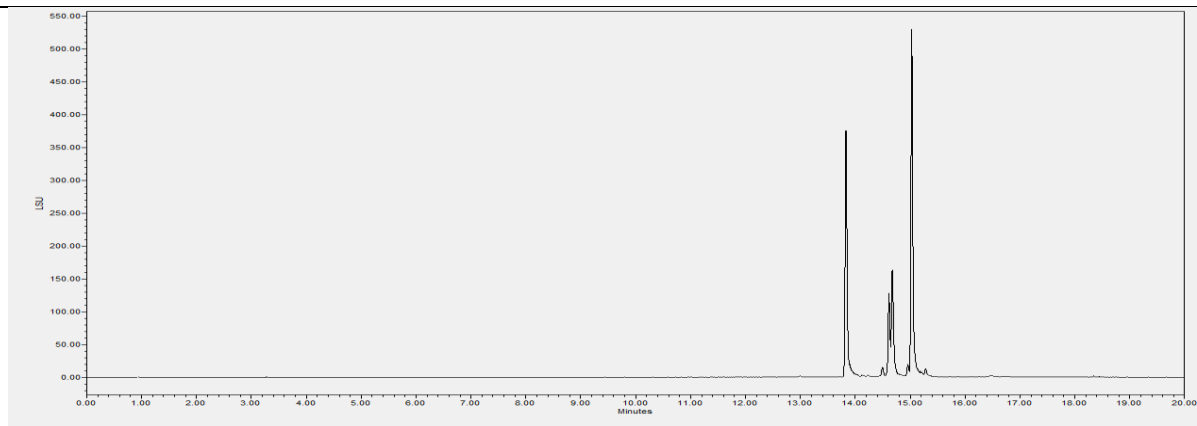
IO#2_PE_8



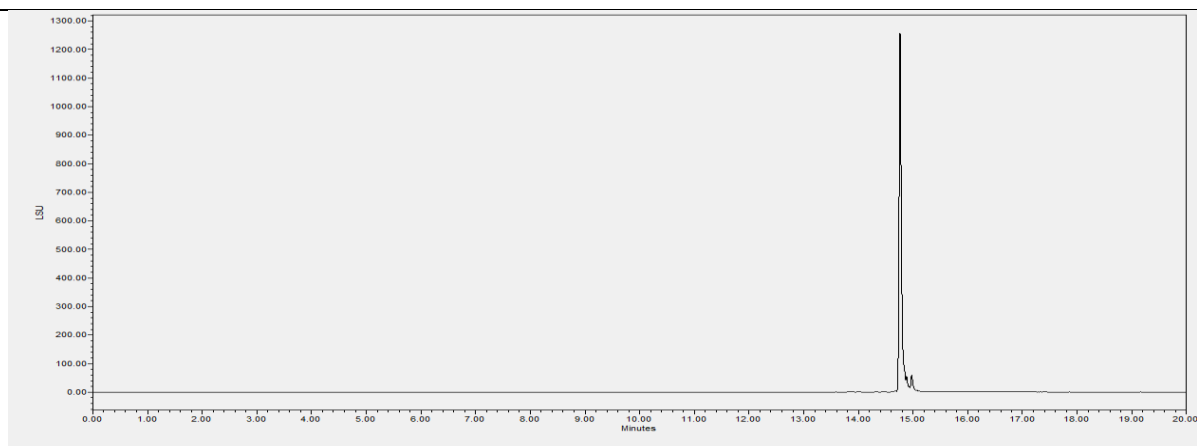
IO#2_PE_9



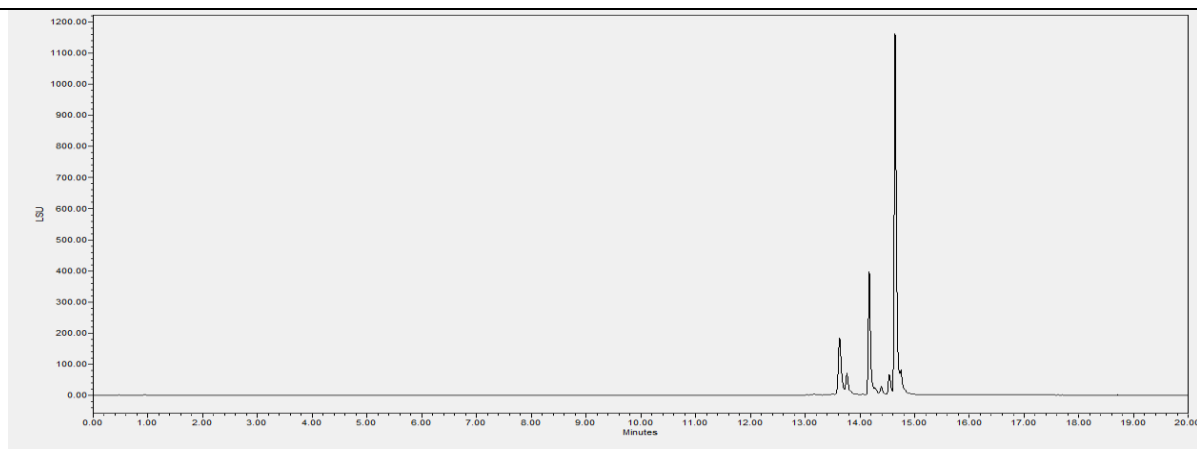
IO#2_PE_10



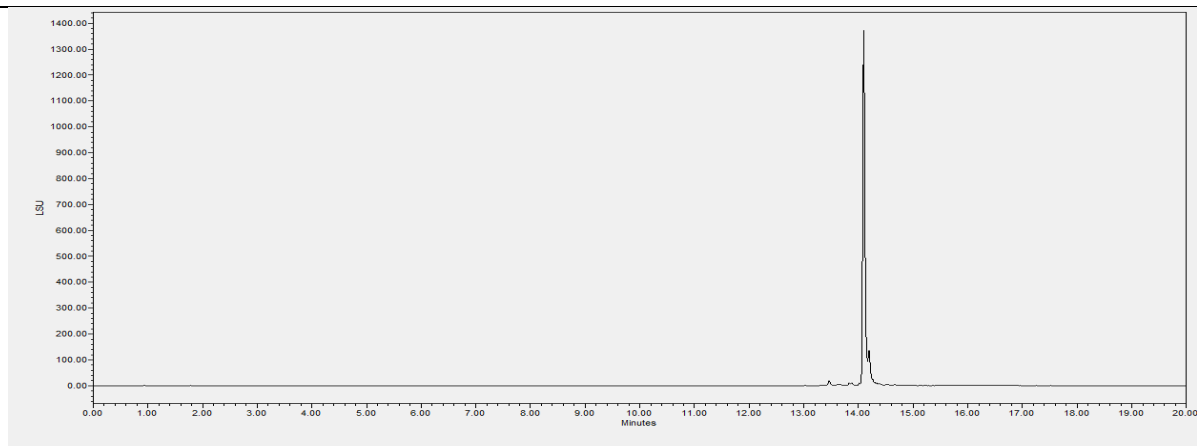
IO#2_PE_11

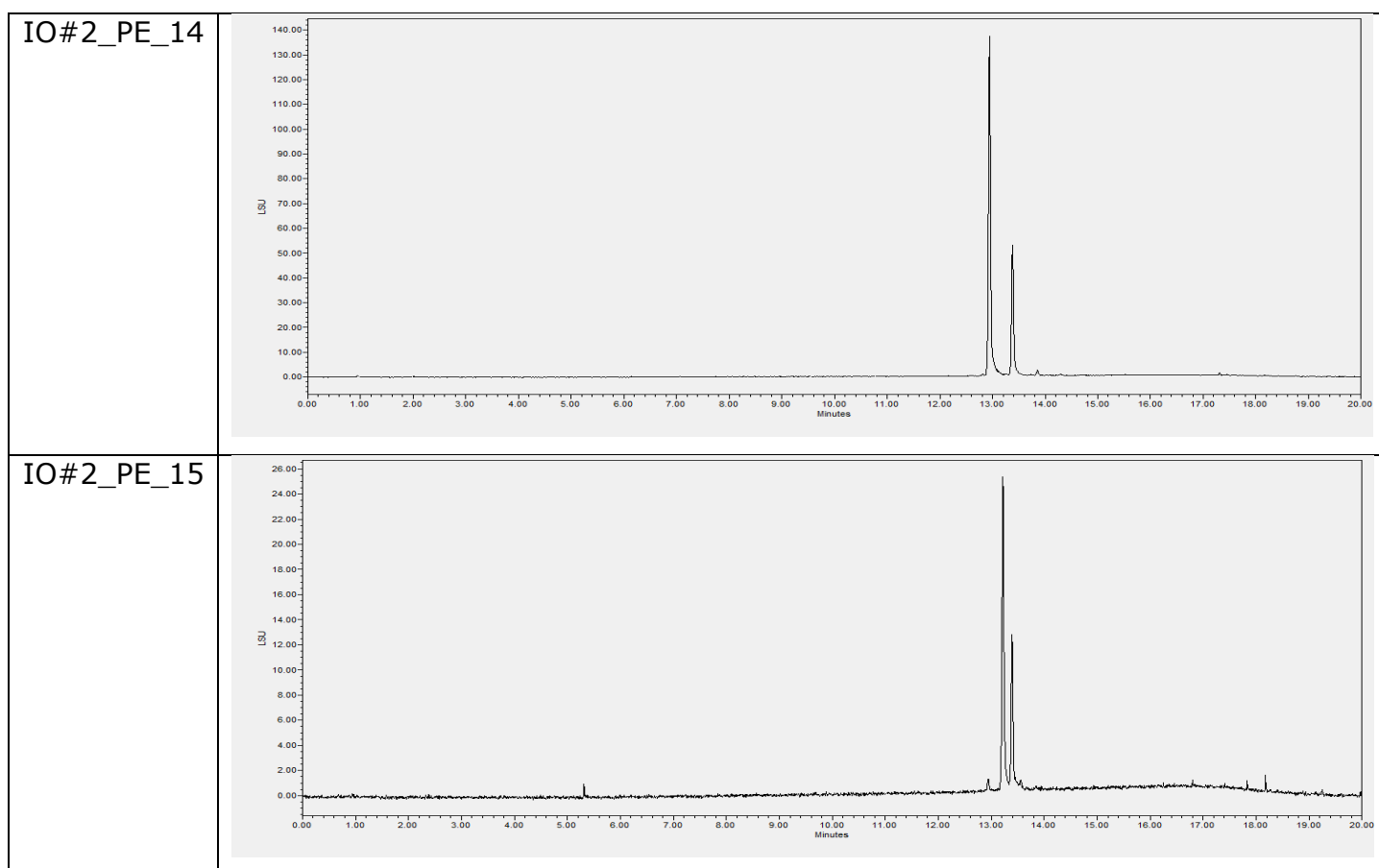


IO#2_PE_12



IO#2_PE_13

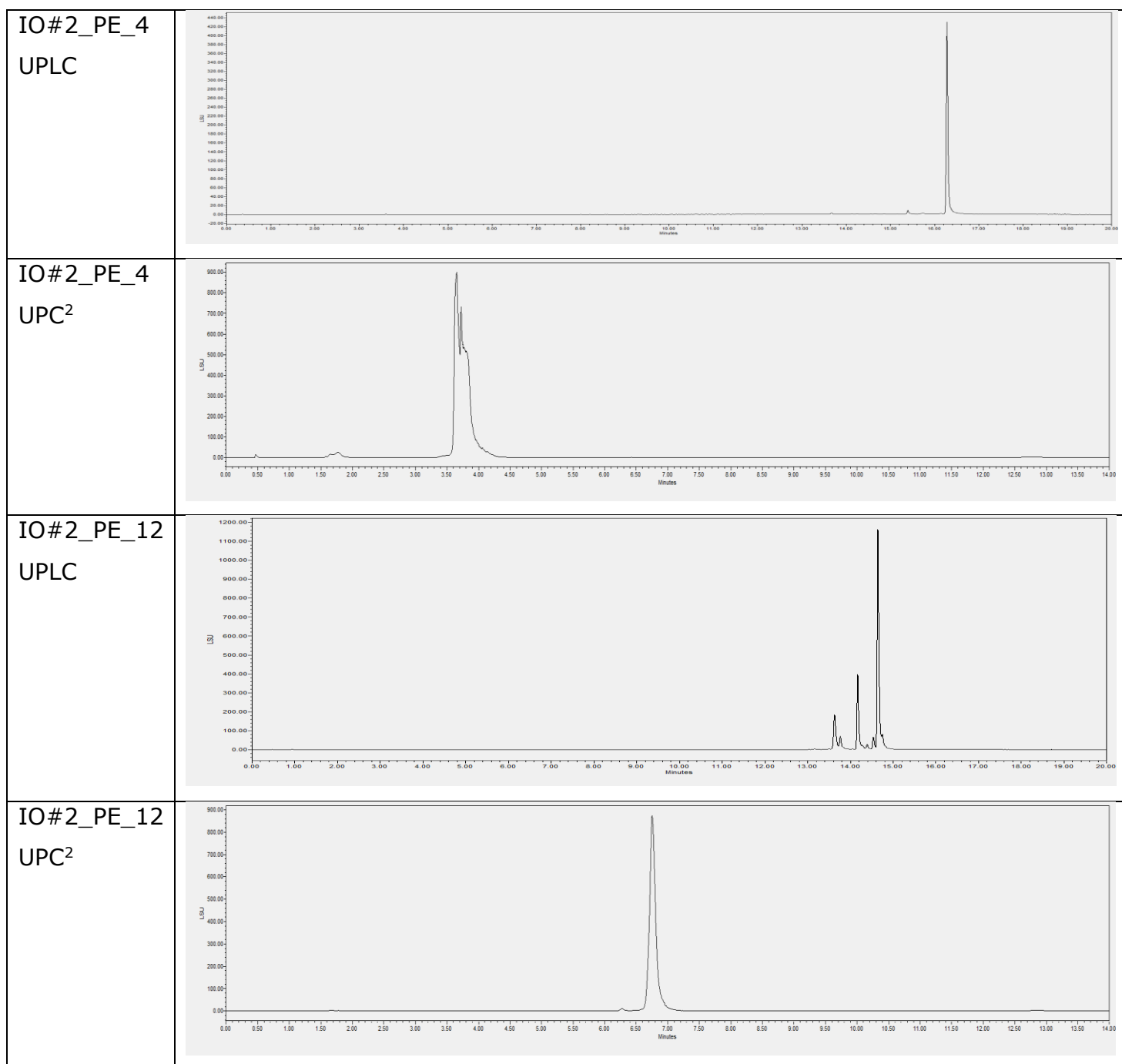




Comparing the UPLC and the UPC² chromatograms with optimized methods, it can be seen, that neither of them sufficiently separated the constituents of our fractions. Table 5 shows a comparison of the UPC² and UPLC chromatograms of sub-fractions IO#2_PE_4 and IO#2_PE_14, as an example for the different separation problems. As the chromatograms display, there is not a superior method for all sub-fractions. Sub-fractions with a single peak on the UPC² show their impurity at the UPLC and vice versa. As mentioned before, plateaus in the gradient might be an explanation for this. The plateaus result in more than one structural similar triterpene arriving at each plateau at once and cause co-elution.

A linear gradient or another co-solvent might have improved separation, although the methods were optimized already in advance. Optimizations are time-consuming and would theoretically have to be tailored to each sub fraction individually for the best separation.

Table 5: Comparison of selected ELSD chromatograms of the same sub-fractions with different chromatographic methods (UPLC and SFC).



The different peaks of the sub fractions IO#2_PE_12 and IO#2_PE_13 were tried to separate with UPLC which was only achieved for IO#2_PE_12. First, the method was optimized, and an attempt was made to unravel the peaks preparative on the UPLC. The optimized ELSD spectrum is shown together with the PDA spectrum in Figure 14. Every run was performed with 10 µl injection of IO#2_PE_12. 200 runs

were performed. The three collected peaks were measured with UPLC-ELSD for purity with the same method. Table 6 shows the results of the three isolated peaks.

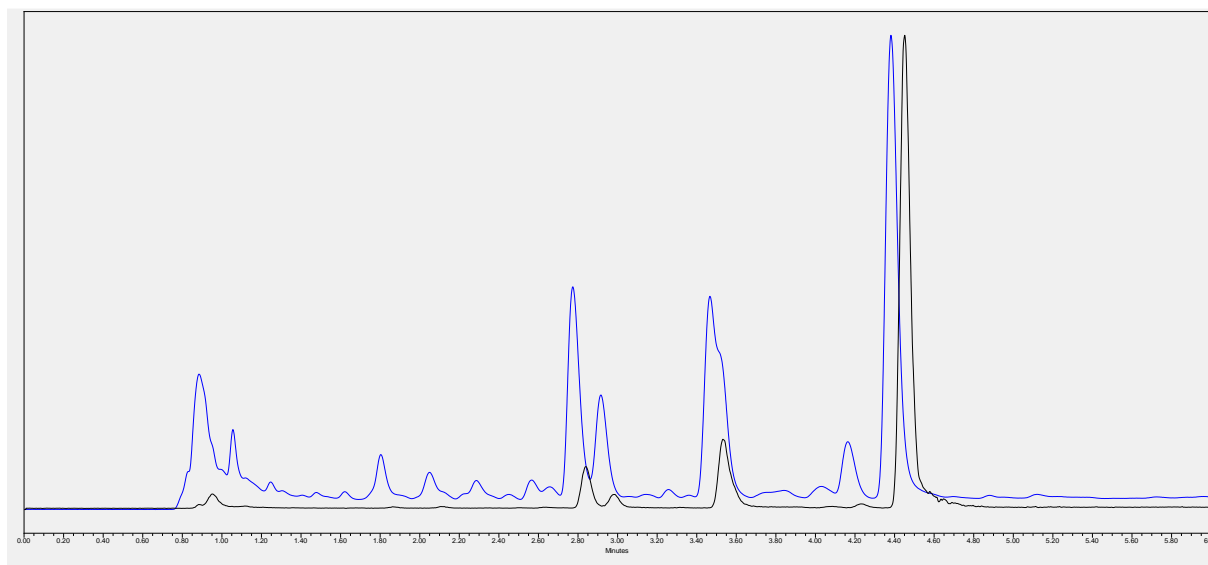


Figure 14: ELSD spectrum (black) and PDA spectrum (200nm, blue) of IO#2_PE_12. Y-axis was normalized.

The isolation cuts and the ULPC PDA-Chromatogram are shown in Figure 15.

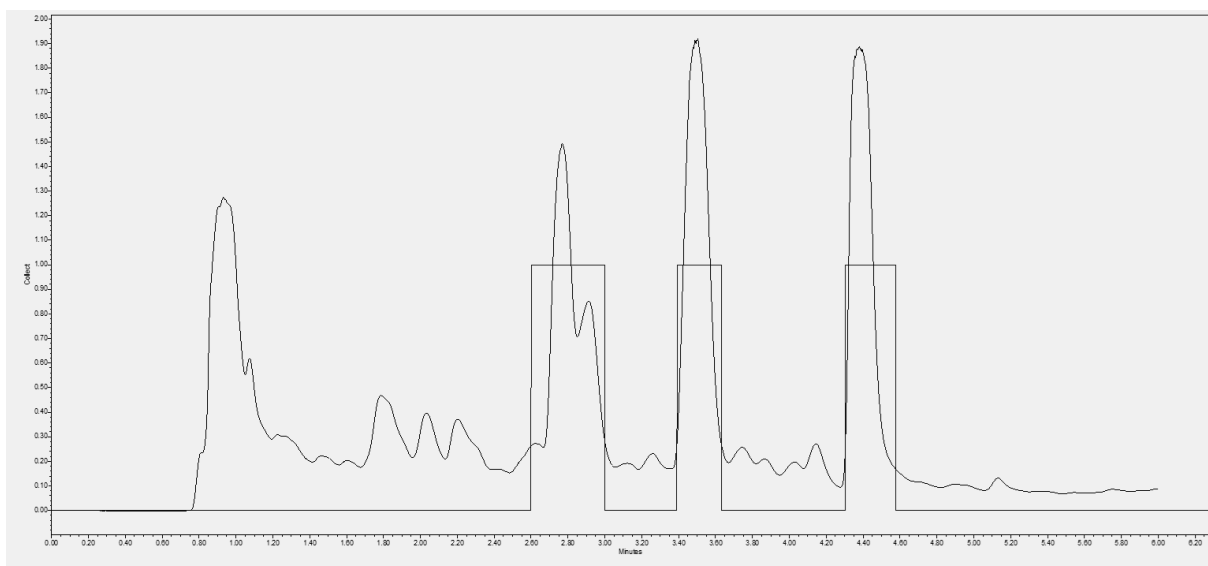
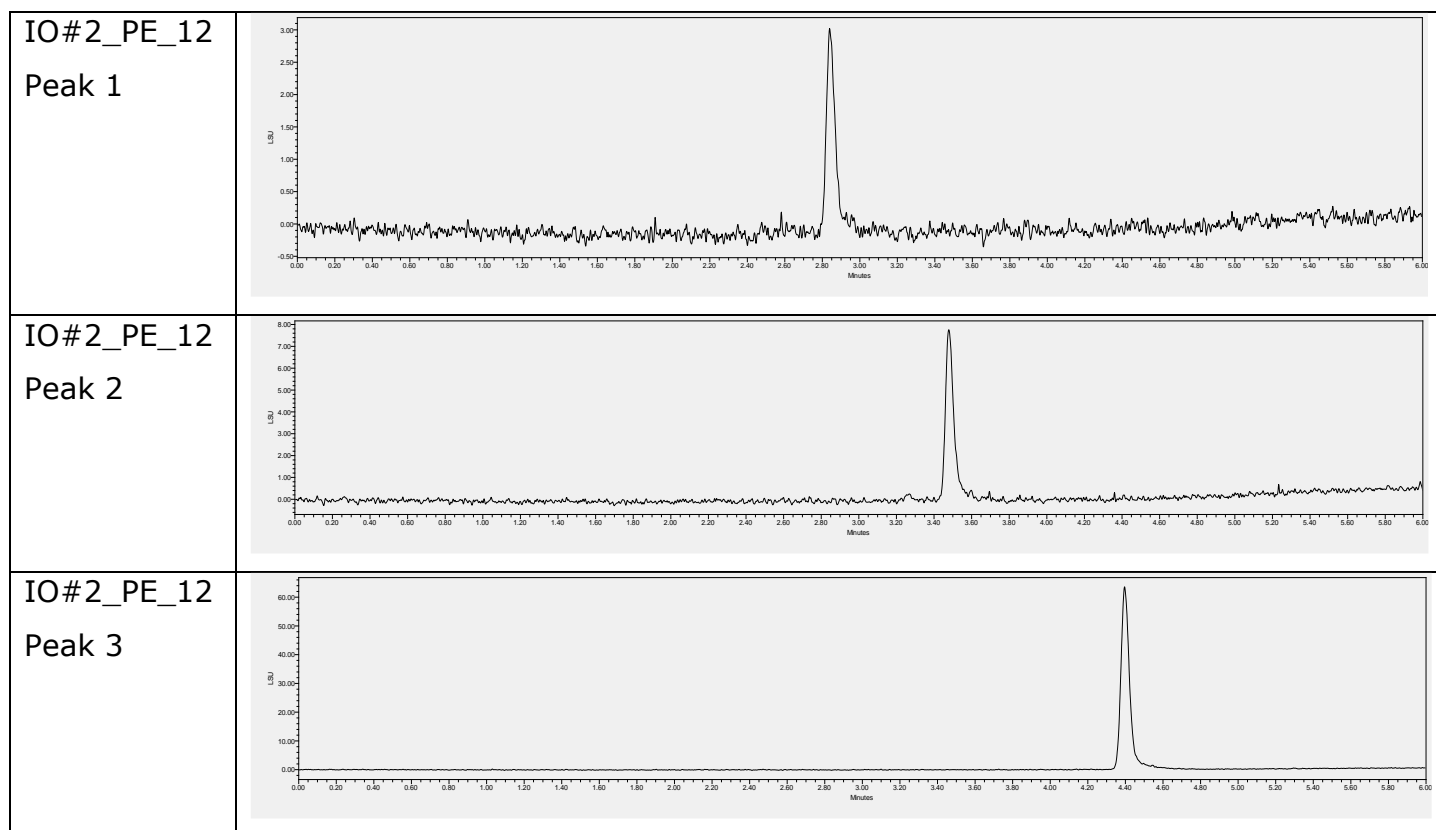


Figure 15: PDA-spectrum of IO#2_PE_12 paired with the preparative isolation cuts of the peaks.

Table 6: ELSD spectra of IO#2_PE_12 isolated Peaks.



Unfortunately, this did not work out this perfectly for all semi-pure fractions. A problem was the loss of material, due to washing processes and slight shifts with

the cuts. Another one, was the low yield of some peaks, which prevented us from analysing them further.

After all, two pure substances could be isolated through preparative SFC. Seven further compounds were isolated, three of them with gel permeation chromatography and four of them with preparative UPLC (Figure 16, Table 7).

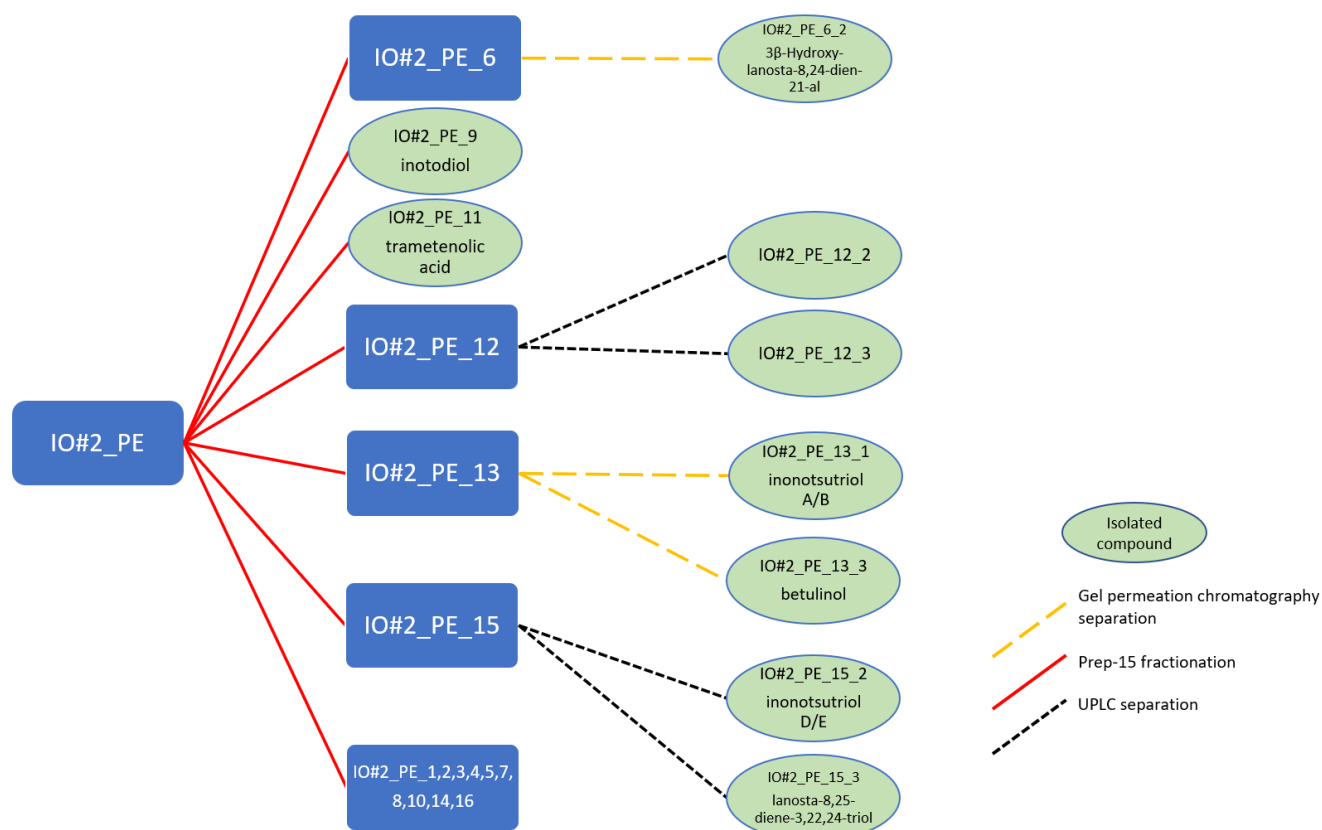
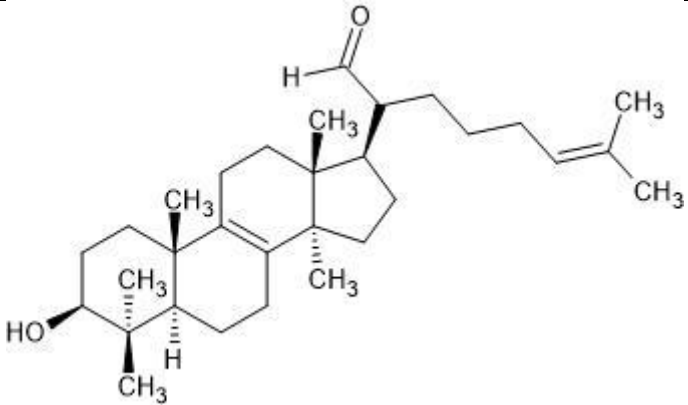
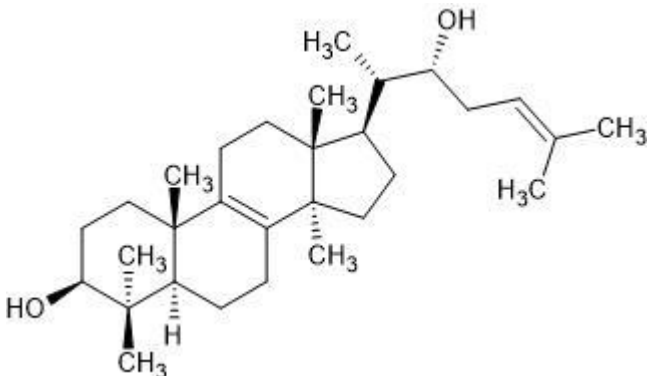
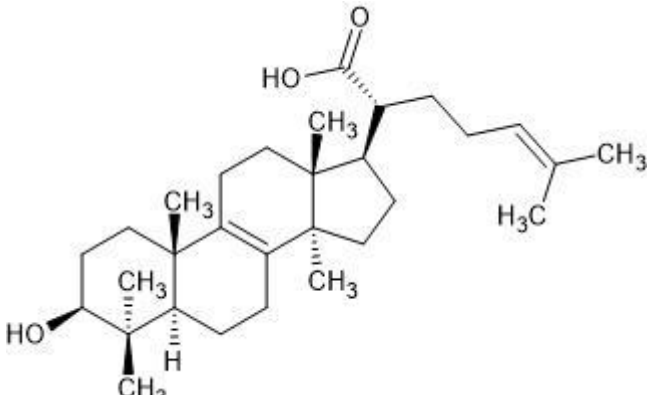
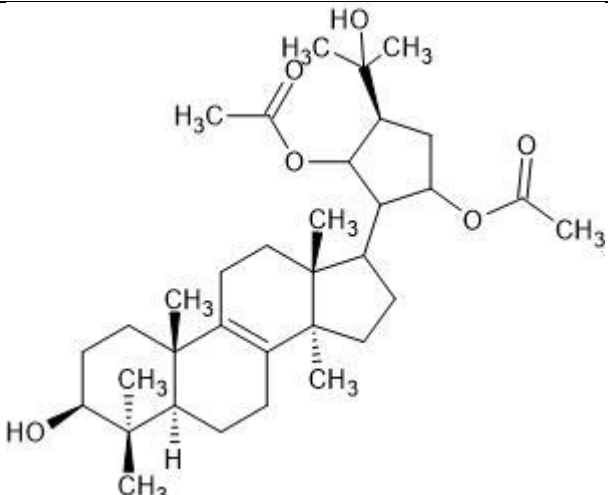


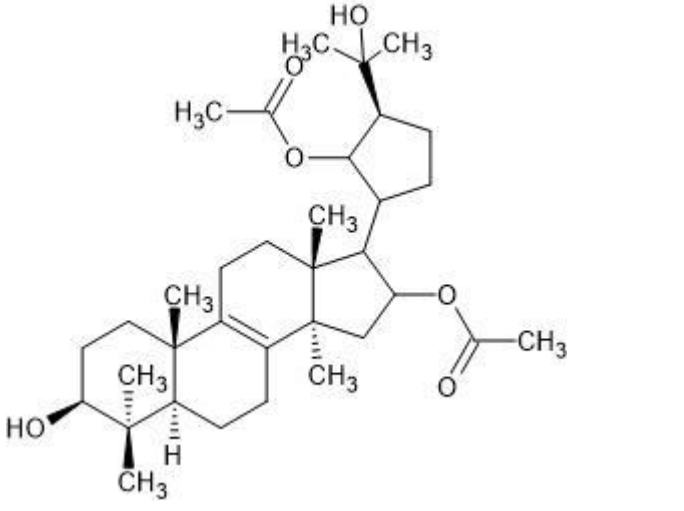
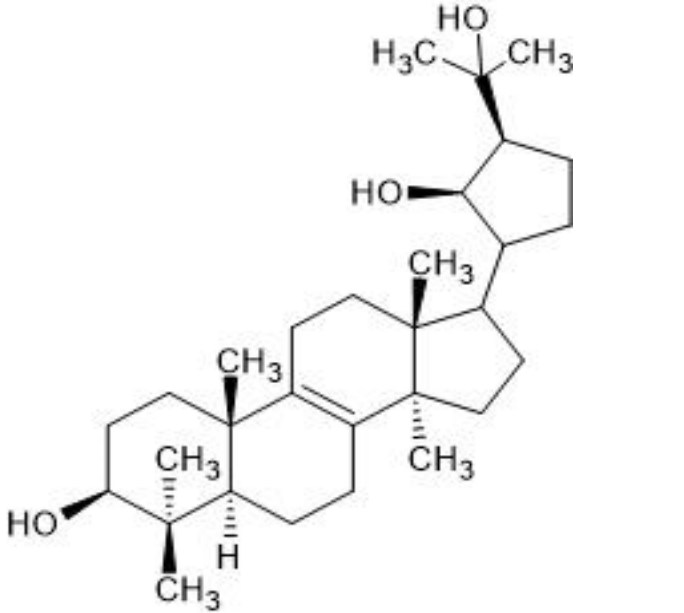
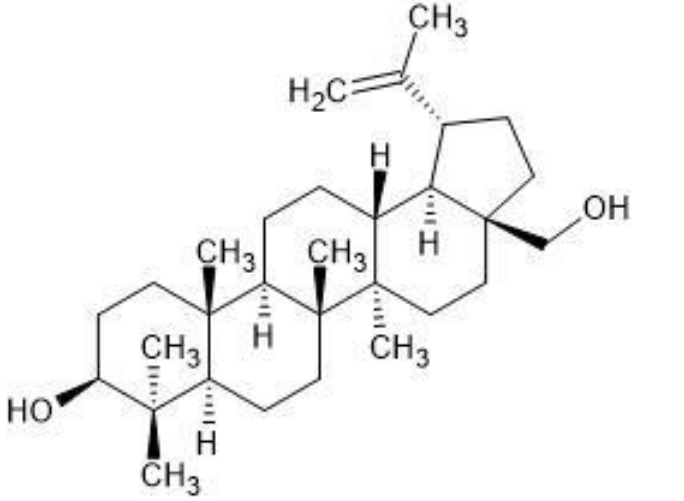
Figure 16: Fractionation tree of IO#2_PE with separation methods and isolated compounds.

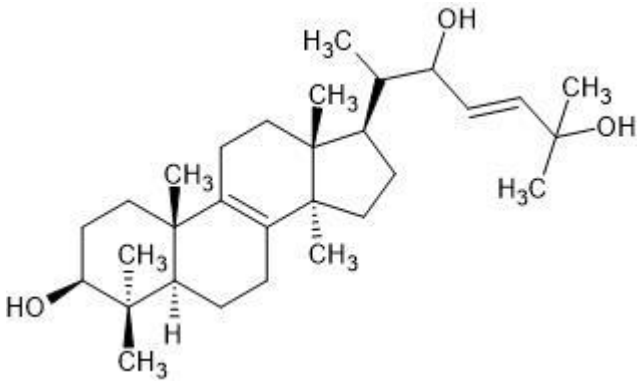
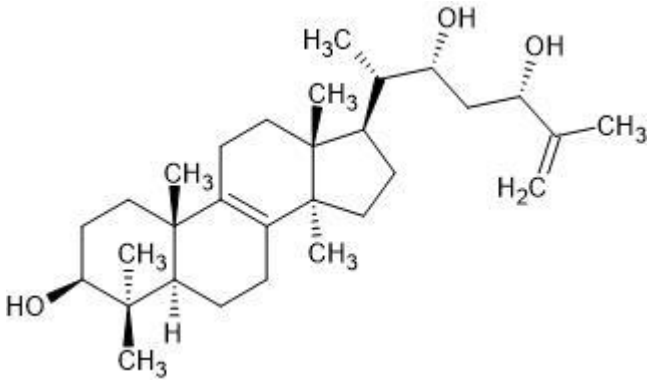
Those pure substances were:

Table 7: Isolated sub-fractions from IO#2_PE with structure and MW.

Sub-fraction	Structure	MW
IO#2_PE_6_2	3β-Hydroxy-lanosta-8,24-dien-21-al	MW: 440.7

		
IO#2_PE_9	<p>Inotodiol</p> 	MW: 442.7
IO#2_PE_11	<p>Trametenolic acid</p> 	MW: 456.7
IO#2_PE_12 Peak 2		MW: 558.80

<p>IO#2_PE_12</p> <p>Peak 3</p>		<p>MW: 558.80</p>
<p>IO#2_PE_13</p> <p>Peak 1</p>	<p>Inonotsutriol A/B</p> 	<p>MW: 458.73</p>
<p>IO#2_PE_13</p> <p>Peak 3</p>	<p>Betulinol</p> 	<p>MW: 442.72</p>

IO#2_PE_15 Peak 2	Inonotsutriol D/E 	MW: 458.73
IO#2_PE_15 Peak 3	Lanosta-8,25-diene-3,22,24-triol 	MW: 458.73

In total 9 pure isolates were identified from the IO#2_PE fraction. Most of the substances have already been described in literature, but IO#2_PE_12_2 and IO#2_PE_12_3 are putatively new compounds (Characterization performed by Dr. Ulrike Grienke). However, the position of the two acetyloxy-groups is not fully proven.

Table 8: Bioactivity data of isolated substances at different concentrations at ROR_{yt} and TGR-5 cell models. The experiment (6.4) was repeated twice, and the mean value calculated. SR2211 acted as positive control. DMSO 0.1% was the control. The significance is represented with * for $p < 0.5$, ** for $p < 0.1$ and *** for $p < 0.01$ ($n=2$).

Compound	ROR _{yt} - activity	TGR-5 - activity
DMSO 0.1% (control)	± 0 %	± 0 %
SR2211 10 µM (positive control)	- 48.59 % (± 17.4) **	not tested
IO#2_PE_6_2 30 µM	not active	not active
IO#2_PE_9 30 µM	not active	not active
IO#2_PE_11 30 µM	not active	+ 220 % ($n=1$)
IO#2_PE_12_2 30 µM	- 53.27 % (± 10.4) **	not active
IO#2_PE_12_2 10 µM	- 44.08 % (± 5.3) *	not active
IO#2_PE_12_3 30 µM	- 68 % (± 13.7) *** (cytotox.)	not active
IO#2_PE_12_3 10 µM	- 45.58 % (± 2.1) *	not active
IO#2_PE_13_1 30 µM	- 56.71 % (± 7.4) **	not active
IO#2_PE_13_1 10 µM	- 37.39 % (± 6.4) *	not active
IO#2_PE_13_3 30 µM	not active	not active
IO#2_PE_15_2 30 µM	not active	not active
IO#2_PE_15_3 30 µM	not active	not active

As shown in Table 8, three compounds show a significant inhibition of ROR_{yt} in cell models. IO#2_PE_12_2 and IO#2_PE_12_3 are putatively new molecules, which were not described in literature before. Both are diacetyloxylated inonotsutriols with a high inhibition on ROR_{yt}. IO#_PE_13_1 is Inonotsutriol A/B, which also significantly inhibits ROR_{yt}. IO#2_PE_11, identified as trametenolic acid, is the only compound of this fraction showing an activity at the TGR-5. All of those molecules, especially the stereochemistry at the fifth ring and the exact position of the acetyloxy groups of the IO#2_PE_12 fractions, should be further investigated. It might be interesting to know if those fractions have synergistic effects on each other.

4.4 Analysis of IO#4-7_DCM

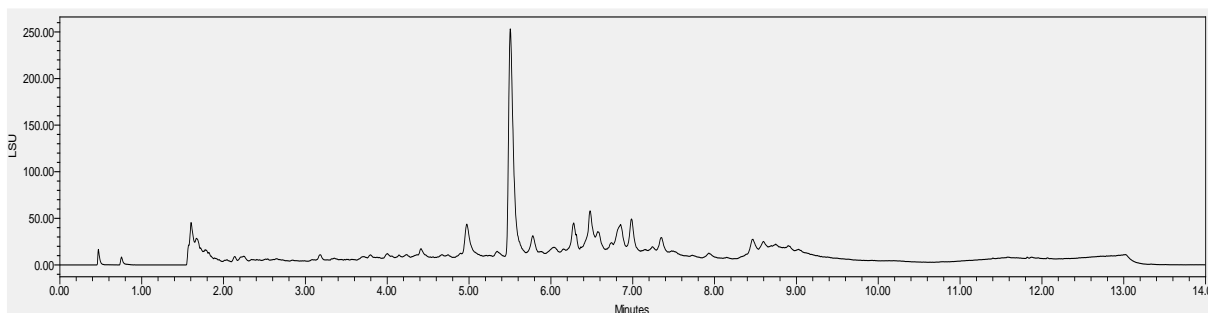


Figure 17: IO#4-7_DCM SFC chromatogram (ELSD detection, Waters UPC², Torus 1-AA column, 40°C, co-solvent B = Methanol, 14 minute method (Table 20))

The fraction IO#4-7_DCM which activated the TGR-5 (4.2) receptor, was selected for mycochemical investigation next. The UPC² chromatogram suggested that IO#4-7_DCM consisted mainly of one constituent, appearing as a major peak at retention time (R_t) = 5.49 min. MS and PDA spectra (Figure 19) suggested a small aromatic compound with a MW under 200. The UPC²-QDa measurement showed, that the whole fraction included substances with a big difference in molecular weight. The fractionation method of choice was therefore sephadex LH-20 column chromatography (5.1.2). Approximately 157 mg of the extract were dissolved in 2 ml of the mobile phase DCM:Acetone (85:15) and applied to a Sephadex column (1000 x 1.5 mm). 140 tubes of 3 ml were collected and monitored via TLC (Figure 18). Based on the TLC fingerprints, the tubes were combined to 19 sub-fractions (IO#4-7_DCM_1 – IO#4-7_DCM_19) whereby 19 was the dried wash solvent and the yield was determined. 53.5 mg could not be recovered.

The 19 sub-fractions were analyzed with TLC (5.1.1). 25 µg of each fraction were applied (Figure 18).

For analysis of composition, all sub-fractions were measured with the UPC² (5.1.3) equipped with PDA-ELSD first, and then the molecular weights were determined using PDA-QDa detection. The ELSD chromatograms of the sub-fractions are shown in Table 9: ELSD Spectra of IO#4-7_DCM fractionsTable 9.

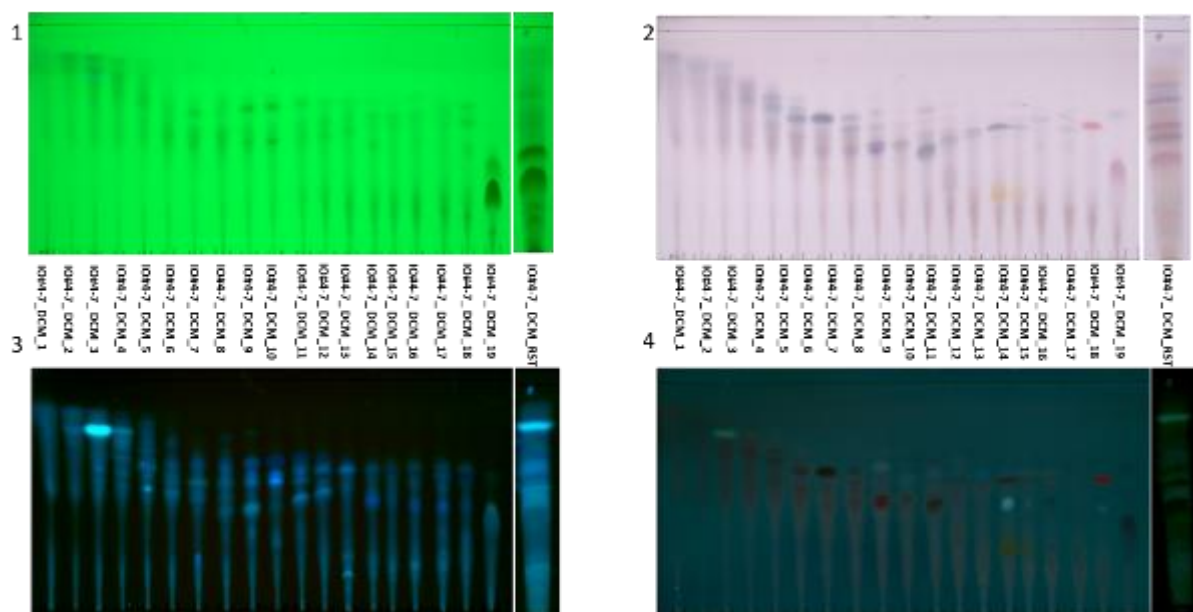
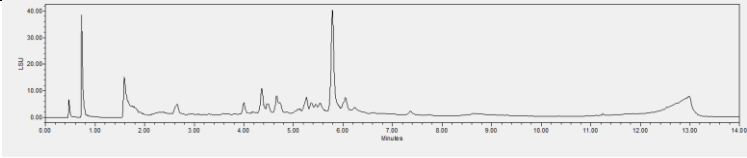
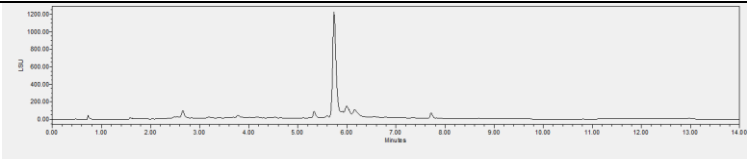
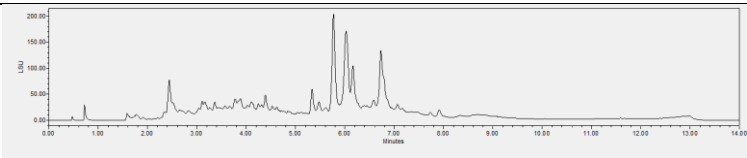
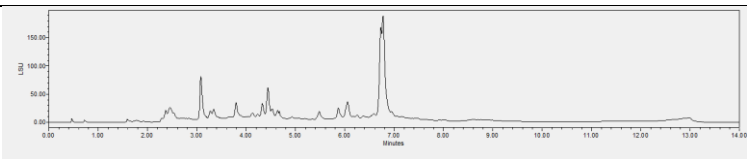
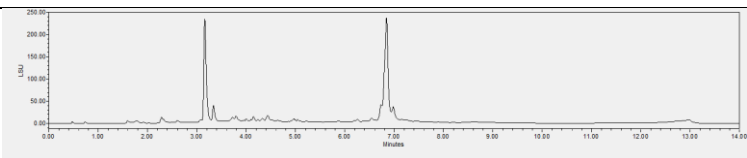
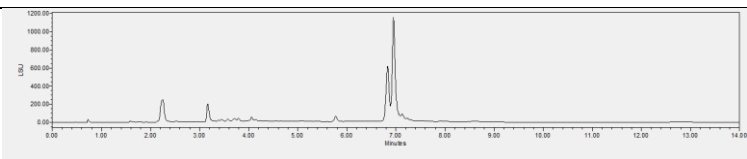
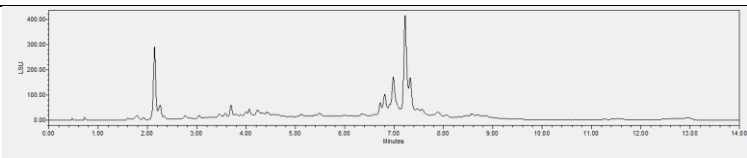
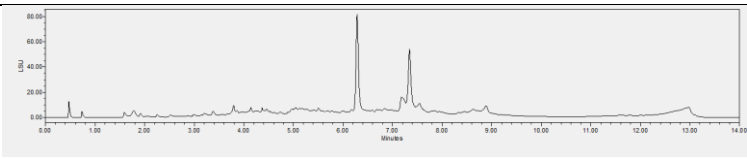
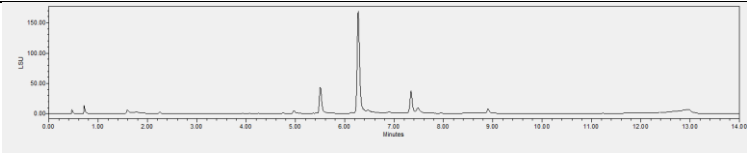
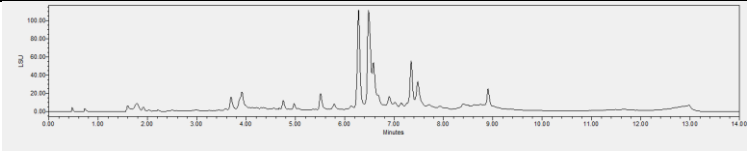
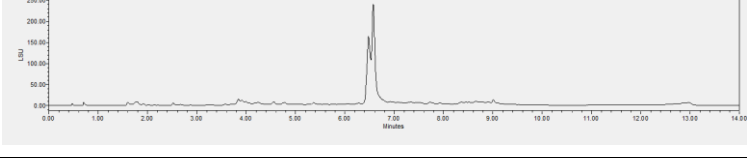


Figure 18: TLC (5.1.1) of IO#4-7_DCM fractions, **1**:254 nm before derivatization with Vanillin/sulphuric acid, **2**: Vis after derivatization, **3**: 366nm before derivatization, **4**: 366 nm after derivatization.

Table 9: ELSD Spectra of IO#4-7_DCM fractions

Name	ELSD - chromatograms	Mass ⁺ [m/z]	Predicted Substance	Yield [mg]
IO#4-7_DCM_1		n.d.		6.84
IO#4-7_DCM_2		n.d.		4.2
IO#4-7_DCM_3		n.d.		5.07
IO#4-7_DCM_4		n.d.		1.59
IO#4-7_DCM_5		n.d.		6.96

IO#4- 7_DCM_6		n.d.		6.18
IO#4- 7_DCM_7		n.d.		2.8
IO#4- 7_DCM_8		n.d.		3.9
IO#4- 7_DCM_9		n.d.		3.88
IO#4- 7_DCM_10		n.d.		2.95
IO#4- 7_DCM_11		n.d.		6.15
IO#4- 7_DCM_12		n.d.		4.58
IO#4- 7_DCM_13		n.d.		6.31
IO#4- 7_DCM_14		n.d.		4.36
IO#4- 7_DCM_15		n.d.		1.48
IO#4- 7_DCM_16		n.d.		3.54

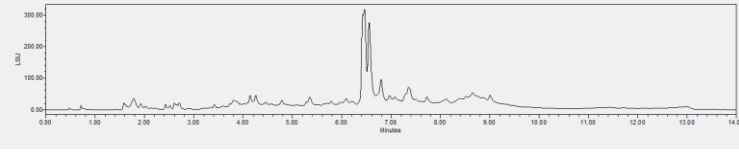
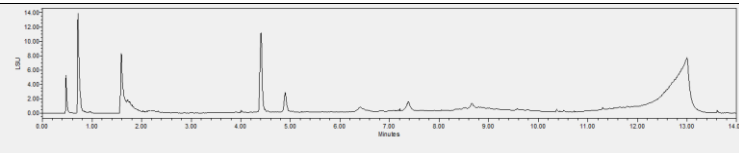
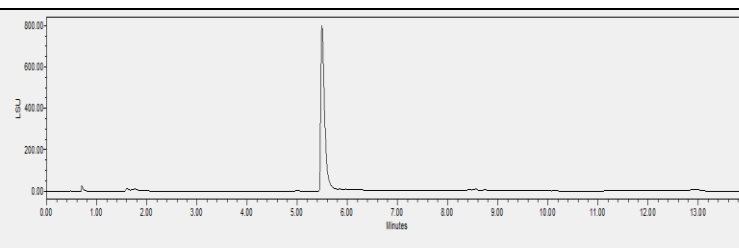
IO#4-7_DCM_17		n.d.		2.56
IO#4-7_DCM_18		n.d.		4.49
IO#4-7_DCM_19		[M+H]⁺ = 179.16 [M-H]⁻ = 177.19 [M+Na]⁺ = 221.2 [M]⁻ = 182.0	Osmund-acetone [MW= 178.18] Syringic-acid [MW= 198.2]	14.67

Table 10: collected tubes and yields of IO#4-7_DCM sub-fractions

Fraction	collected tubes	yield [mg]
IO#4-7_DCM_RST	-	11.03
IO#4-7_DCM_1	15-18	6.84
IO#4-7_DCM_2	19-20	4.2
IO#4-7_DCM_3	21-23	5.07
IO#4-7_DCM_4	24	1.59
IO#4-7_DCM_5	25-28	6.96
IO#4-7_DCM_6	29-32	6.18
IO#4-7_DCM_7	33-34	2.8
IO#4-7_DCM_8	35-38	3.9
IO#4-7_DCM_9	39-42	3.88
IO#4-7_DCM_10	43-45	2.95
IO#4-7_DCM_11	46-52	6.15
IO#4-7_DCM_12	53-60	4.58
IO#4-7_DCM_13	61-75	6.31
IO#4-7_DCM_14	76-84	4.36
IO#4-7_DCM_15	85-88	1.48
IO#4-7_DCM_16	89-100	3.54
IO#4-7_DCM_17	101-110	2.56
IO#4-7_DCM_18	111-128	4.49
IO#4-7_DCM_19	129-140	14.67
total		103.54

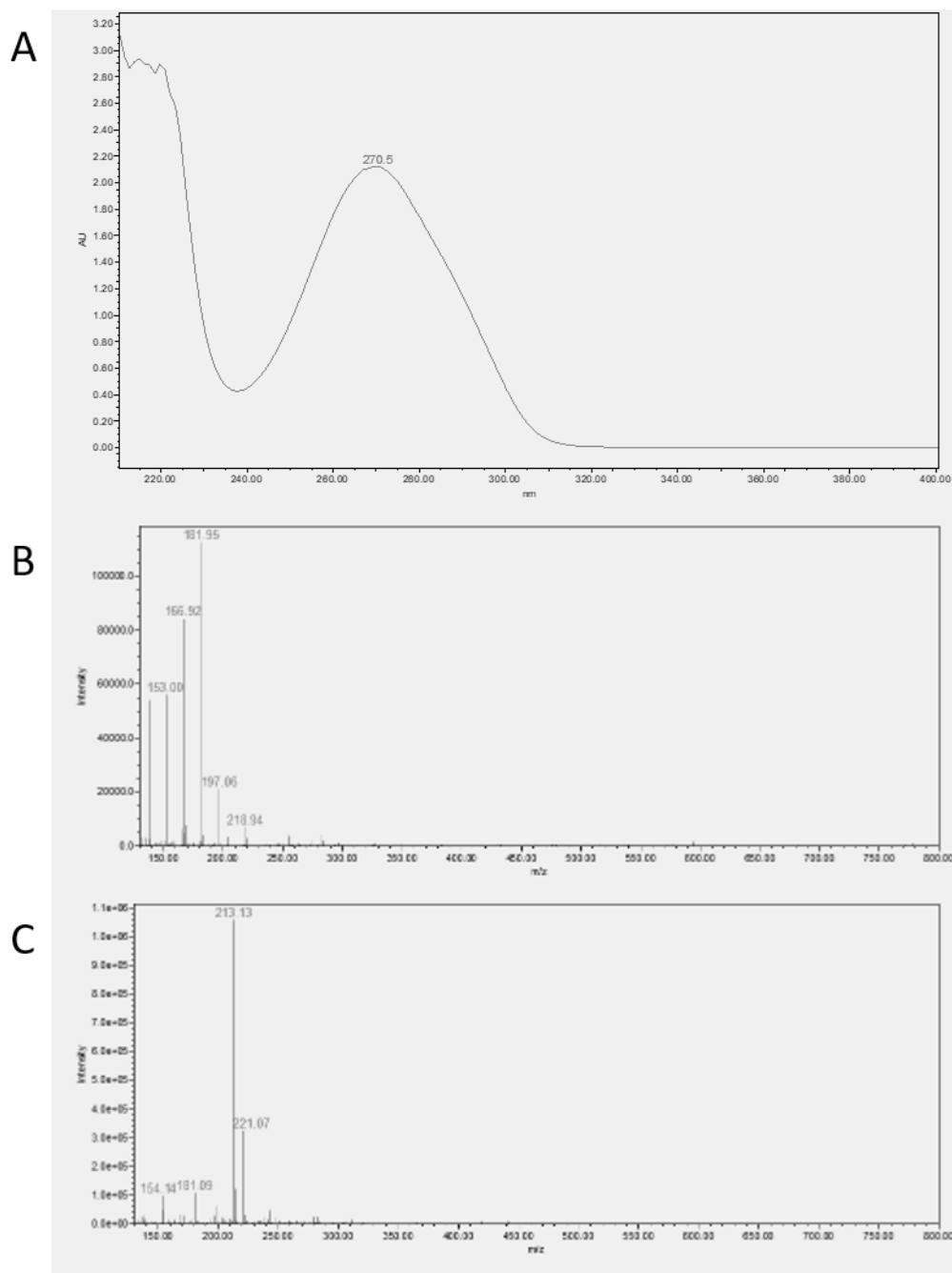


Figure 19: **A** PDA spectrum of main constituent of IO#4-7_DCM, **B** $[m/z]^+$ MS of main constituent of IO#4-7_DCM **C** $[m/z]^-$ MS of main constituent of IO#4-7_DCM

IO#4-7_DCM_19 was the dried fraction and seemed like a putatively pure substance in the UPC²-ELSD spectrum. It could also be determined as the main compound of the fraction. Because of the late elution time, it had to be a small molecule.

The TLC showed two bands (R_f 0.28 and R_f 0.38) with 254 absorption. After derivatization with vanillin/sulphuric acid, the band at R_f 0.38 was of red-violet colour, whereas the second band at R_f 0.28 was invisible. The m/z values typical

for osmundacetone $[M+H]^+ = 179$ were found in the QDa – measurement. A reference TLC with osmundacetone (98% abcr, Germany) was then performed, to confirm the presence of osmundacetone in the sub-fraction. Finally, to prove that osmundacetone is the main constituent, the sub fraction was measured with NMR (Figure 20). In the ^1H -NMR, the osmundacetone shifts were clearly recognisable, but other signals had a higher intensity. The two singlet signals, which appeared in a ratio of 6:2, with the 6 protons in the region of the O-methyl groups, and the 2 signals in the region of the substituted aromatics, were much stronger. By elucidating the NMR spectrum in more detail, another substance was found: syringic acid (Figure 21). By integration of ^1H NMR shifts, a ratio of 20:1 for syringic acid: osmundacetone was determined.

Osmundacetone and syringic acid were measured again at the UPC² with the BEH Phenyl column (instead of BEH C18), to get a better separation, and in different variations to confirm the ratio of 20:1, syringic acid:osmundacetone.

Table 12 shows that IO#4-7_DCM_19 consists of both, osmundacetone and syringic-acid in a 20:1 ratio.

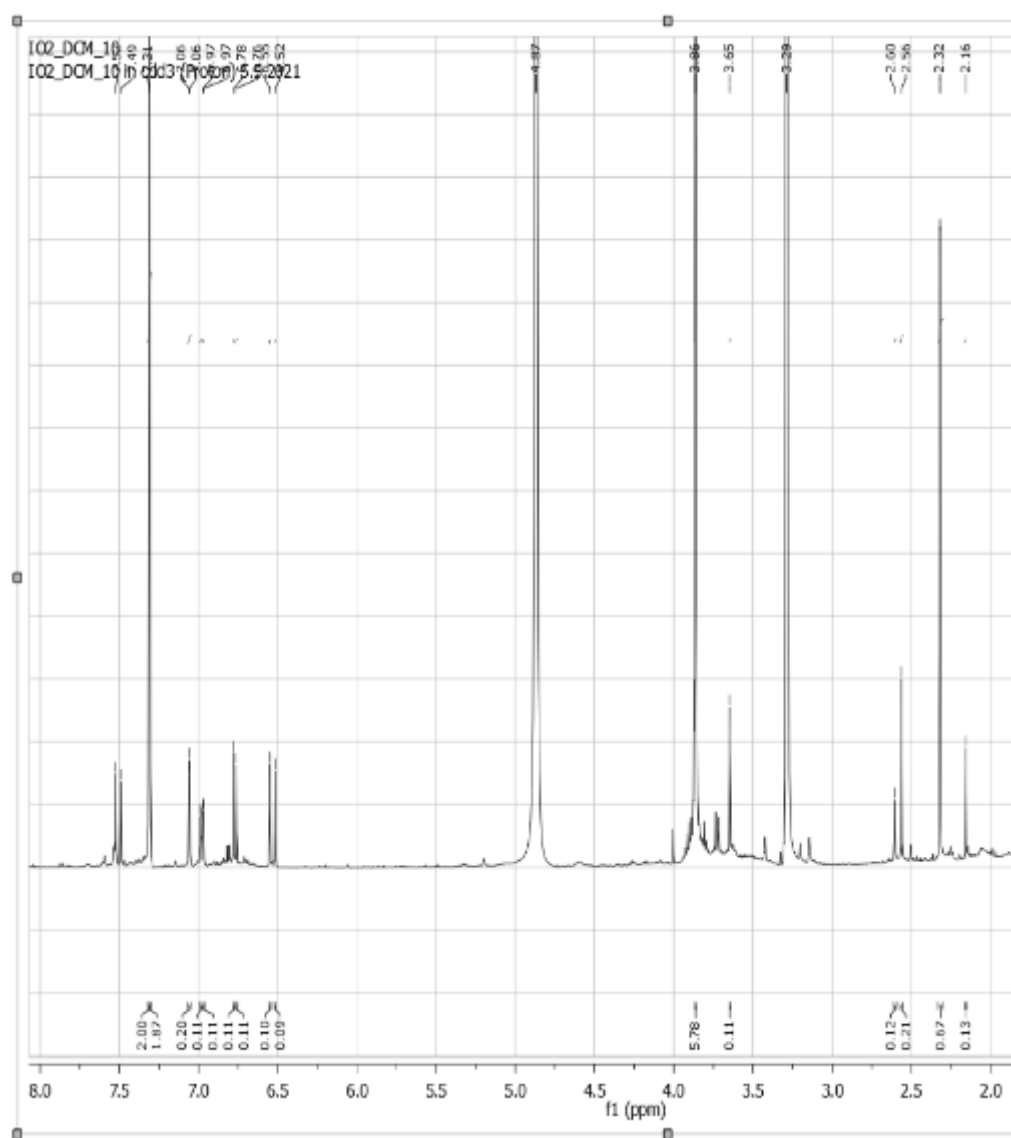


Figure 20: ^1H -NMR spectrum of IO#4-7_DCM_19 in MeOD

Table 11: ^1H and ^{13}C -NMR spectral data for syringic acid

Carbon no.	δ_{C}	δ_{H}
1	124.54	
2	110.78	7.31
3	151.41	
4	144.54	
5	151.41	
6	110.78	7.31
7	172.52	
8	59.27	3.86
9	59.27	3.86

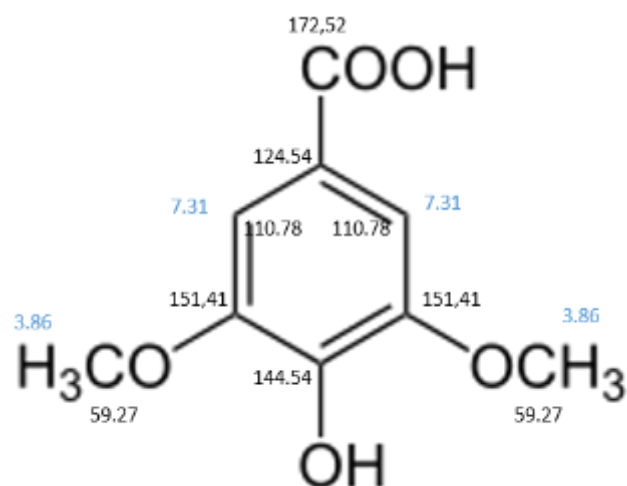


Figure 21: Structure of syringic acid and the assigned NMR shifts.

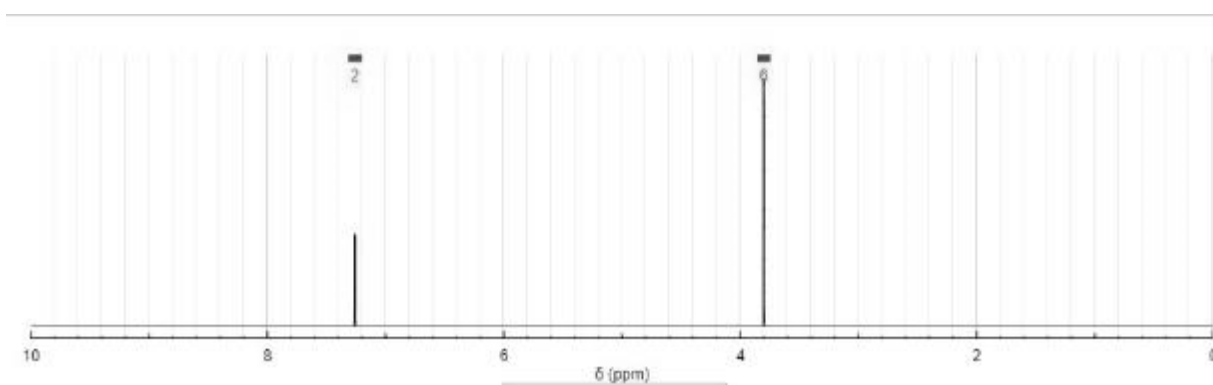


Figure 22: Predicted ^1H -NMR spectrum for syringic acid at nmrd.b.org

Table 12: ELSD chromatogram of IO#4-7_DCM_19, osmundacetone, syringic acid and their mixtures in the ratio of 1:1 and 1:20

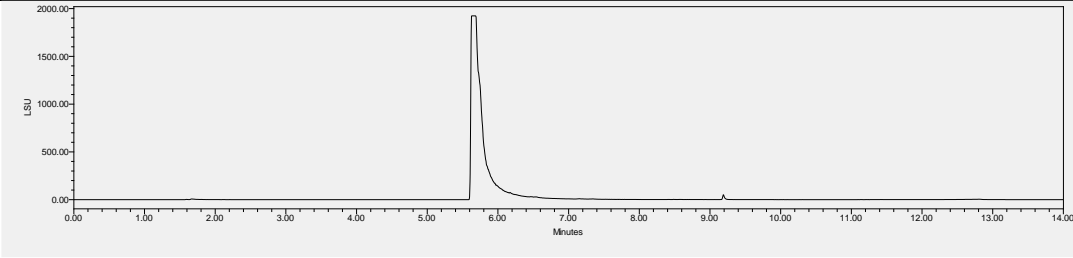
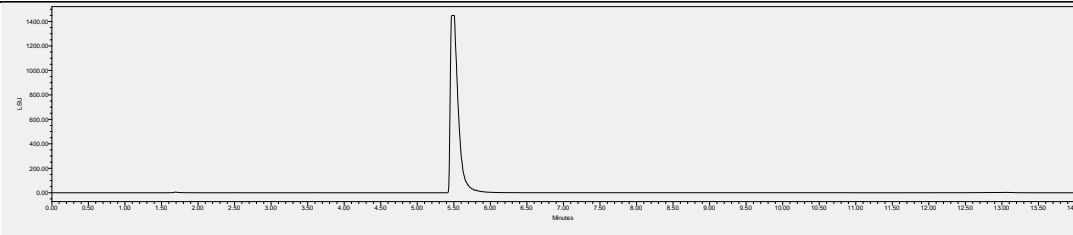
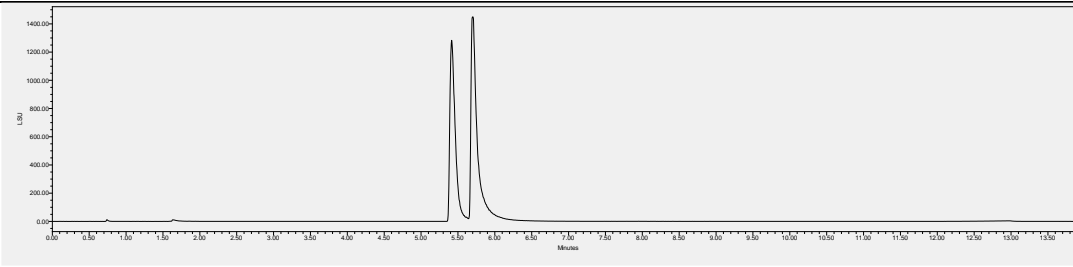
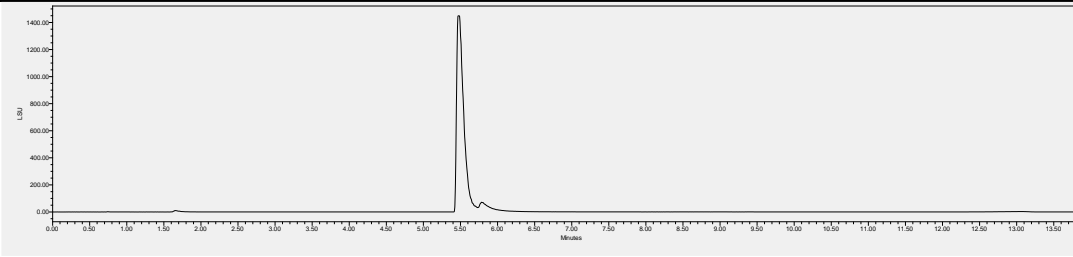
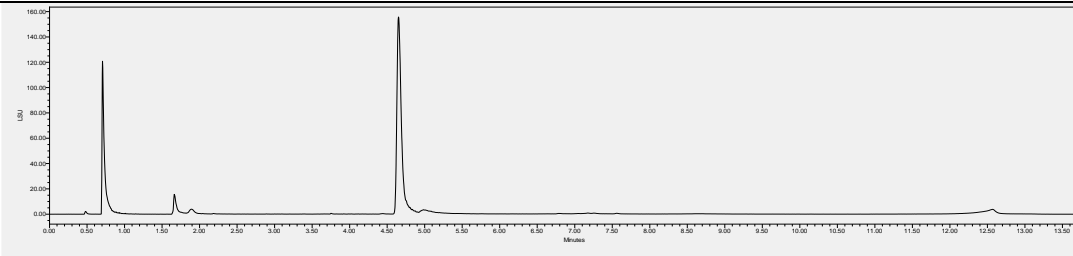
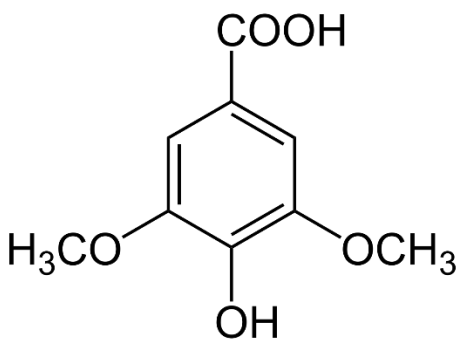
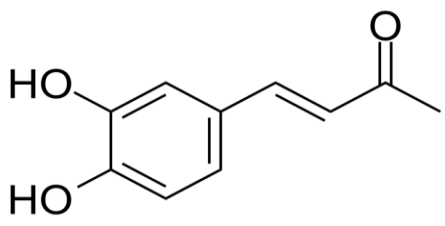
Osmundacetone	 <p>The chromatogram for Osmundacetone displays a single, prominent, sharp peak at approximately 5.5 minutes. The y-axis represents intensity in LSI units, ranging from 0.00 to 2000.00. The x-axis represents time in minutes, ranging from 0.00 to 14.00. A very small, barely visible peak is present at approximately 9.2 minutes.</p>
Syringic acid	 <p>The chromatogram for Syringic acid shows a single, sharp peak at approximately 5.5 minutes. The y-axis (LSI) ranges from 0.00 to 1400.00. The x-axis (Minutes) ranges from 0.00 to 14.00.</p>
Syringic acid: Osmundacetone 1:1	 <p>The chromatogram for the 1:1 mixture of Syringic acid and Osmundacetone shows two distinct, sharp peaks. The first peak is at approximately 5.2 minutes and the second, slightly taller peak is at approximately 5.5 minutes. The y-axis (LSI) ranges from 0.00 to 1400.00. The x-axis (Minutes) ranges from 0.00 to 14.00.</p>
Syringic acid: Osmundacetone 20:1	 <p>The chromatogram for the 20:1 mixture of Syringic acid and Osmundacetone shows a single, sharp peak at approximately 5.5 minutes, similar to the pure components. The y-axis (LSI) ranges from 0.00 to 1400.00. The x-axis (Minutes) ranges from 0.00 to 14.00.</p>
IO#4-7_DCM_19 The shift of one minute is due to the change of the column.	 <p>The chromatogram for IO#4-7_DCM_19 shows a complex profile with several peaks. A major peak is at approximately 5.5 minutes. Another significant peak is at approximately 0.8 minutes. There are also smaller peaks at approximately 1.8 and 12.5 minutes. The y-axis (LSI) ranges from 0.00 to 160.00. The x-axis (Minutes) ranges from 0.00 to 14.00.</p>

Table 13: Identified constituent of IO#4-7_DCM

Identified compound	Molecular weight
<p>Syringic acid</p> 	198.18
<p>Osmundacetone</p> 	178.18

Two constituents (Table 13), including the main compound, of the IO#4-7_DCM fraction could be determined. All fractions, including the identified compounds were tested for bioactivity at the TGR-5.

Table 14: Bioactivity data of isolated substances at TGR-5 cell model. The experiment (6.4) was repeated three times with three replicates (n=3), and the mean value was calculated. Forskolin 10 μ M and LCA 10 μ M acted as positive control. DMSO 0.1 % was the control.

Compound/Sub-fraction	TGR-5 activity	ROR _{yt} activity
DMSO 0.1%	\pm 0 %	\pm 0 %
Forskolin 10 μ M	+ 74.52 %	not tested
LCA 10 μ M	+ 74.10 %	not tested
Syringic acid	not active	not tested
Osmundacetone	not active	- 29.9 % _(n=1)
IO#4-7_DCM_15 30 μ M	+ 32.44 %	not tested
IO#4-7_DCM_16 30 μ M	+ 16.52 %	not tested

The activity measurements show, that both compounds were inactive at the TGR-5 (Table 14). However, sub-fractions IO#4-7_DCM_15 and IO#4-7_DCM_16 showed an activity at TGR-5 and osmundacetone showed an activity at the ROR_{vt}. A further separation and isolation of the compounds from the sub-fractions would be a good starting point for further research.

4.5 Analysis of IO#3_DCM

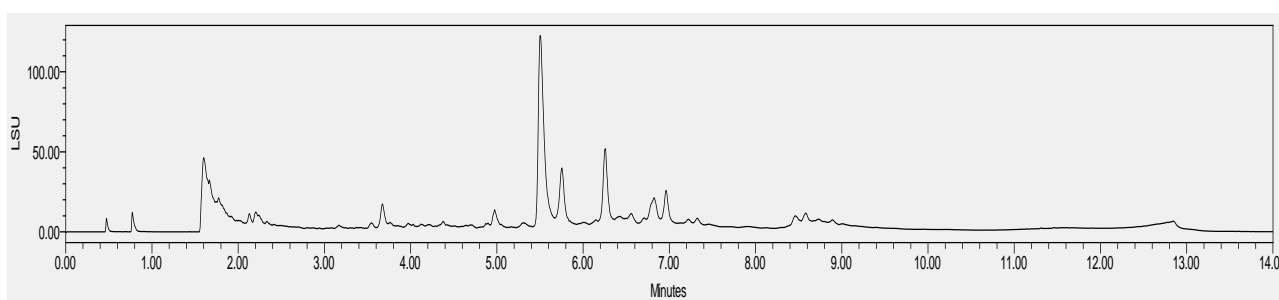


Figure 23: IO#3_DCM SFC chromatogram (ELSD detection, Waters UPC², Torus 1-AA column, 40°C, co-solvent B = Methanol, 14 minute method (Table 20))

The third bioactive fraction, IO#3_DCM, showed a lot of similarities to IO#4-7_DCM. As shown in 4.2, the bioactivity at the TGR-5 was lower but still significant. One main compound, with the same retention time as syringic-acid in IO#4-7_DCM was determined in the UPC² - ELSD spectrum. In relation to the other compounds, the concentration of the main compound was lower compared to IO#4-7_DCM.

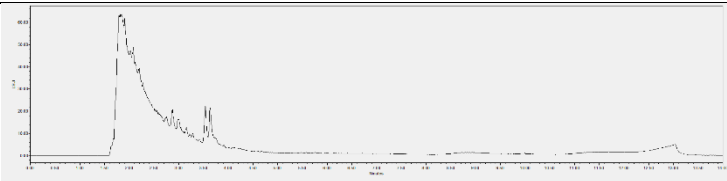
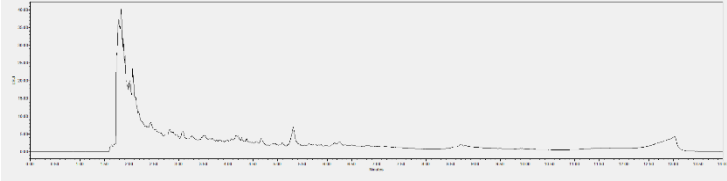
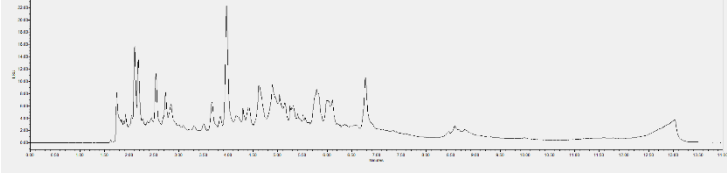
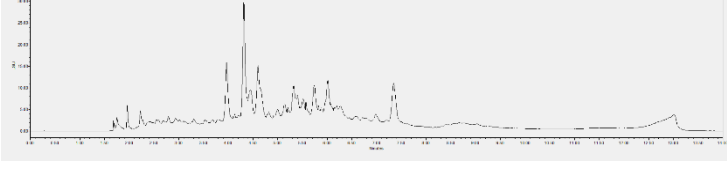
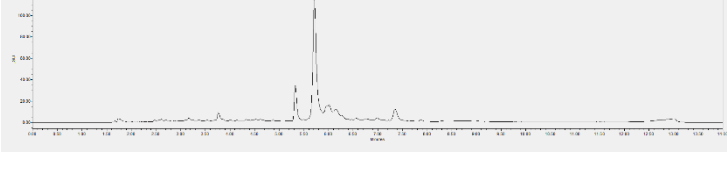
Because of the molecular weight differences measured by the UPC²-QDa detector, a separation with a Sephadex LH-20 column was performed.

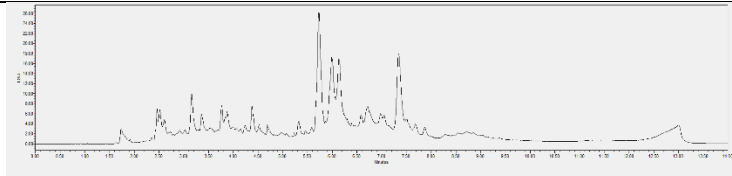
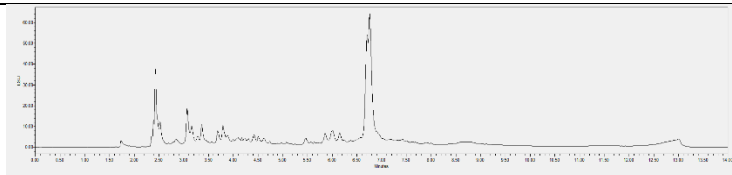
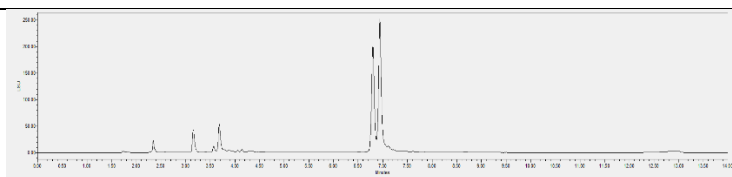
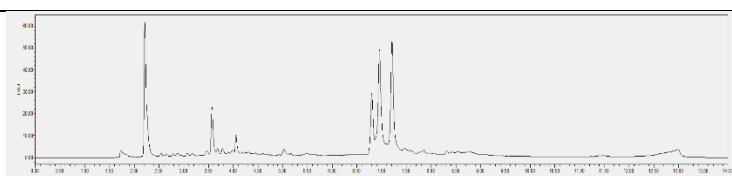
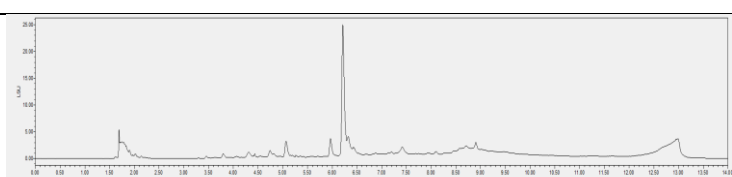
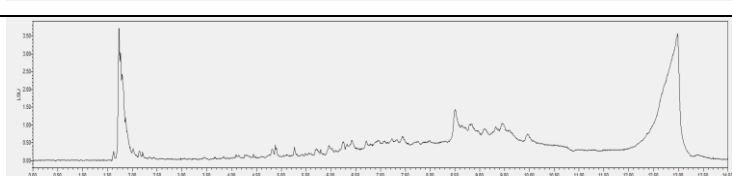
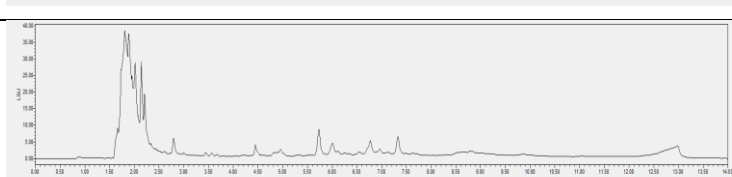
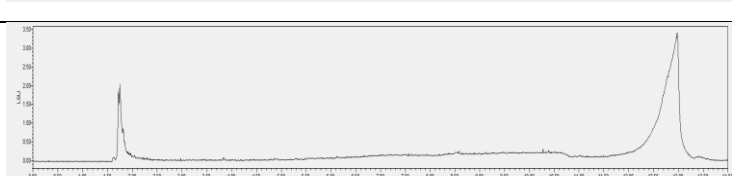
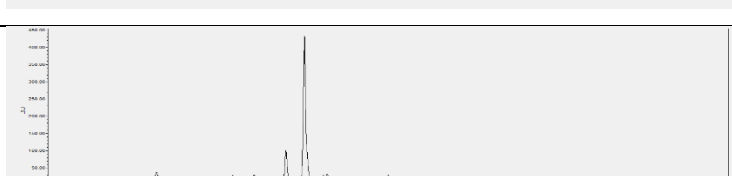
Approximately 250 mg of the extract were dissolved in 2 ml of the mobile phase DCM:acetone (85:15) and applied to a Sephadex column (500 x 40 mm). 70 tubes of 3 ml were collected and monitored via TLC. Based on their TLC fingerprints, the tubes were combined into 13 sub-fractions (IO#3_DCM_1 – IO#3_DCM_13) and the yield was determined. 72.74 mg could not be recovered. As the Sephadex material was coloured yellow-orange after the run and could not be cleaned with different solvents, it was assumed that the lost material were polymerized pigments (i.e. melanin).

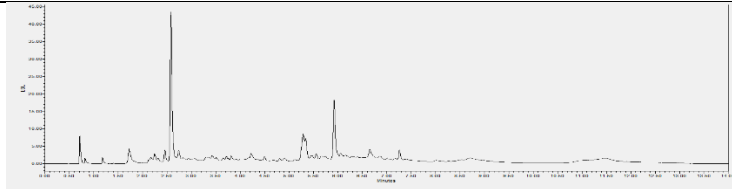
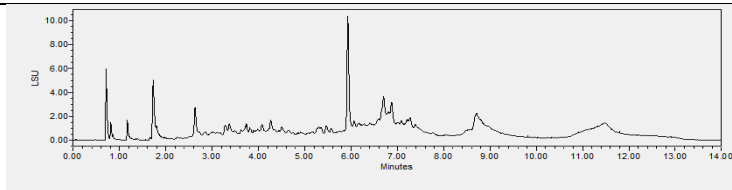
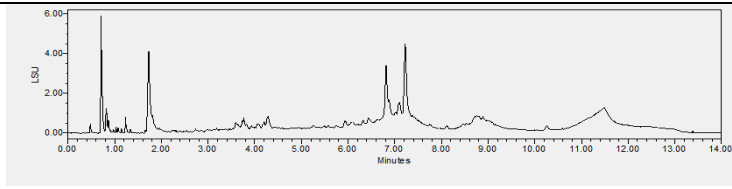
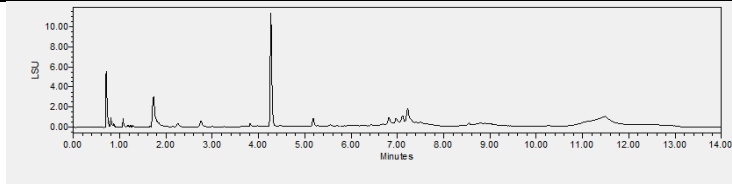
The fractionation was repeated a second time with approximately 90 mg of material dissolved in 1 ml DCM:acetone (85:15). Hereby, minor changes were made: The amount of collected tubes was increased to 100 with less volume collected per tube (2 ml). Nine sub-fractions were created (IO#3.2_DCM_1-9) of which four were merged with the sub-fractions of the first run. IO#3.2_DCM_1 and IO#3.2_DCM_2 were merged with IO#3_DCM_1, IO#3.2_DCM_3 was merged with IO#3_DCM_4 and IO#3.2_DCM_4 was merged with IO#3_DCM_5. Five new sub-fractions were created during the second fractionation (IO#3_DCM_I – IO#3_DCM_V).

The TLC of both fractionations before merging is shown in Figure 24. The SFC ELSD - chromatograms of the merged sub-fractions are shown in Table 15.

Table 15: ELSD chromatograms of IO#3_DCM sub fractions, mass, predicted Substance and yield

Name	ELSD - chromatograms	Mass ⁺ [m/z]	Predicted Substance	Yield [mg]
IO#3_DCM_1		n.d.		30,60
IO#3_DCM_2		n.d.		10,38
IO#3_DCM_3		n.d.		11,02
IO#3_DCM_4		n.d.		18,39
IO#3_DCM_5		n.d.		13,87

IO#3_DCM_6		n.d.		4,12
IO#3_DCM_7		n.d.		9,30
IO#3_DCM_8		n.d.		10,64
IO#3_DCM_9		n.d.		5,18
IO#3_DCM_10		n.d.		2,04
IO#3_DCM_11		n.d.		3,65
IO#3_DCM_12		n.d.		8,65
IO#3_DCM_13		n.d.		20,63
IO#3_DCM_I		n.d.		12,96

IO#3_DCM_II		n.d.		5,53
IO#3_DCM_III		n.d.		4,43
IO#3_DCM_IV		n.d.		3,87
IO#3_DCM_V		n.d.		2,00

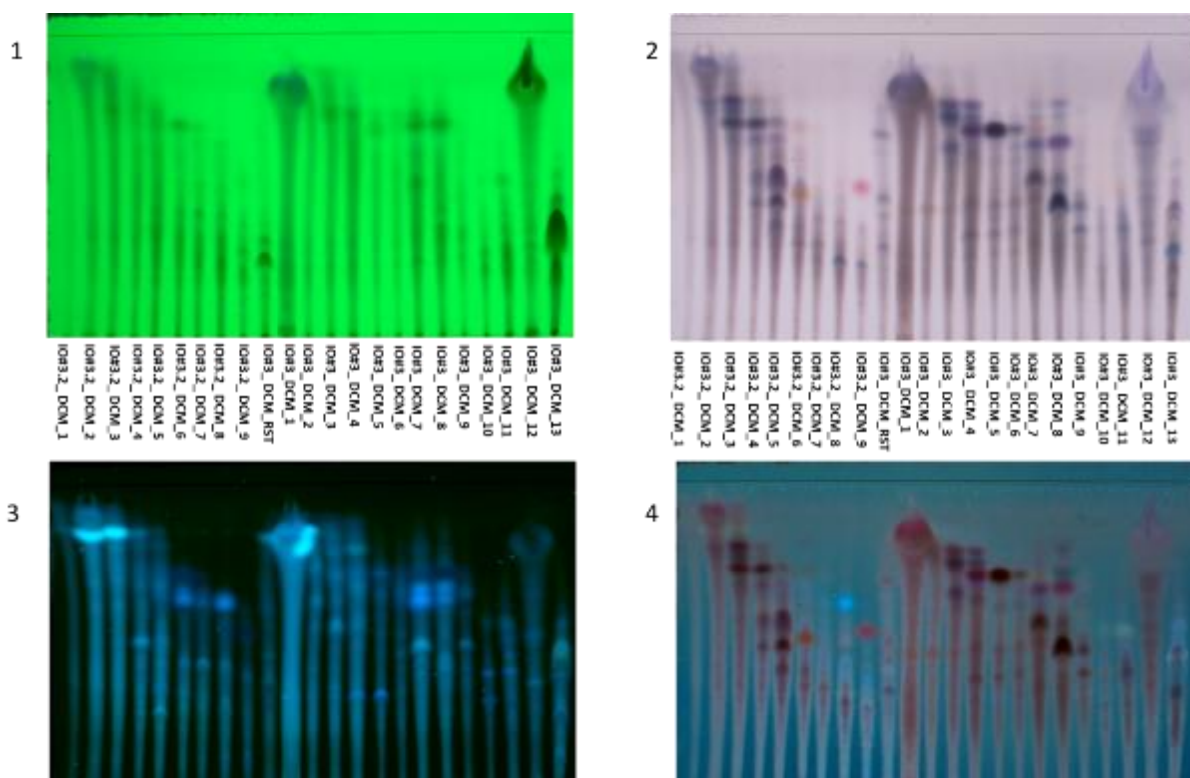


Figure 24: TLC (5.1.1) of IO#3_DCM fractions, 1:254 nm before derivatization with Vanillin/sulphuric acid, 2: Vis after derivatization, 3: 366 nm before derivatization, 4: 366 nm after derivatization.

As shown by the UPC² (Table 15) and TLC, none of the yielded sub-fractions comprised a single constituent. However, by comparison of UPC² and TLC

chromatograms, syringic acid could be determined as the main compound. Other substances like inotodiol, inonotsutriol A/B and trametenolic acid were putatively identified based on retention times.

Due to the very similar molecular weight of the fractions' constituents gel permeation chromatography was inadequate for fractionation. Possibly another type of chromatography (such as column chromatography with silica gel) would have been better, since on the TLC, the separation seems better. It might also would have been helpful, to collect less mL per tube, since the separation of constituents with similar diffusion volume could have improved.

In conclusion, this extract has a lot of different substances, some with similar molecular weights in it, and to isolate pure substances, a Sephadex column run is insufficient.

Since there were no isolated compounds, all fractions were tested for bioactivity.

Table 16: Bioactivity data of isolated substances at TGR-5 cell model. The experiment (6.4) was done with three replicates, and the mean value was calculated (n=1). Forskolin 10 μ M and LCA 10 μ M acted as positive control. DMSO 0.1 % was the control.

Compound/Sub-fraction	TGR-5 activity
DMSO 0.1%	\pm 0 %
Forskolin 10 μ M	+ 74.52 %
LCA 10 μ M	+ 74.10 %
IO#3_DCM_V 30 μ M	+ 15.09 %

The activity measurements show that only one sub-fraction caused an activation of the TGR-5 (Table 16). A further separation, isolation, and comparison with the active IO#4-7_DCM sub-fractions of the compounds from this sub-fraction would be a good starting point for further research.

4.6 Analysis of IO#2_DCM

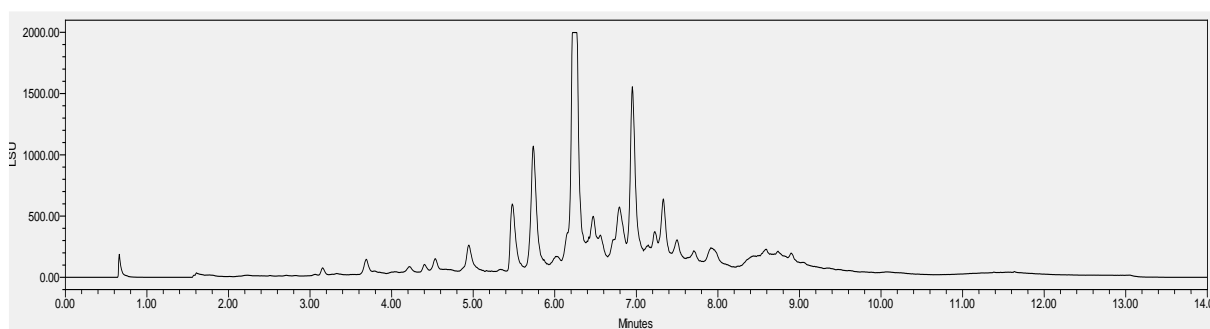


Figure 25: IO#2_DCM ELSD chromatogram

The last fraction prepared for analysis was not tested for bioactivity.

Since there was only a limited, small amount of fraction IO#4-7_DCM and IO#3_DCM, it was expected that these amounts would not be sufficient to isolate several pure substances. Additionally, these two fractions turned out to be particularly complex during mycochemical workup. The chromatograms of IO#2_DCM suggest a similar composition to the tested fractions. This fraction was analyzed and separated into sub-fractions for the purpose of obtaining more material in the analysis of various sub-fractions of IO#4-7_DCM and IO#3_DCM.

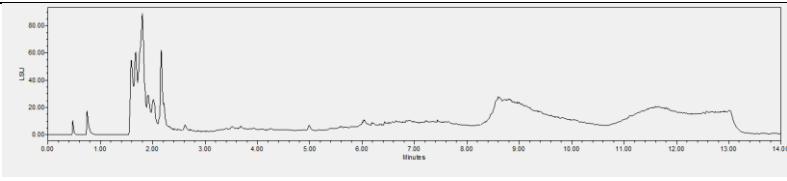
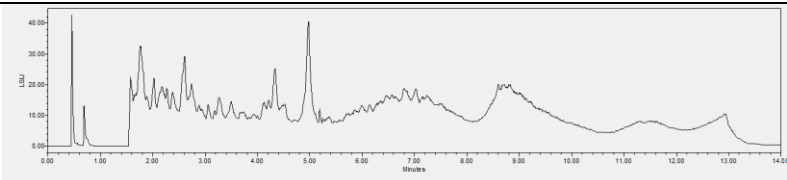
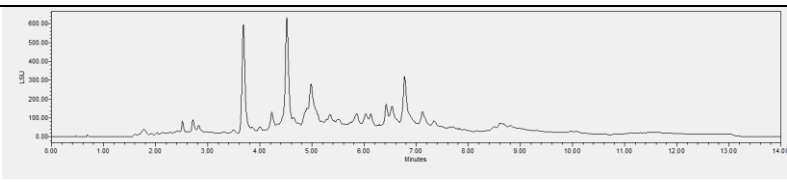
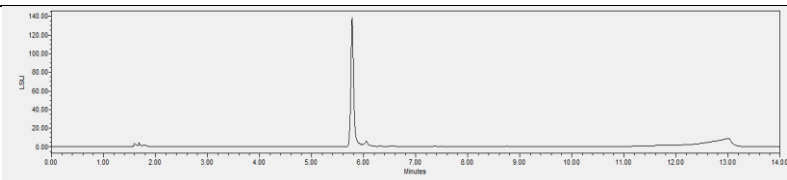
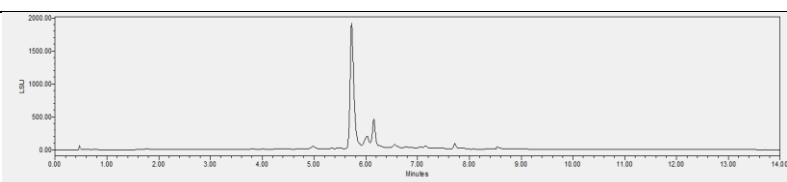
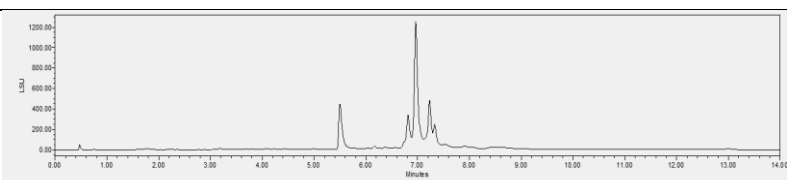
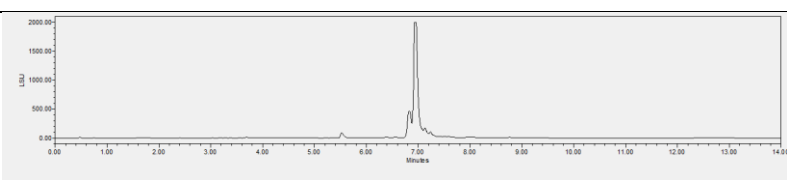
Four main compounds were determined in the ELSD chromatogram of IO#2_DCM. These were assigned to the respective peaks in the chromatograms of IO#4-7_DCM and IO#3_DCM and the whole fraction was attempted to separate into similar sub-fractions using the same Sephadex method.

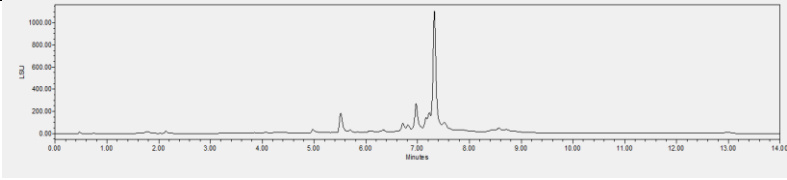
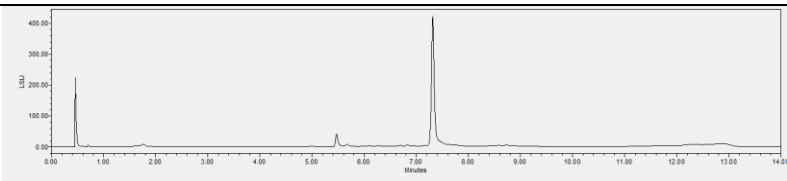
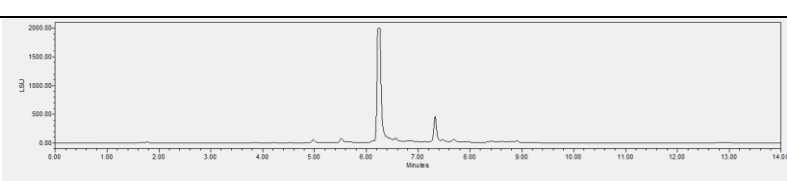
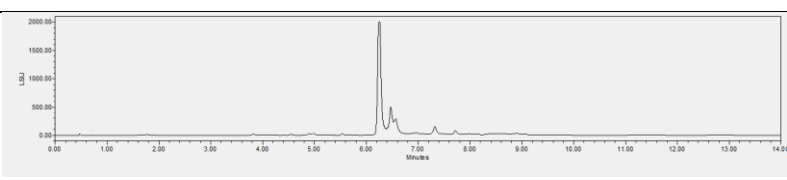
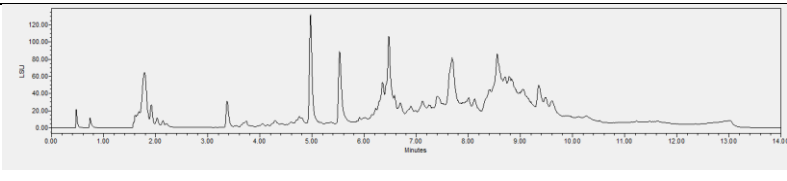
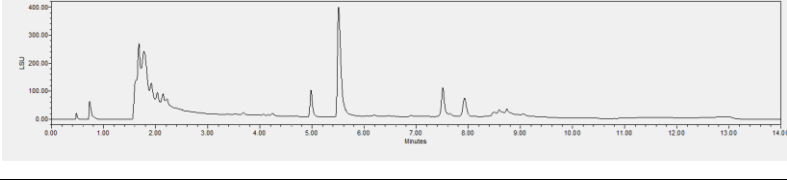
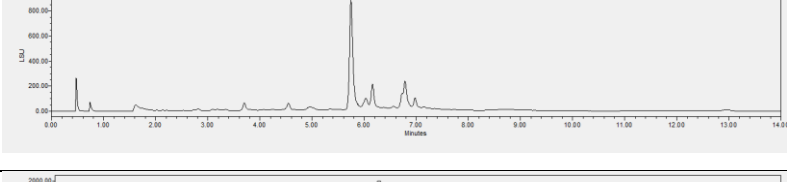
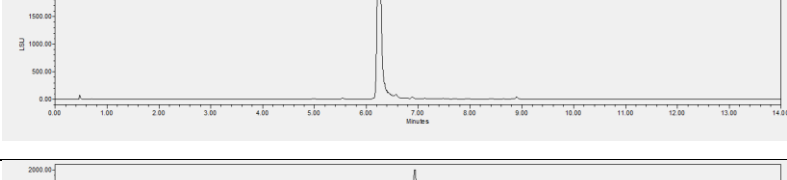
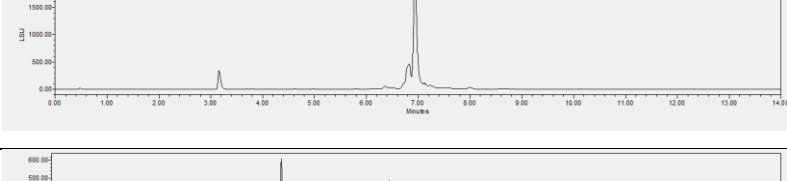
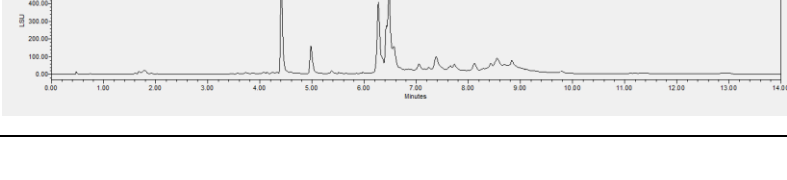
15.83 mg were diverted as reference (IO#2_DCM_RST). The other 300 mg had to be splitted into 3 parts of 100 mg and each was dissolved in 1.5 ml of mobile phase (DCM:acetone, 85:15). The parts were applied to a Sephadex column (1000 x 1.5 mm). In run 1, 70 tubes with 5 ml were collected and monitored via TLC; in run 2, 67 tubes were collected; in run 3, 77. Unfortunately, due to an error of the sample collector and pigments not eluting, 145 mg were lost. Based on the TLC fingerprints, the tubes were merged to 18 fractions and the yield was determined. The fractionation yields, and the distribution of the tubes are shown in Table 18. Two fractions (IO#2_DCM_18 run 1 and 2) were combined with IO#4-7_DCM_18 because both fractions seemed semi pure on the TLC.

The 18 new fractions were analyzed with TLC (**5.1.1**). Figure 26 shows the TLC of the merged fractions of IO#2_DCM. For further purity measurements all fractions, except IO#2_DCM_17 (not enough yield), were measured with analytical SFC

(5.1.3) equipped with PDA-ELSD. The ELSD chromatograms are shown in Table 17.

Table 17: ELSD spectra of IO#2_DCM fractions

Name	ELSD - chromatograms	Mass+ [m/z]	Predicted Substance
IO#2_DCM_1		n.d.	
IO#2_DCM_2		n.d.	
IO#2_DCM_3		n.d.	
IO#2_DCM_4		[M+Na] ⁺ =465.1 [M-OH] ⁺ = 425.5	Inotodiol [M=442.7]
IO#2_DCM_5		[M+Na] ⁺ =465.1 [M-OH] ⁺ = 425.5	Inotodiol [M=442.7]
IO#2_DCM_6		[M+Na] ⁺ =481.5 [M-OH] ⁺ =441.5	Inonot- sutriol [M=458.7] + ?
IO#2_DCM_7		[M+Na] ⁺ =481.5 [M-OH] ⁺ =441.5	Inonot- sutriol [M=458.7] + ?

IO#2_DCM_8		n.d.	
IO#2_DCM_9		n.d.	
IO#2_DCM_10		[M-H]⁻ =455.5	Trametenolic acid
IO#2_DCM_11		[M-H]⁻ =455.5	Trametenolic acid [M=456.7]
IO#2_DCM_12		n.d.	
IO#2_DCM_13		n.d.	
IO#2_DCM_14		n.d.	
IO#2_DCM_15		[M-H]⁻ =455.5	Trametenolic acid
IO#2_DCM_16		[M+Na]⁺ =481.5 [M-OH]⁺ =441.5	Inonot- sutriol [M=458.7]
IO#2_DCM_18			

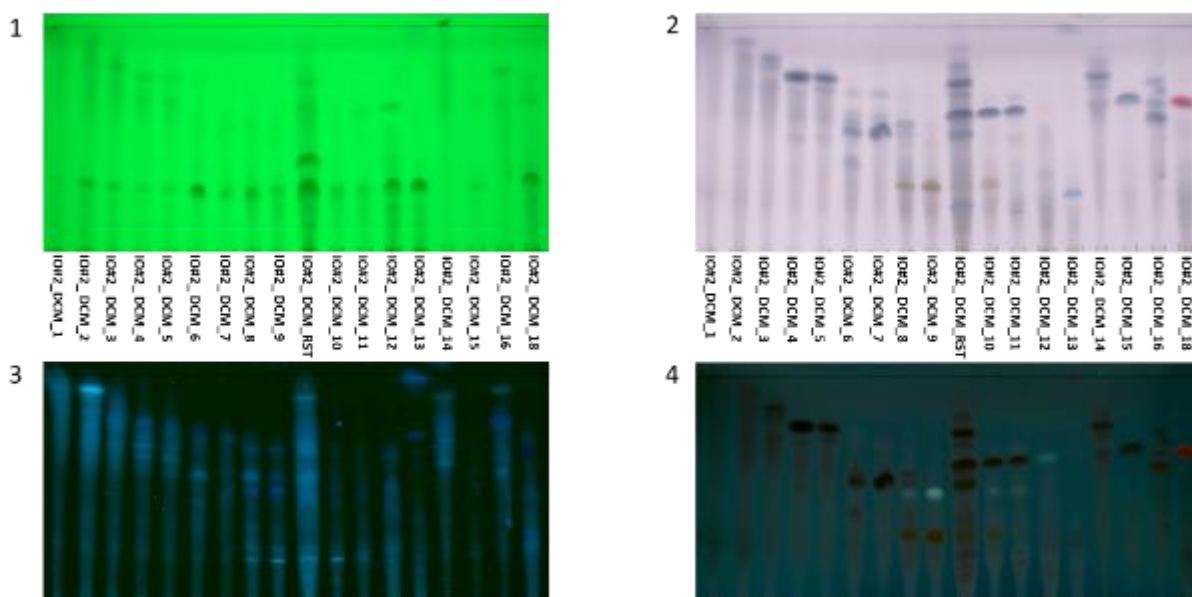


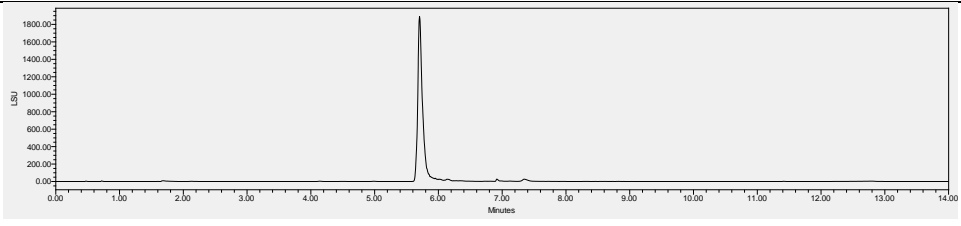
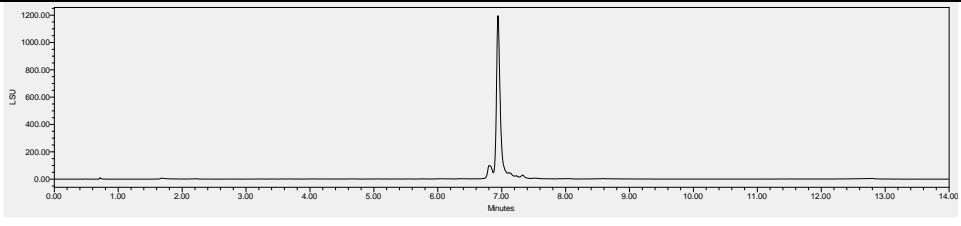
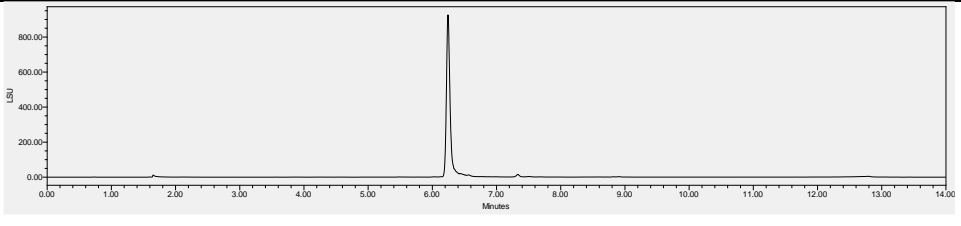
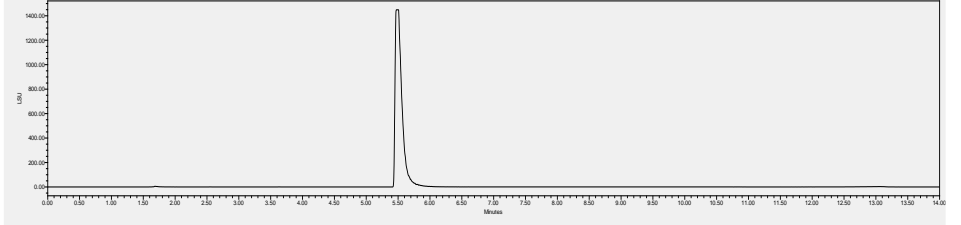
Figure 26: TLC (5.1.1) of IO#2_DCM fractions. 1:254 nm before derivatization with Vanillin/sulphuric acid, 2: Vis after derivatization, 3: 366nm before derivatization, 4: 366 nm after derivatization.

Table 18: IO#2_DCM sub-fraction yields

Sub-fraction	collected tubes 1	collected tubes 2	collected tubes 3	yield [mg]
IO#2_DCM_RST				15.83
IO#2_DCM_1	1-4	1-10	1-19	8.33
IO#2_DCM_2	5-6			0.66
IO#2_DCM_3	7-9			1.43
IO#2_DCM_4	11			0.57
IO#2_DCM_5	10,12,13			2
IO#2_DCM_6	14-18	13-17	26-31	15.86
IO#2_DCM_7	19	12	25	4.85
IO#2_DCM_8	20-27	18-21	32-35	8.22
IO#2_DCM_9	28-29	22		1.03
IO#2_DCM_10	30-41	23-26	36-39	12.73
IO#2_DCM_11	42-45	32-38	45-53	13.13
IO#2_DCM_12	52-70	46-61	61-77	9.63
IO#2_DCM_13		62-NI		11.23
IO#2_DCM_14		11	20-22	22.84
IO#2_DCM_15		27-31	40,41,43,44	15.99
IO#2_DCM_16			23.24	5.48
IO#2_DCM_17			42	0.11
IO#2_DCM_18			54-60	4.2
IO#4-7_DCM_18	46-51	39-45		1.05
total				155.17

All of the four main components could be putatively assigned as syringic acid, inotodiol, inonotsutriol A/B, and trametenolic acid based on comparison to available reference compounds the retention times of previous isolations (Table 19) and their [m/z] values.

Table 19: Reference retention time chromatograms of pure substances, UPC², optimized 14 min method (5.1.3)

Inotodiol	
Inonotsutriol	
Trametenolic acid	
Syringic Acid	

5. Material and Methods

5.1 Chromatography

Chromatography is a separation method which makes use of the different interactions of the different analytes with a stationary and/or a mobile phase. Every analyte distributes differently in different phases. This distribution or separation can be used analytically and for preparative systems (Gey M. H., 2015).

Following methods i.e. thin-layer chromatography, gel permeation chromatography, supercritical fluid chromatography, ultra-performance liquid chromatography and liquid chromatography - mass spectrometry were used.

5.1.1 Thin-layer chromatography

Thin-layer chromatography consists of a stationary phase that is applied as a thin layer to a supporting material such as a glass plate or aluminium foil. Generally, this thin layer is made of a polar material such as silica gel. However, there are also other layers used, like aluminium oxide, cellulose, or polyamide.

The mobile phase usually consists of different apolar solvents with different elution powers. The selection of the stationary and mobile phase depends on the chemical features of the analytes (Gey M.H., 2015).

Thin-layer chromatography in this work was performed with the following system:

Mobile phase: DCM: Methanol: H₂O, 9: 1: 0.25

Stationary phase: Merck silica gel 60 F₂₅₄

Detection: Vanillin (1% in MeOH)/H₂SO₄ (5% in MeOH)

The samples were first dissolved in DCM. Then 5 µl of sample solution (5 mg/ml) were applied to the TLC plate with a glass capillary. After evaporation of the solvent, the TLC plate was transferred to the already mobile phase saturated developing chamber. Because of the stationary phase capillaries, the mobile phase moves over the stationary phase's surface. During this movement, the compounds

with higher affinity to the silanol groups of the stationary phase, move slower compared to low affinity compounds which results in their separation over time. The time is limited by the length of the TLC plate. After separation, the plate was dried, and for visualisation derivatised.

The first TLC detection was performed before derivatisation, with CAMAG TLC visualizer, under visible light, UV₂₅₄ and UV₃₆₆. For derivatisation the plate was sprayed with vanillin/sulphuric acid and heated for 3 minutes at around 100 °C. After that, the plate was detected again with the same settings.

5.1.2 Gel permeation chromatography

Gel permeation chromatography is a form of liquid-chromatography, where the constituents are separated by their diffusion volumes with an organic solvent. The mobile phase is an organic solvent, the stationary phase is a beaded, cross-linked dextran which has been hydroxypropylated to yield a chromatographic media with both hydrophilic and lipophilic character (Sephadex). The extracts are "filtered" according to the size of their constituents between the pores of the separation phase (gel) and the mobile phase. Smaller molecules can enter and migrate through the pores. The smaller the molecules, the longer the residence times in the pore system, so that they are retained longer and elute at the end. Very large molecules that do not fit into the pores are excluded and pass the stationary phase within the liquid volume. Thus, they elute faster (Gey M.H., 2015).

The LH-20 Sephadex granulate was swelled overnight in the mobile phase to form a gel with uniform pore size. It was then packed into a column. The gel permeation chromatography was performed in two different solvents. The fractionation of the extracts IO#4-7_DCM, IO#3_DCM and IO#2_DCM was performed in DCM:acetone, 85:15. The isolation of pure substances of the sub fractions IO#2_PE6 and IO#2_PE_13 was performed in methanol. Unless otherwise stated the DCM:acetone column had a diameter of 20 mm and a length of 1000 mm, while the methanol column had a diameter of 10 mm and a length of 500 mm.

The respective extract or sub-fraction was applied, and the eluting mobile phase was collected into test tubes. Those tubes contained the collected solvent of 1-3 min (constant per column) flow time each, at atmospheric pressure. The flow rate

was around 2 ml/min, so every collected tube contained between 2 - 6 ml. After collection, the solvent in the tubes was evaporated under reduced pressure using the Genevac EZ-2 Mk3 with the "very low BP mix" evaporation method. Dried fractions were dissolved again in 500 μ l DCM and 5 μ l were applied to a TLC.

5.1.3 Supercritical fluid chromatography

Supercritical fluid chromatography (SFC) is a chromatographic method which employs a supercritical fluid as mobile phase. When a certain temperature and pressure is reached, a substance turns into a supercritical fluid (Figure 27). At 31°C and 73.75 bar, CO₂ is at that critical point and enters a supercritical fluid condition, which leads to high diffusivity and low viscosity. That enables a high flow rate compared

to other chromatographic methods like HPLC or UPLC. These conditions are easy to achieve with most of the ordinary HPLC instruments, which makes CO₂ an attractive substance for SFC. Also, CO₂ is cheap, inert, non-flammable and considered environmentally friendly since it is an industrial by-product. The polarity of CO₂ is like hexane (normal-phase chromatography), therefore modifiers like methanol, ethanol or acetonitrile are necessary to adjust the elution strength to the samples.

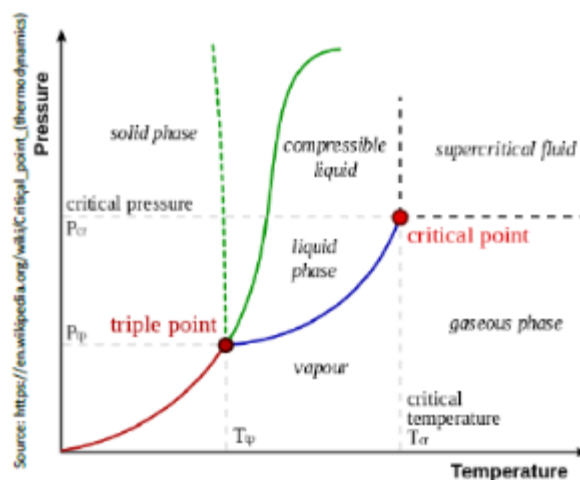


Figure 27: Pressure-temperature phase diagram. At critical point, a supercritical fluid emerges. Accessed: 01.10.2021

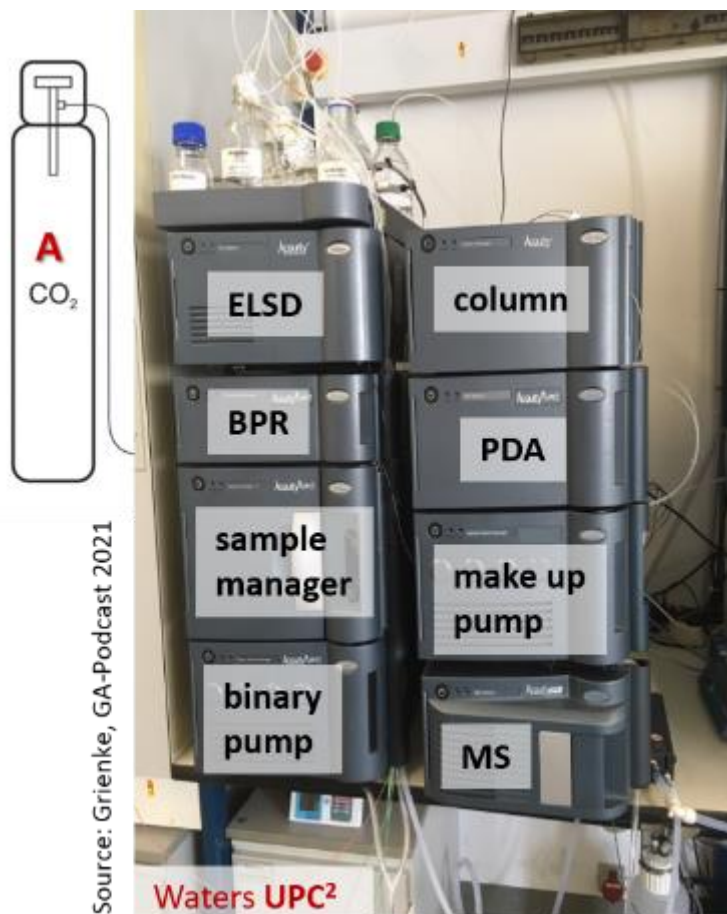


Figure 28: SFC instrumentation, back pressure regulator (BPR), electric light scattering detector (ELSD), mass spectrometer (MS), photodiode array detector (PDA). Image kindly provided by Ulrike Grienke, 2021.

For analytical supercritical fluid chromatography, the Waters Acuity UPC² instrument was used (Figure 28). It consists of a sample-, binary solvent-, convergence-, and column manager and a PDA detector. In addition, an Acuity-ELS-detector or an Acuity-ISM-QDa-detector was connected. As nebulising gas for QDa operation, nitrogen was used. Empower 3 was the operating software. The method used was optimized by refinement of the co-solvent methanol gradient. The initial and the optimized method, with the best separation reached, is given in Table 20.

Table 20: SFC parameters per method at UPC²

SFC technique	Initial method			Optimized method		
injection volume [μl]	5 μl			5 μl		
flow rate [ml/min]	1.200			1.200		
mobile phase A	CO ₂			CO ₂		
mobile phase B	MeOH			MeOH		
	time [min]	% A	% B	time [min]	% A	% B
gradient	0	90	10	0	100	0
	3	90	10	1	95	5
	6	87.60	12.40	2	95	5
	8	84	16	3	90	10
	12	56	44	4	90	10
	14	50	50	5	86	14
	16	50	50	6.5	80	20
	17	90	10	7.5	80	20
	19	90	10	8	70	30
				10	70	30
				11	56	44
				12	50	50
				12.5	50	50
				13	100	0
				14	100	0
back pressure	3250 psi			3250 psi		
temperature [°C]	40			40		
stationary phase	Torus 1-AA Column (3.0 * 100 mm, 1.7 μm, 130 Å)			Torus 1-AA Column (3.0 * 100 mm, 1.7 μm, 130 Å)		

For preparative SFC, the Waters Prep-15 SFC system was used (Figure 29). It consists of a fluid delivery module which is connected to an Accel 500 LC chiller (Thermo Fisher Scientific), a ten-port column manager, a Waters 2767 sample manager, a back pressure regulator, a heat exchanger, a make-up pump, a Waters 2998 Photo Diode Array and a Waters 2424 ELSD. MassLynx V4.1 was the operating software. With the sample collector and the high flowrate, separation

and isolation of certain peaks was possible. The method used for fractionations, was optimized at the start. It is shown in Table 21.

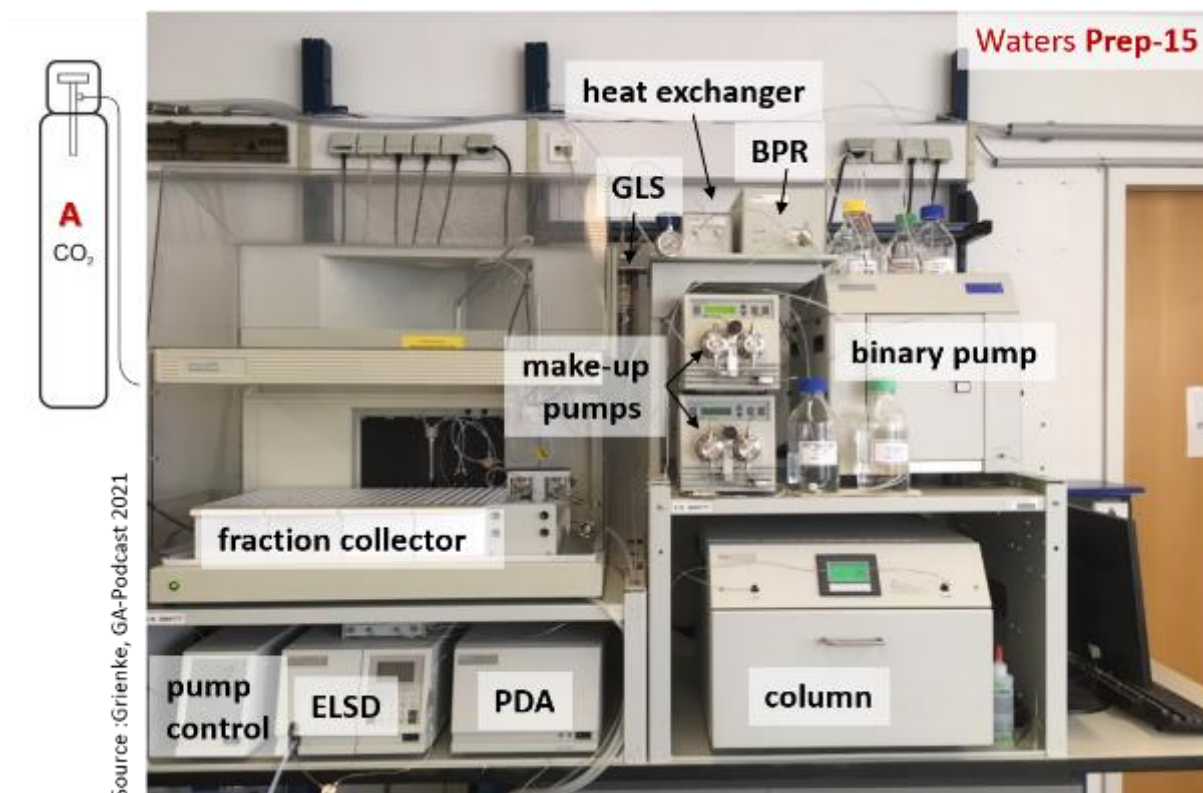


Figure 29: preparative SFC instrumentation; back pressure regulator (BPR), electric light scattering detector (ELSD), gas liquid separator (GLS), photodiode array detector (PDA)

Table 21: SFC isolation method parameters at Prep-15.

SFC technique	isolation method		
injection volume [μl]	100		
flow rate [ml/min]	15		
mobile phase A	CO_2		
mobile phase B	MeOH		
	time [min]	% A	% B
gradient	0	95	5
	3	95	5
	4	86	14
	7	86	14
	8	83	17
	9	83	17

	11	60	40
	12	60	40
	12,5	95	5
	14	95	5
backpressure	120bar		
temperature [°C]	40° C		
stationary phase	Torus 1-AA Column (10 mm * 250 mm)		

5.1.4 Ultra-performance liquid chromatography

The ultra-performance liquid chromatography is an advanced high resolution LC technology. It is a widely used analysis technique that allows separation, identification and quantification of substances. Usually reversed phase material is utilized (Figure 30), which means that the mobile phase consists of a mixture of polar solvents, for example a mix of water and acetonitrile. The mobile phase is pumped continuously, under high pressure through the column. The particle size of the adsorptive stationary phase is smaller (1.7 - 1.8 μm) than those of conventional HPLC devices. The pressure at which the mobile phase is pumped through the columns is up to 1030 bar (15.000 psi). This shortens the time of the analysis and provides a higher sensitivity and resolution of the chromatographic performance (Waters, 2021).

The sample is applied under normal pressure conditions with the help of a valve.

Source: Gey M. H., 2015

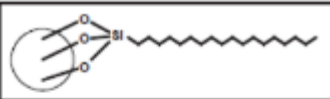
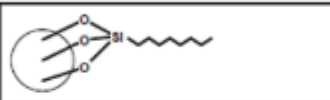
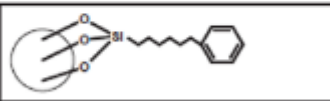
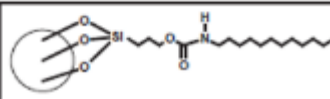
	A: ACQUITY UPLC BEH C18
	B: ACQUITY UPLC BEH C8
	C: ACQUITY UPLC BEH Phenyl
	D: ACQUITY UPLC BEH Shield RP18

Figure 30: Separation phases for UPLC

The instrument used in this work was the Waters Acquity-UPLC. As stationary phase, the Acquity UPLC BEH C18 (1.7 μm) was used. The mobile phase consisted of water and acetonitrile. The initial gradient is shown in Table 22. The measured samples were dissolved in methanol. The UPLC was used analytically and preparative to collect single peaks. ELSD and PDA served as detectors in the analytical process. For preparative steps the PDA at a wavelength of 200 nm was employed and coupled to a sample collector. The gradient was optimized for faster analyzation and isolation. The optimized isolation-gradient is shown in Table 23.

Table 22: 20 min gradient at UPLC. Solvent A is water and Solvent B is acetonitrile. Flowrate was 0.3 ml/min

Time [min]	Solvent A (water) [%]	Solvent B (acetonitrile) [%]
0	95	5
2	95	5
10	55	45
14	5	95
15	5	95
16	95	5
20	95	5

Table 23: optimized gradient for the isolation of IO#2_PE_12_2 and IO#2_PE_3 at UPLC. Solvent A is water and Solvent B is acetonitrile. Flowrate was 0.3 ml/min

Time [min]	Solvent A (water) [%]	Solvent B (acetonitrile) [%]
0	20	80
3	5	95

4.5	5	95
5	20	80
6	20	80

5.2 Mass spectrometry

Mass spectrometry (MS) is an analytical technique for identification and mass elucidation of unknown compounds and quantification of known compounds. The determination of the mass-to-charge ratio (m/z) of a molecule's ions is key to the analysis. This enables the possibility of quantitative and qualitative measurements.

First, the sample gets ionized in vacuum. There are two different ionization methods. The first is hard ionization through electron impact ionization (EI) and the second one is soft ionization. Later methods are chemical ionization (CI) or electron spray ionization (ESI). After ionization, the molecules are separated through their mass-to-charge ratio in mass analyzers like ion-trap -, quadrupole - or time of flight - instruments. The last step is the detection of the ions through the faraday-cup or the secondary electron multiplier. At the end, the measurement results in a mass spectrum that plots the abundance against the mass-to-charge ratio (m/z) (Maher S. et al., 2015; Gey M. H., 2008).

In this work, MS is combined either with liquid chromatography (LC-MS) or with SFC, to elucidate the mass of components at a certain retention time. The SFC linked QDa settings are shown in Table 24. The LC and the linked MS-device used are described in Table 25. The MS was equipped with a 3D quadrupole ion trap and an orthogonal ESI-source. All Samples analyzed by LC-MS were dissolved in methanol.

Table 24: SFC linked QDa settings

QDa settings	
Probe temperature	500°C
Capillary voltage (positive and negative)	0.8 kV
Cone voltage positive	15V
Cone voltage negative	30V
Mass Range	130-800 Da
ISM Solvent	95% MeOH 5% Water + 10mM ammoniumformiate
Flowrate	0.6 ml/min

Table 25: Hardware, Software, stationary phase and mobile phase for LC-MS

HPLC-Instrumentation	DIONEX UltiMate 3000 RS Pump
	DIONEX UltiMate 3000 RS Autosampler
	DIONEX UltiMate 3000 RS Column Compartment
	DIONEX UltiMate 3000 Diode Array Detector
MS-Instrumentation	BRUKER Daltonics HCT
Software	DIONEX Chromeleon XPress
	BRUKER esquire control
	BRUKER HyStar 3.2
	BRUKER Compass Data Analysis
Stationary phase	Licrosphere 100 RP 18e 5µm (Number: 098) dimension: 250 x 4 mm
Mobile phase	Solvent A: H ₂ O + 0,1 % FA
	Solvent B: Acetonitrile + 0,1 % FA

5.3 Nuclear magnetic resonance spectroscopy (NMR)

Nuclear magnetic resonance (NMR) spectroscopy is based on the excitation of atomic nuclei by radio waves. Compared to electrons, nuclei (protons) are much heavier, which is why a homogeneous magnetic field must be applied for their transfer to a higher (excited) energy state. The NMR technique is one of the most important and informative instrumental analytical methods in organic chemistry. It has been gaining increasing importance in recent years for the structural elucidation of complex biomolecules such as proteins, glycoproteins and oligosaccharides. The atoms are exposed to a strong homogeneous magnetic field and a radiated high frequency. A resonance is created between the oscillating field and the rotating atomic nuclei. At the end of the pulse, the nuclei return to their equilibrium state, which is called relaxation. A magnetic field is generated in the receiver, producing an electric current that is amplified and detected.

The most common excitation is of protons (^1H -NMR-spectroscopy) and of carbon nuclei (^{13}C -NMR-spectroscopy/Attached Proton Test (APT)). Those are the two used in this work as well (Gey M.H., 2015).

^1H -NMR and ^{13}C -NMR spectroscopy contribute very significantly to the structural elucidation of chemical and biochemical molecules. From an NMR spectrum the chemical shift, the spin-spin coupling pattern and the peak areas (intensities) are important information. Based on the chemical shift of proton nuclei, individual functional groups can be assigned, and the structure of the entire molecule can be predicted or characterized.

In this work, the BRUKER Avance 500 NMR spectrometer instrument (UltraShield) was used in combination with a switchable 5 mm probe (TCI Prodigy cryoprobe head, 5 mm, triple resonance inverse detection probe head) with z-axis gradients, automatic tuning and matching accessories (BRUKER BioSpin) for increased sensitivity (Table 26). For the ^1H NMR, the frequency 500.13 MHz was used, and for the ^{13}C NMR/APT, the frequency 125.75 MHz was used. The solvents were fully deuterated methanol or chloroform. The measurement temperature was 298 K. 1D and gradient-enhanced (ge) 2D spectra were recorded. Heteronuclear single quantum coherence (HSQC), heteronuclear multiple bond correlation (HMBC), and correlation spectroscopy (COSY) were utilized as supplied by the manufacturer. The chemical shifts are internally related to the residual, non-deuterated solvent signal for methanol ^1H (δ 3.31 ppm) or chloroform ^1H (δ 7.26 ppm) and to the solvent carbon signal for methanol ^{13}C (δ 49.00 ppm) or chloroform ^{13}C (δ 77.00 ppm). Both, the two-dimensional experiments such as HSQC, HMBC and COSY and the one-dimensional experiments such as proton and carbon spectra were recorded. For two-dimensional spectra, the frequency axes consist of the chemical shifts of ^1H or ^{13}C nuclei. This results in a plot indicating the intensities of the coupling pairs. With HSQC, the direct bound of a proton to a specific carbon atom were determined. HMBC couples ^1H and ^{13}C nuclei over two or more bonds. It also visualizes couplings between protons and quaternary carbons (Langeder Julia, 2019).

In this work, proton and carbon spectra/APT, HSQC, HMBC and COSY were performed. The findings were compared by alignment with spectra of available reference compounds and using an online NMR spectrum predictor called nmrd.org.

Table 26: NMR instrumentation

NMR-Instrumentation	BRUKER 500 UltraShield™ Prodigy CryoProbe (TCI) for enhanced sensitivity
Calibration	Residual, non-deuterated solvent signal Methanol: 1H (δ 3,31 ppm) and 13C (δ 49,00 ppm) Chloroform: 1H (δ 7,26 ppm) and 13C (δ 77,00 ppm)
Software	MESTRELAB RESEARCH MestReNova

5.4 *In vitro* testing

In this work, we focused on two specific target receptors. The activity of the isolated compounds was measured *in vitro* by Alexander Perhal, Patrik Schwarz and Johanna Raab in the laboratory of Prof. Dr. Verena Dirsch (molecular targets University of Vienna). The two target receptors were the TGR-5 or GPBAR-1 receptor, a bile acid receptor, and the ROR_{yt} receptor, a retinoic acid receptor-related orphan receptor.

Activation measurement of the TGR5: HEK-293 cells were cotransfected with a TGR5 expression plasmid, a CRE luciferase reporter plasmid and an EGFP plasmid as internal control. Cells were treated with 10 μ M LCA as positive control or 30 μ g/ml of the three I. obliquus fractions for 18 h. The measured luciferase-derived luminescence was normalized to the obtained EGFP-derived fluorescence. Results are expressed as fold activation compared to vehicle control (Control, 0,1% DMSO). Each bar represents the mean \pm SD of four independent experiments. IO#2_PE was only tested in one experiment.

Fold activation measurement of the ROR_{yt}: HEK-293 cells were transiently transfected employing the calcium phosphate method using a plasmid encoding full-length human ROR_{yt}, a plasmid containing a luciferase reporter under the control of a ROR response element and a plasmid carrying eGFP as internal control. Cells were treated with 1 μ M SR2211 as positive control, and with the fractions at the indicated concentrations and incubated at 37 °C overnight (18 hours total). Luminescence values were measured, normalized to fluorescence values, and then normalized to the solvent control. Results are expressed as fold activation relative to the vehicle control. Data are shown as means \pm SEM of (at least) three biological replicates measured in technical quadruplicates.

5.5 Material

The material used was provided to us by Pakuso, LLC, Finland. It was *Inonotus obliquus* (Ach. ex Pers.) Pilát sclerotia, collected from birch trees grown in Finland above the arctic circle.

6 References

- Balandaykin, M. E., & Zmitrovich, I. V., 2015, Review on Chaga Medicinal Mushroom, *Inonotus obliquus* (Higher Basidiomycetes): Realm of Medicinal Applications and Approaches on Estimating its Resource Potential, *Int J Med Mushrooms*, 17(2), 95–104.
- Beutler J.A., 2019, Natural Products as a Foundation for Drug Discovery, *Curr. Protoc. Pharmacol.*, 86, e67.
- Broeders E.P., Nascimento E.B., Havekes B., Brans B., Roumans K.H., Tailleux, A., et al., 2015, The bile acid chenodeoxycholic acid increases human brown adipose tissue activity. *Cell Metab.* 22,418–426
- Caesar L. K., & Cech N. B., 2019, Synergy and antagonism in natural product extracts: when 1 + 1 does not equal 2. *Nat. Prod. Rep.*, 36(6), 869–888.
- Cui Y, Kim D-SS, Park K-CC., 2005, Antioxidant effect of *Inonotus obliquus*. *J Ethnopharmacol.*; 96 (1-2): 79e85
- Cvijic, M. E., Sum, C. S., Alt, A., & Zhang, L., 2015, GPCR profiling: from hits to leads and from genotype to phenotype. *Drug Discov. Today: Technologies*, 18, 30–37.
- Day K., Alfonzo M., Chen Y., Guo Z., Lee KK., 2013, Overweight, obesity, and inactivity and urban design in rapidly growing Chinese cities. *Health & place*; 21: 29-38
- Duru K.C., Kovaleva E.G., Danilova I.G., van der Bijl P., 2019, The pharmacological potential and possible molecular mechanisms of action of *Inonotus obliquus* from preclinical studies. *Phytother Res.*;1–15.
- Flanagan J. J., Neklesa, T. K., 2019, Targeting Nuclear Receptors with PROTAC degraders. *Mol Cell Endocrinol*, 110452.
- Foord S.M., Bonner T.I., Neubig R.R., Rosser E.M., Pin J. P., Davenport A. P., et al., 2005, International union of pharmacology. XLVI. G protein-coupled receptor list. *Pharmacol.Rev.* 57,279–288.

- Gey M. H., 2015. Instrumentelle Analytik und Bioanalytik: Biosubstanzen, Trennmethoden, Strukturanalytik, Applikationen. 3. Auflage, SpringerSpektrum-Verlag, Berlin Heidelberg.
- Guo C., Chen W.-D. and Wang Y.-D., 2016, TGR5, Not Only a Metabolic Regulator. *Front. Physiol.* 7:646.
- Hartmann A., Ganzera M., 2015. Supercritical Fluid Chromatography - Theoretical Background and Applications on Natural Products. *Planta Med.* 81 (17), 1570–1581.
- Jetten A. M., 2007, Retinoid-related orphan receptors (RORs): critical roles in development, immunity, circadian rhythm, and cellular metabolism. *Nucl Recept Signal*, 4.
- Katsuma S., Hirasawa A., and Tsujimoto G., 2005, Bile acids promote glucagon-like peptide-1 secretion through TGR5 in a murine enteroendocrine cell line STC-1. *Biochem. Biophys. Res. Commun.* 329,386–390.
- Kumar D.P., Rajagopal S., Mahavadi S., Mirshahi F., Grider J.R., Murthy K.S., et al., 2012, Activation of transmembrane bile acid receptor TGR5 stimulates insulin secretion in pancreatic beta cells. *Biochem. Biophys. Res. Commun.* 427, 600–605.
- Ladurner A., Zehl M., Grienke U., Hofstadler C., Faur N., Pereira F. C., Rollinger J. M., 2017. Allspice and Clove As Source of Triterpene Acids Activating the G Protein-Coupled Bile Acid Receptor TGR5, *Front Pharmacol*, 8.
- Ladurner A., Schwarz P. F., & Dirsch V. M., 2021, Natural products as modulators of retinoic acid receptor-related orphan receptors (RORs). *Nat Prod Rep*, 38(4), 757–781
- Langeder J., 2017, Isolation and characterization of constituents in an aqueous NaHCO₃-extract of Norway spruce balm, Diploma Thesis, University of Vienna.
- Liu, C., Zhao, C., Pan, H. H., Kang, J., Yu, X. T., Wang, H. Q., ... Chen, R. Y., 2014, Chemical constituents from *Inonotus obliquus* and their biological activities. *J Nat Prod*, 77, 35–41.
- Lockemann, G., 1951, Friedrich Wilhelm Serturmer, the discoverer of morphine. *J chem educ*, 28, 279.
- Manka K, Sobiczewski P, Manka M, Fiedorow Z., 2005, *Fitopatologia Lesna*. Warszawa: Panstwowe Wydawnictwo Rolnicze i Leśne;
- Maruyama T., Miyamoto Y., Nakamura T., Tamai Y., Okada H., Sugiyama E., et al., 2002, Identification of membrane-type receptor for bile acids (M-BAR). *Biochem. Biophys. Res. Commun.* 298, 714–719.
- McGlone, E. R., Bloom, S. R., 2018, ANNALS EXPRESS: Bile acids and the metabolic syndrome. *Annals of Clinical Biochemistry: Int J Lab Med*, 000456321881779.
- Moore, T. W., Mayne, C. G., & Katzenellenbogen, J. A., 2010, Minireview: Not picking pockets: Nuclear receptor alternate-site modulators (NRAMs). *Mol Endocrinol*, 24(4), 683–695.
- Nestle M., Jacobson M.F., 2000, Halting the obesity epidemic: A public health policy approach. *Public health reports*; 115: 12

- Nolan C.J., Prentki M., 2019 Insulin resistance and insulin hypersecretion in the metabolic syndrome and type 2 diabetes: Time for a conceptual framework shift. *Diabetes and vascular disease research*; 16: 118-127
- Patridge E., Gareiss P., Kinch M. S., Hoyer D., 2016, An analysis of FDA-approved drugs: natural products and their derivatives, *Drug Discov. Today*, Vol. 21, Issue 2, 204-207
- Popkin B. M., Adair L. S., & Ng S. W., 2012, Global nutrition transition and the pandemic of obesity in developing countries. *Nutr Rev*, 70(1), 3–21.
- Redvers N., & Blondin B., 2020, Traditional Indigenous medicine in North America: A scoping review. *PLOS ONE*, 15(8), e0237531.
- Revels S., Kumar S.A., Ben-Assuli O., 2017, Predicting obesity rate and obesity-related healthcare costs using data analytics. *Health policy and technology*; 6: 198-207
- Saar M., 1991, Fungi in khanty folk medicine. *J Ethnopharmacol.*; 31(2): 175e179.
- Schwendicke F., Stolpe M., 2017, Taxing sugar-sweetened beverages: Impact on overweight and obesity in Germany. *BMC Public Health*; 17: 88
- Shashkina MY, Shashkin PN, Sergeev AV., 2006, Chemical and medicobiological properties of chaga. *Pharm Chem J.*; 40(10): 560e568
- Shin, Y., 2000, Chemical constituents of *Inonotus obliquus* I. A new triterpene, 3 β -hydroxy-8,24-dien-lanosta-21,23-lactone from sclerotium. *Eurasian J Forest Res*, 1, 43–50.
- Smeriglio, A., De Francesco, C., Denaro, M., & Trombetta, D., 2021, Prickly Pear Betalain-Rich Extracts as New Promising Strategy for Intestinal Inflammation: Plant Complex vs. Main Isolated Bioactive Compounds. *Front pharmacol*, 12, 722398.
- Sun, N., Guo, H., & Wang, Y. 2019. Retinoic acid receptor-related orphan receptor gamma-t (ROR γ t) inhibitors in clinical development for the treatment of autoimmune diseases: a patent review (2016-present). *Expert Opinion on Therapeutic Patents*.
- Szczepkowski A, Piećka J, Grzywacz A.; 2013, Biology and medicinal properties of the chaga mushroom *Inonotus obliquus* (Fr.) Pilat]. *Sylvan.*; 157(3): 223e233.
- Szychowski, K. A., Bartosz, S., Tadeusz, P., & Jan, G., 2020, *Inonotus obliquus*—from folk medicine to clinical use. *Journal Tradit Complement Med*.
- Thomford N. E., Senthebane D.A., Rowe A., Munro D., Seele P., Maroyi A., Dzobo K., 2018, Natural Products for Drug Discovery in the 21st Century: Innovations for Novel Drug Discovery, *IJMS*, Vol. 19, no. 6, p. 1578
- Tiwari A., Maiti P., 2009, TGR5:an emerging bile acid G-protein-coupled receptor target for the potential treatment of metabolic disorders. *Drug Discov. Today* 14,523–530.
- Watanabe M., Houten S.M., Matak C., Christoffolete M.A., Kim B.W., Sato H., Messaddeq N., Harney J.W., Ezaki O., Kodama T., Schoonjans K., Bianco A.C., Auwerx J., 2006, Bile acids induce

energy expenditure by promoting intracellular thyroid hormone activation. *Nature* 439,484–489.

Wen M.C., Wei C.H., Hu Z.Q., Srivastava K., Ko J., Xi S.T., Mu D.Z., Du J.B., Li G.H., Wallenstein S., et al., 2005, Efficacy and tolerability of anti-asthma herbal medicine intervention in adult patients with moderate-severe allergic asthma, *J. Allergy Clin. Immunol.*, 116, 517–524.

WHO, 2016, WHO fact sheet - Obesity and overweight, <https://www.who.int/news-room/fact-sheets/detail/obesity-and-overweight> (accessed 10.11.2021)

Zheng C., Zhou W., Wang T., You P., Zhao Y., Yang Y., et al., 2015, A novel TGR5 activator WB403 promotes GLP-1 secretion and preserves pancreatic b-cells in type 2 diabetic mice. *PLoS ONE* 10:e0134051.

Zheng W., Miao K., Liu Y., Zhao Y., Zhang M., 2010, Chemical diversity of biologically active metabolites in the sclerotia of *Inonotus obliquus* and submerged culture strategies for up-regulating their production. *Appl Microbiol Biotechnol.*; 87(4): 1237e1254.

Zwirschmayr J., Kirchweiger B., Lehner T., Tahir A., Pretsch D., & Rollinger J. M., 2020. A robust and miniaturized screening platform to study natural products affecting metabolism and survival in *Caenorhabditis elegans*. *Sci Rep*, 10 (1):12323.

7 Appendix

7.1 Zusammenfassung

Inonotus obliquus ist ein parasitärer Pilz aus der Klasse der Hymenochaetaceae. Seine Sklerotien, als Chaga bekannt, werden in der traditionellen Medizin vieler nordischer Länder verwendet. Ihm werden therapeutische Wirkungen wie die Verbesserung der Herzfunktion, krebshemmende, entzündungshemmende und antidiabetische Eigenschaften zugeschrieben.

Die Wirkungsweise von *I. obliquus* ist jedoch nicht ausreichend geklärt. Einige Rezeptoren sind vielversprechende molekulare Ziele, z. B. Modulatoren des Takeda G-protein-coupled receptor 5 (TGR-5) und des retinoic acid receptor-related orphan receptor-gamma ($ROR_{\gamma t}$), da sie ähnliche Wirkungen vermitteln, wie sie Chaga zugeschrieben werden. Darüber hinaus werden beide Rezeptoren von natürlichen Produkten wie Triterpenen vom Lupan-Typ aktiviert. Ähnliche Metaboliten, z.B. Lanostan-Triterpene, sind aus dem Pilz bekannt. Daher lag die Vermutung nah, dass Bestandteile von *I. obliquus* diese Rezeptoren modulieren und so die therapeutische Wirkung vermitteln. Drei Fraktionen von *I. obliquus* zeigten in einem früheren Screening eine modulierende Wirkung.

Ziel dieser Arbeit war es, die für die TGR-5/ $ROR_{\gamma t}$ -Aktivität verantwortlichen Inhaltsstoffe in den Fraktionen des Pilzes zu isolieren und identifizieren. Die durch verschiedene chromatographische Methoden gewonnenen Reinsubstanzen wurden durch Massenspektrometrie (MS) und Kernspinresonanzspektroskopie (NMR) charakterisiert.

Es wurden 11 Inhaltsstoffe isoliert und identifiziert: Diese sind: Inotodiol, 3 β -Hydroxy-lanosta-8,24-dien-21-al, Trametenolsäure, Betulinol, Inonotsutriol A/B, Osmundaceton, Syringinsäure, Inonotsudriol D/E und Lanosta-8,25-dien-3,22,24-triol sowie zwei nicht vollständig charakterisierte diacetylierte Kongenere von Inonotsutriol A/B.

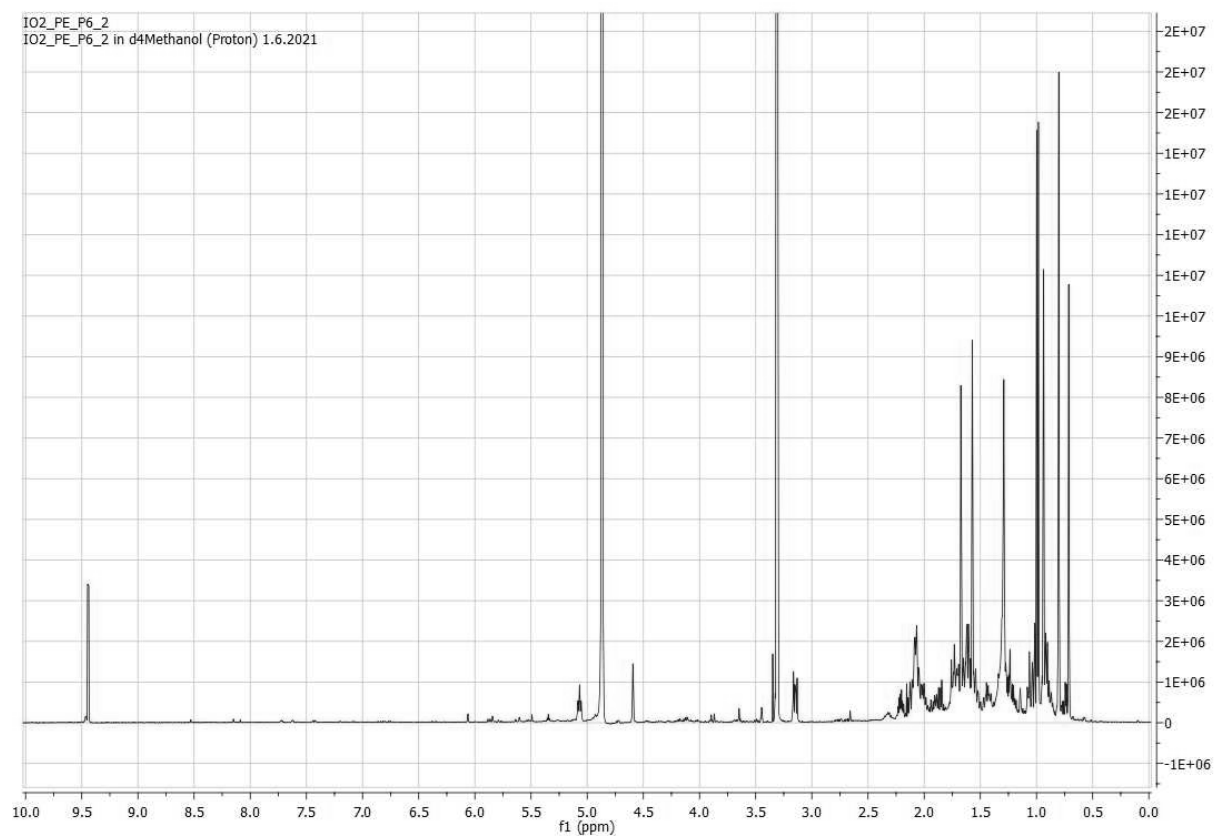
Bioaktivitätsmessungen ergaben eine starke $ROR_{\gamma t}$ -Hemmung bei drei isolierten Verbindungen und eine signifikante TGR-5-Aktivierung bei einer Verbindung.

Zusammenfassend lässt sich sagen, dass weitere Studien erforderlich sind, um die $ROR_{\gamma t}$ /TGR-5-Aktivität von *Inonotus obliquus* besser zu verstehen, z. B. im Hinblick auf synergistische Effekte.

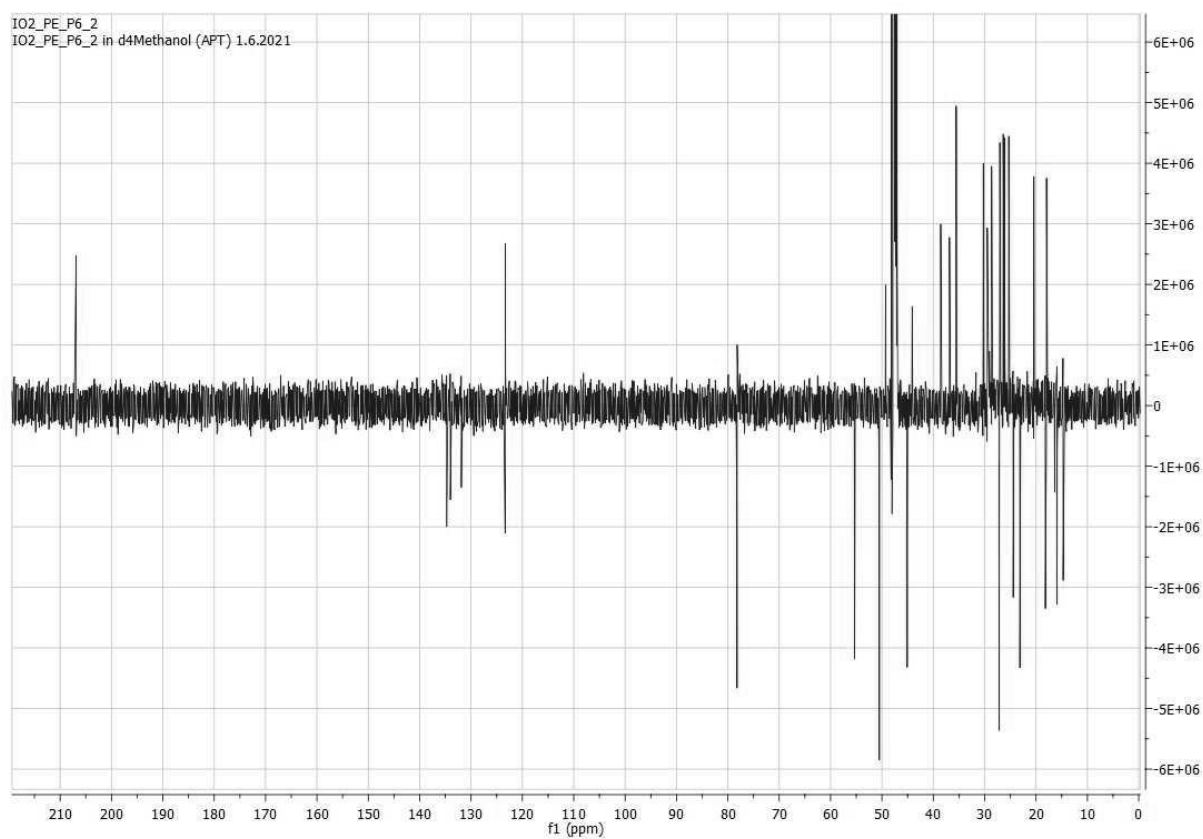
7.2 NMR spectra of pure substances

IO#2_PE_6_2

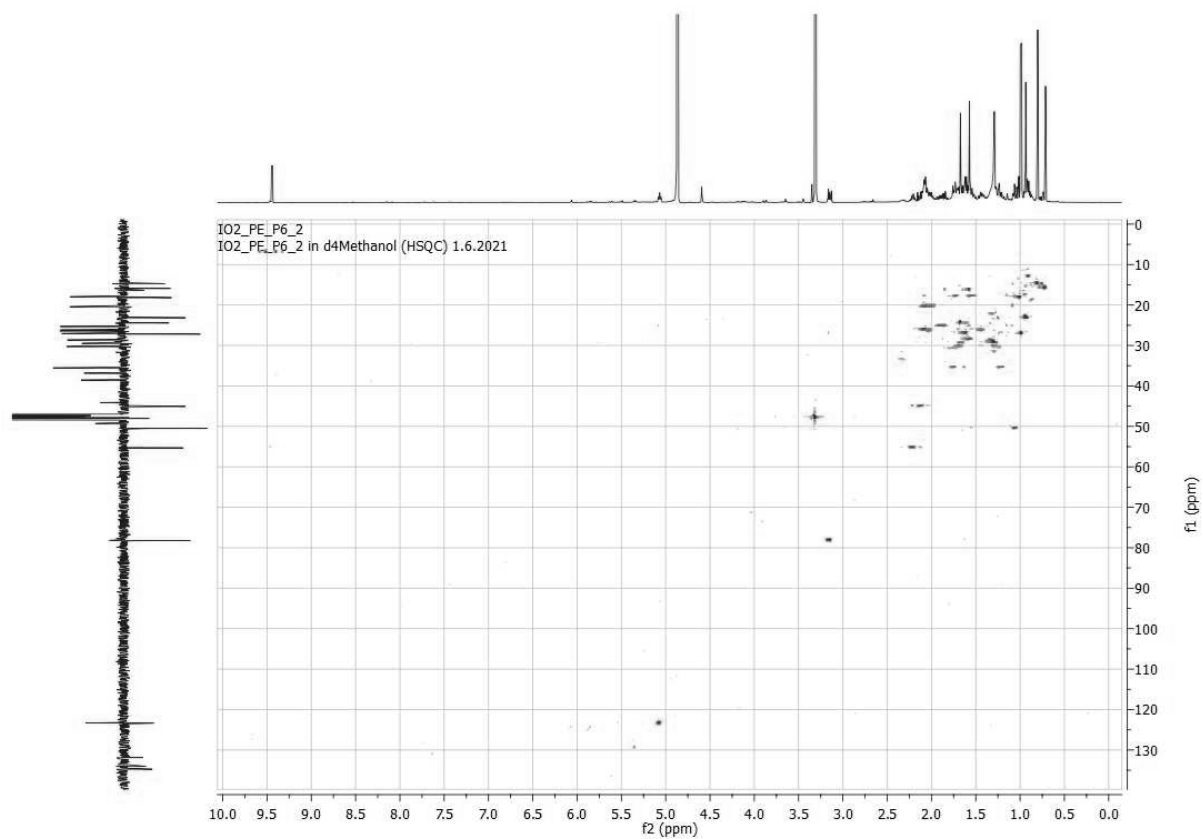
^1H

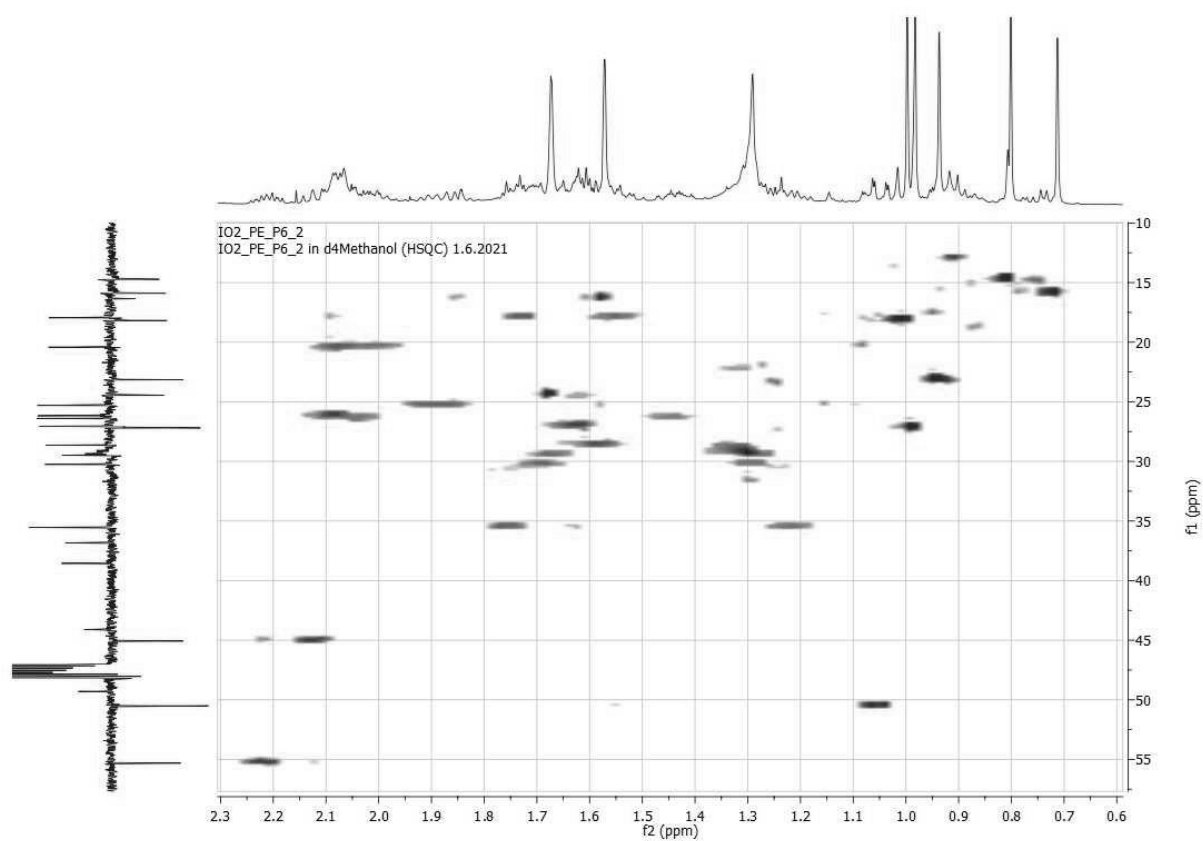


^{13}C

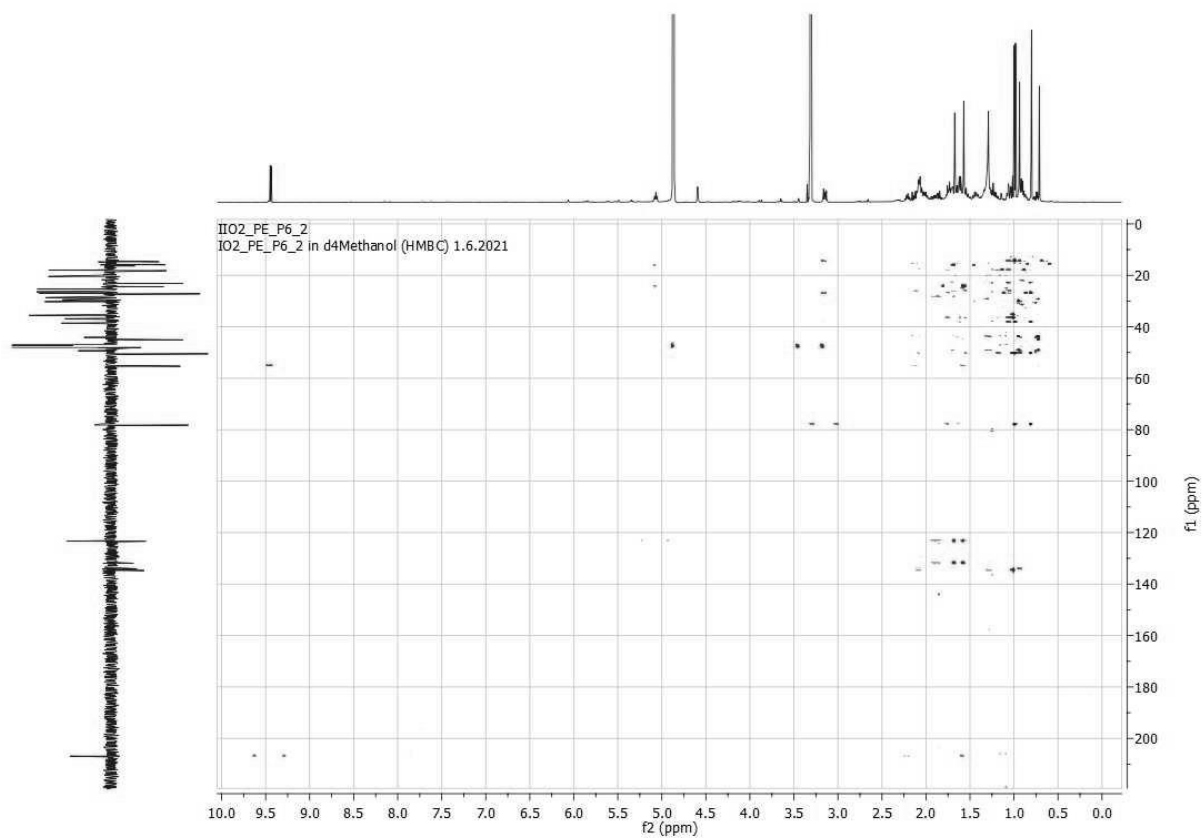


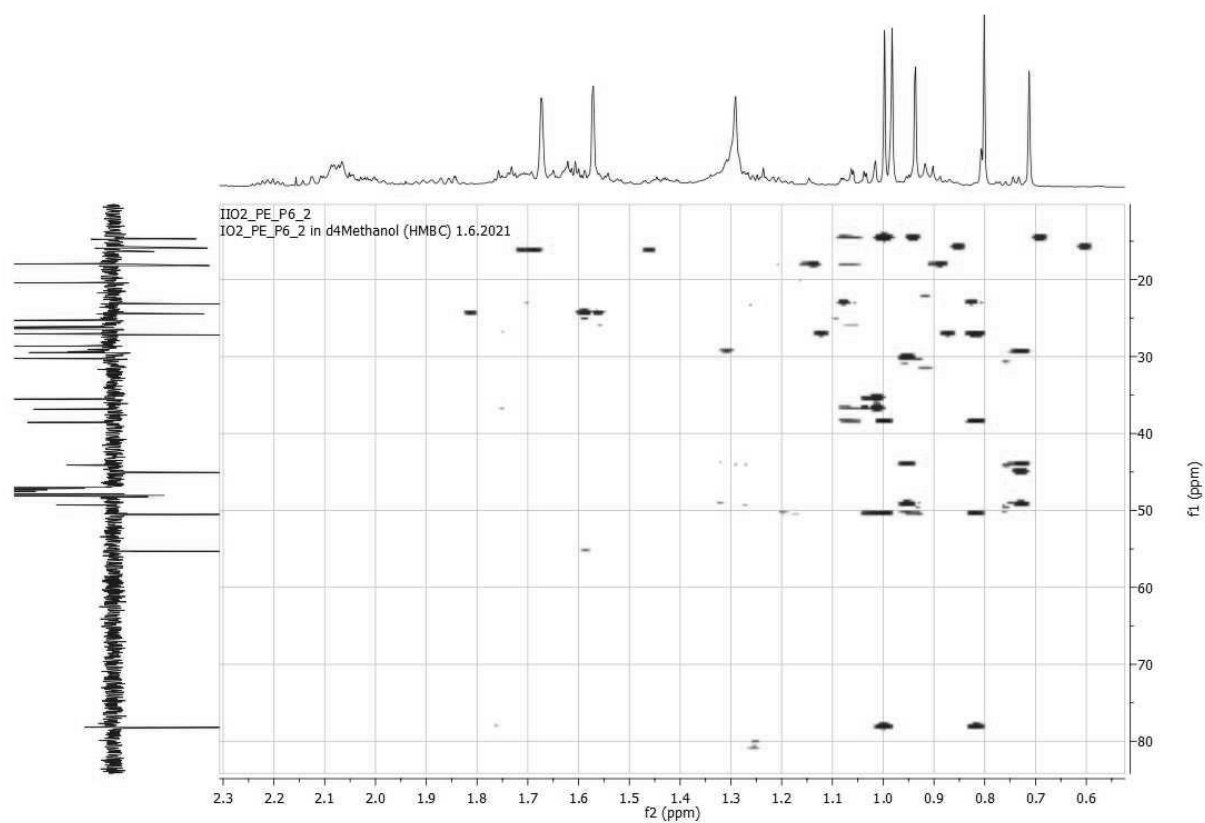
HSQC





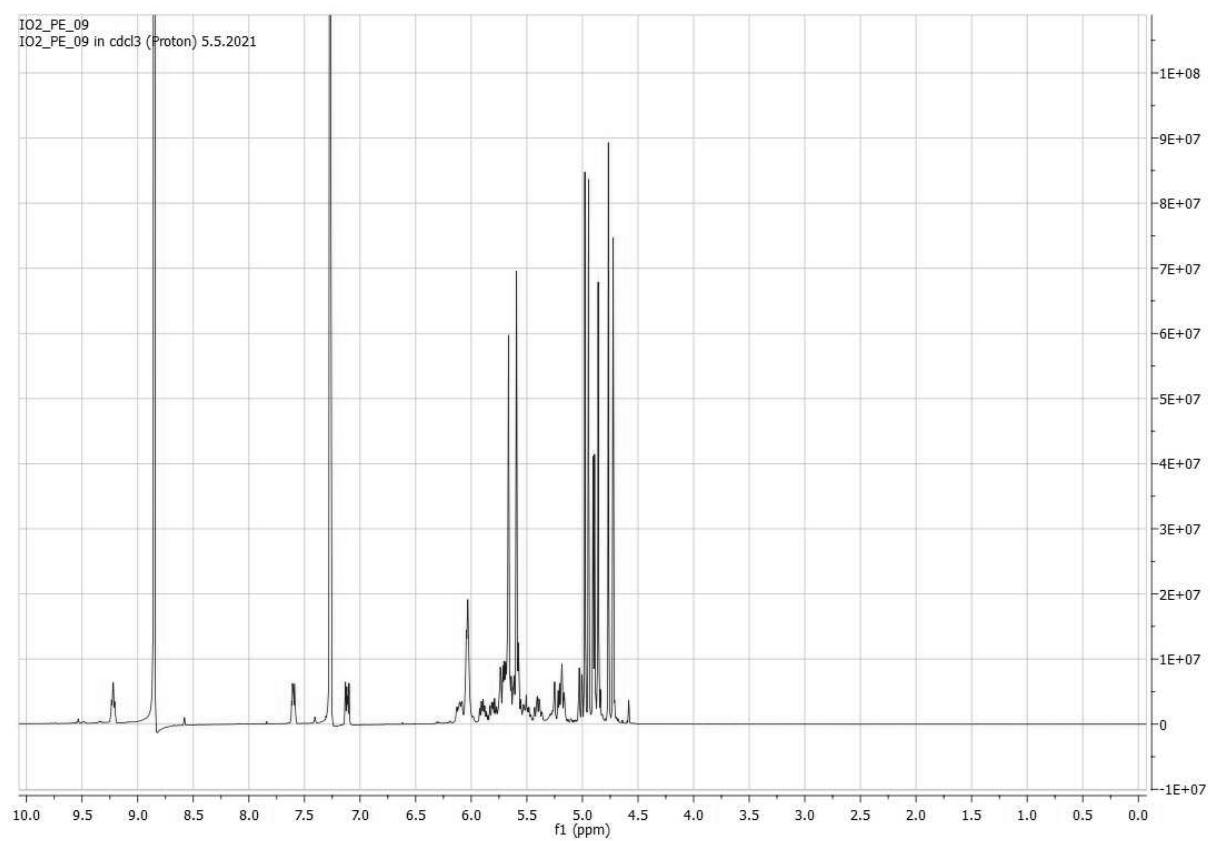
HMBC



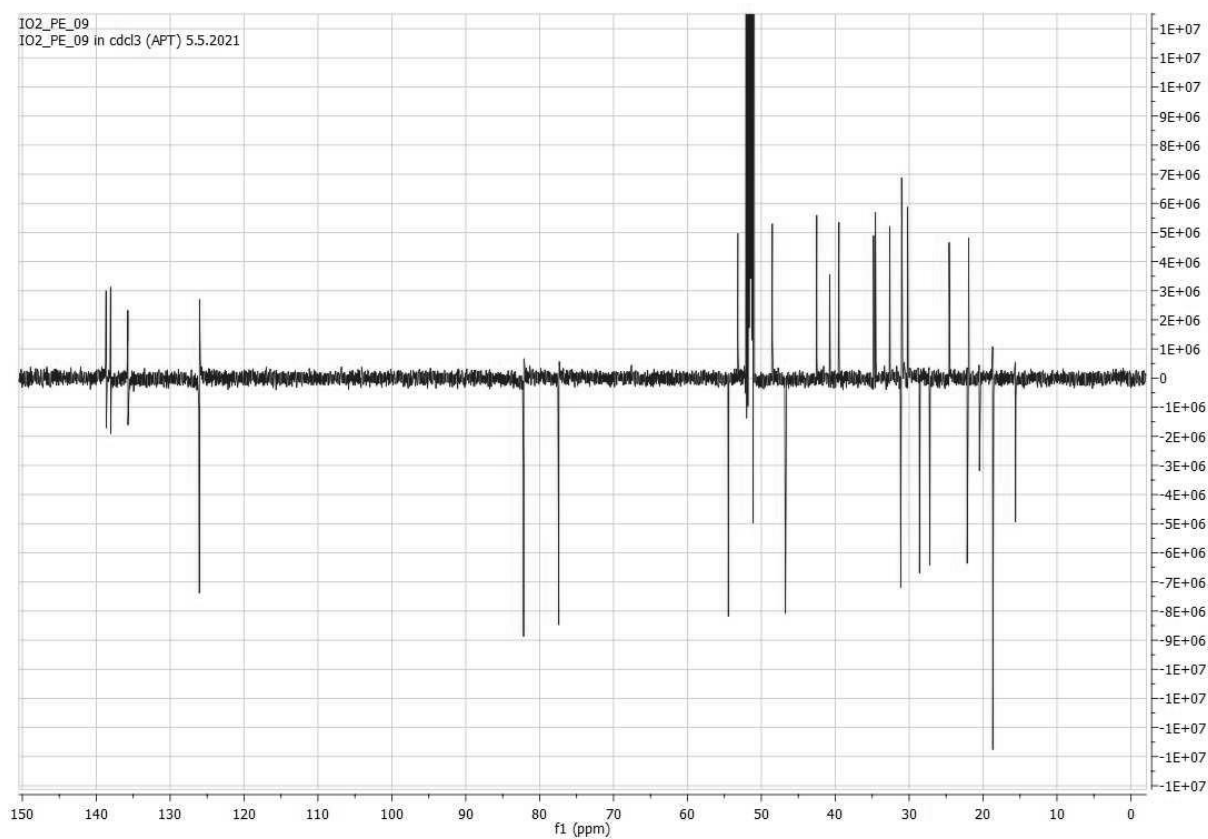


IO#2_PE_9

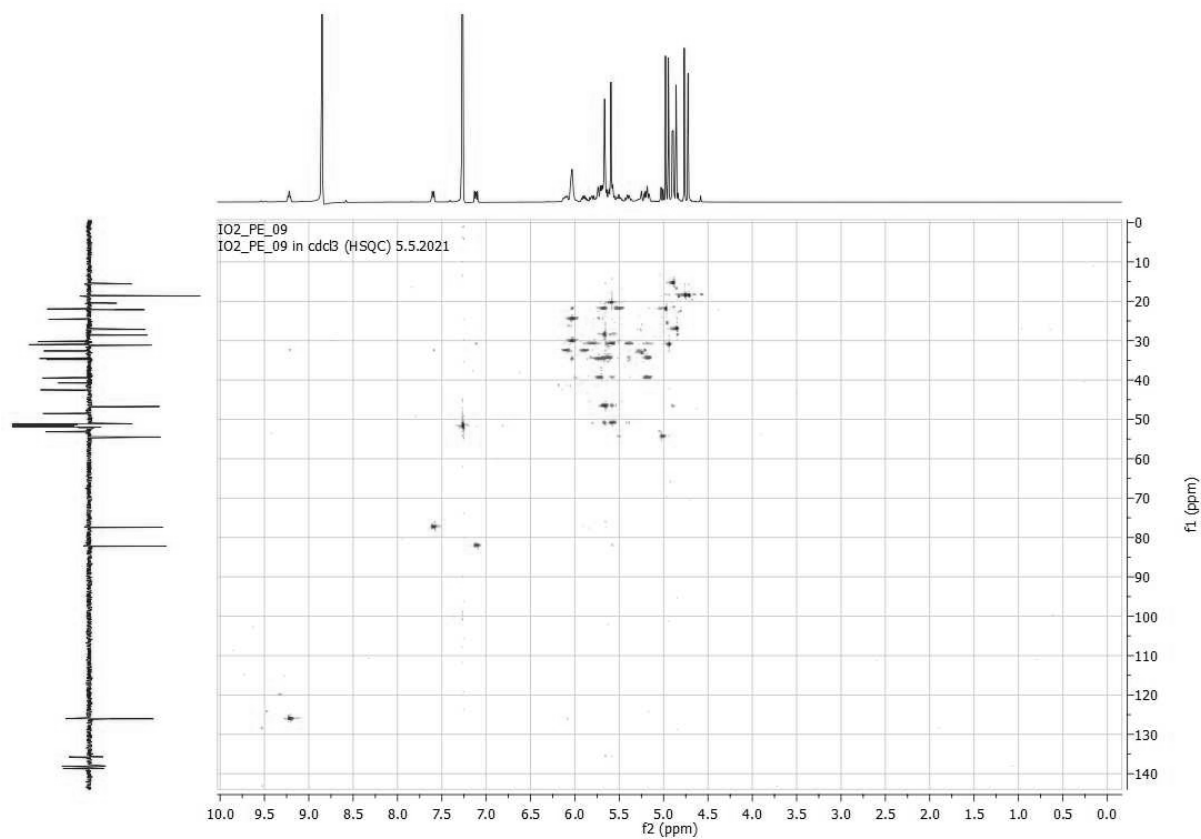
^1H

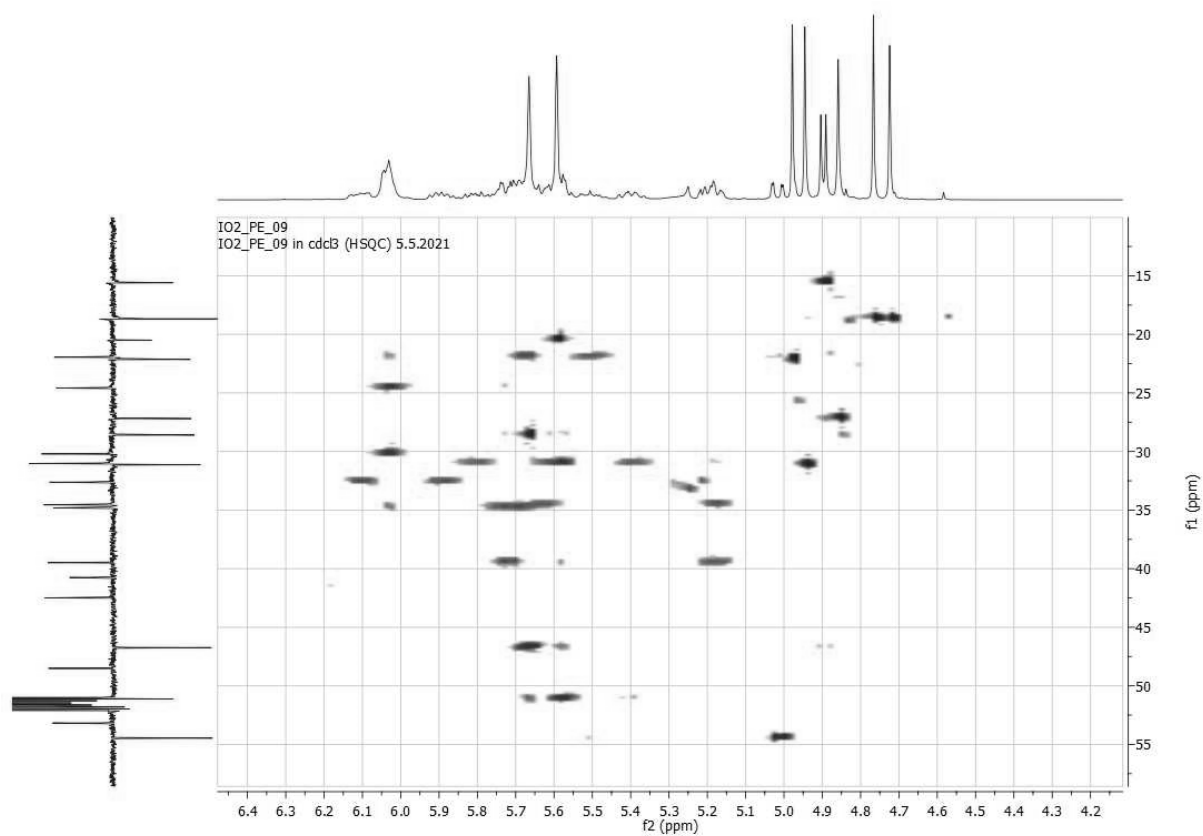


^{13}C

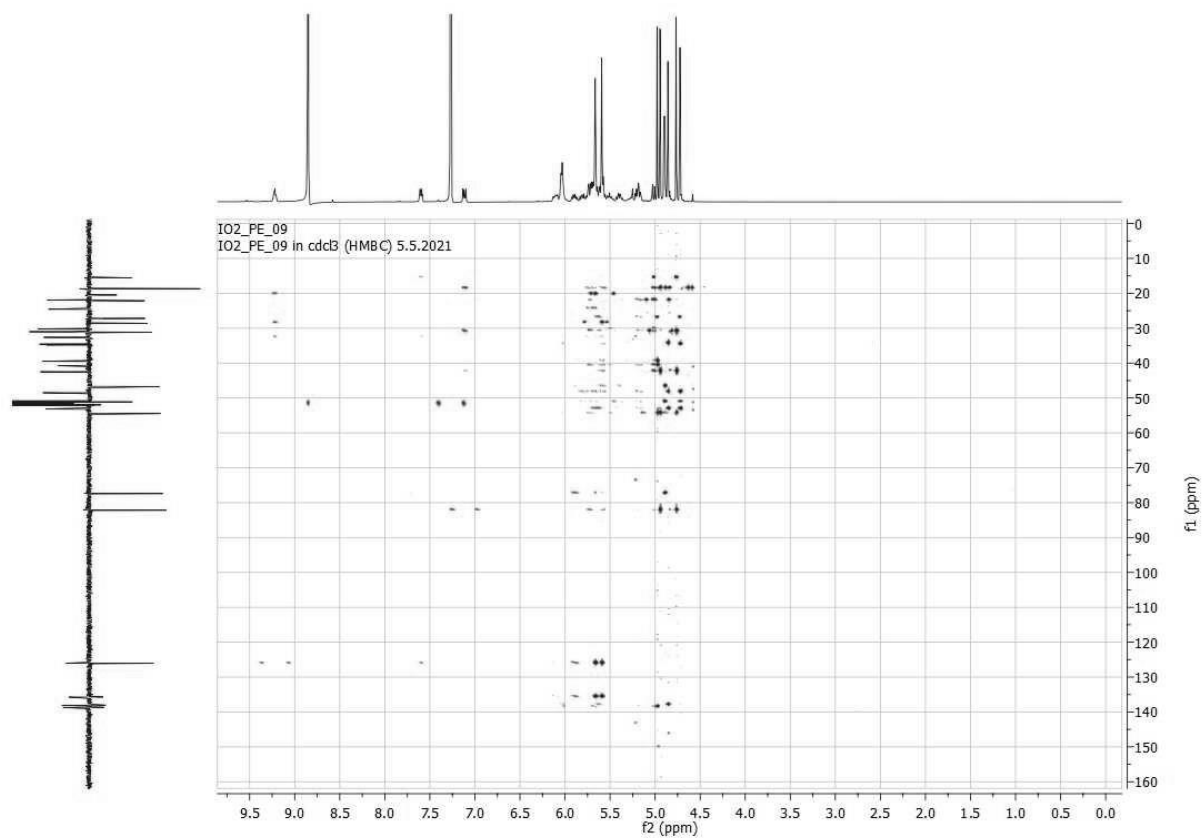


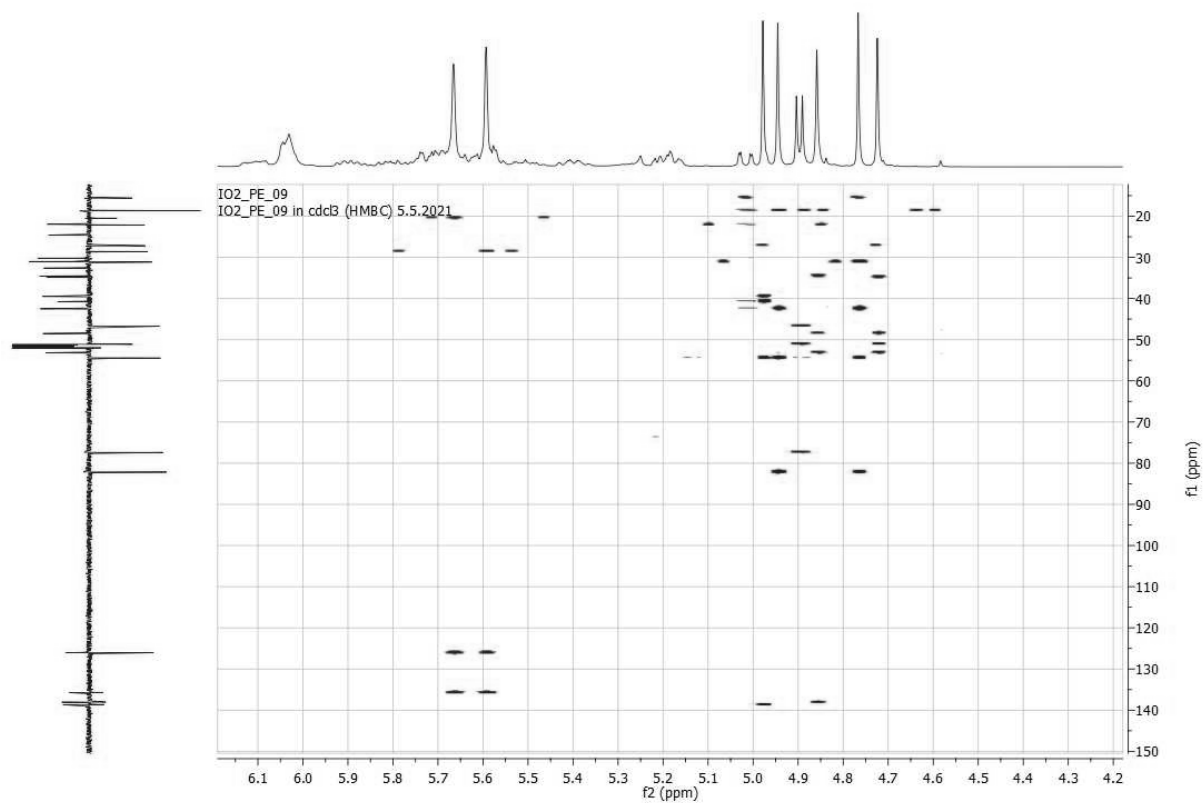
HSQC





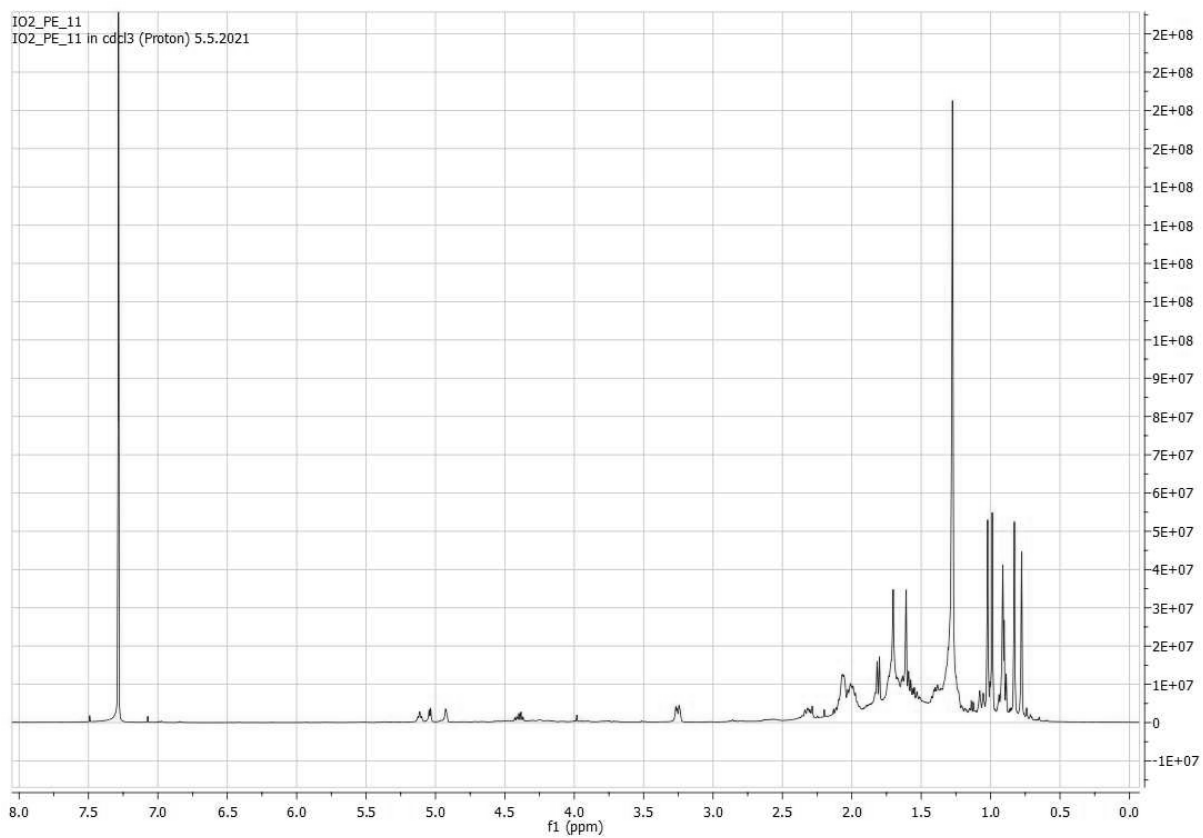
HMBC



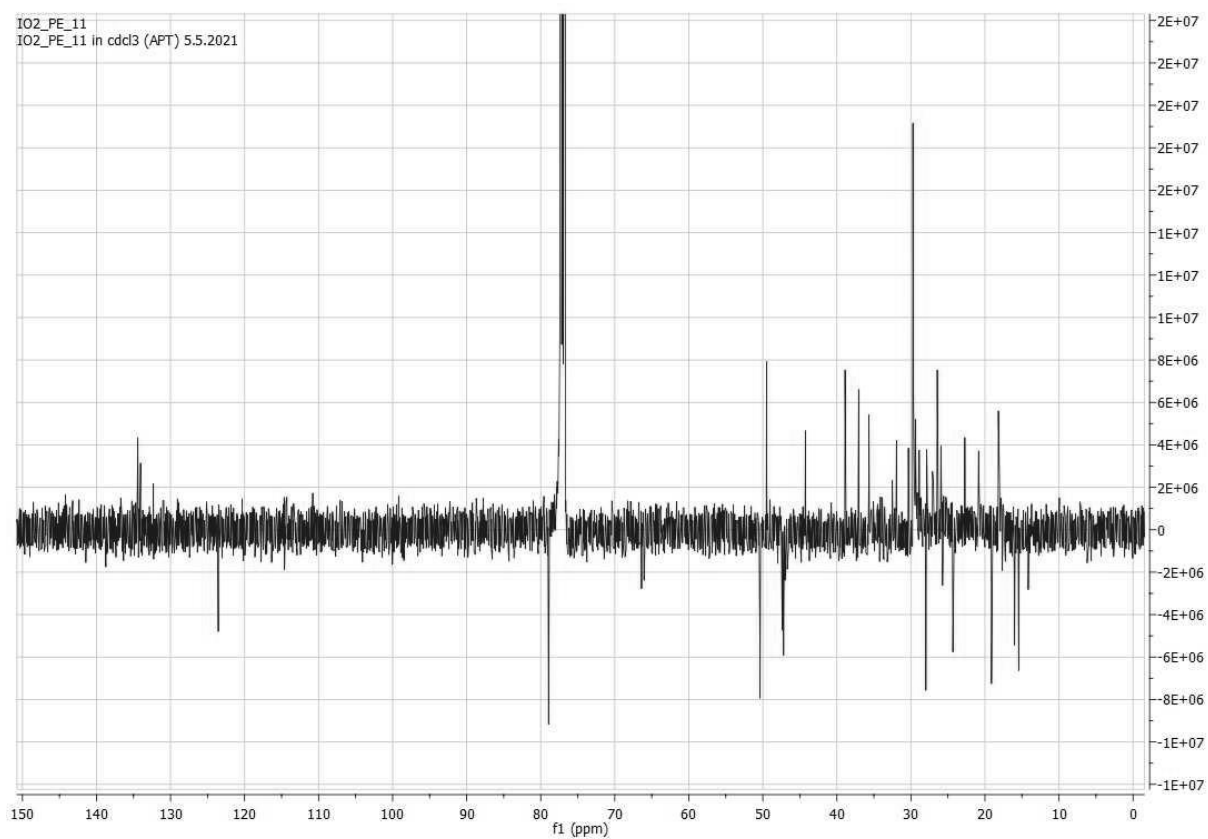


IO#2_PE_11

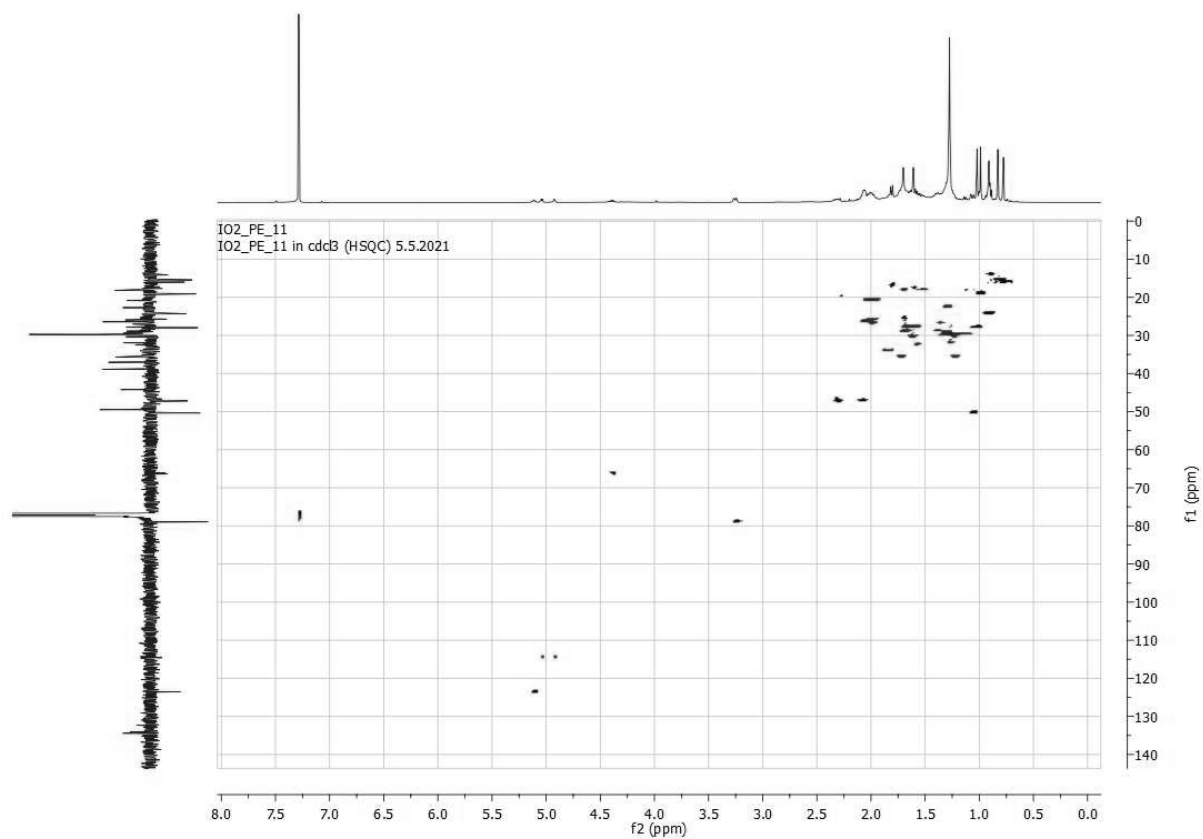
^1H

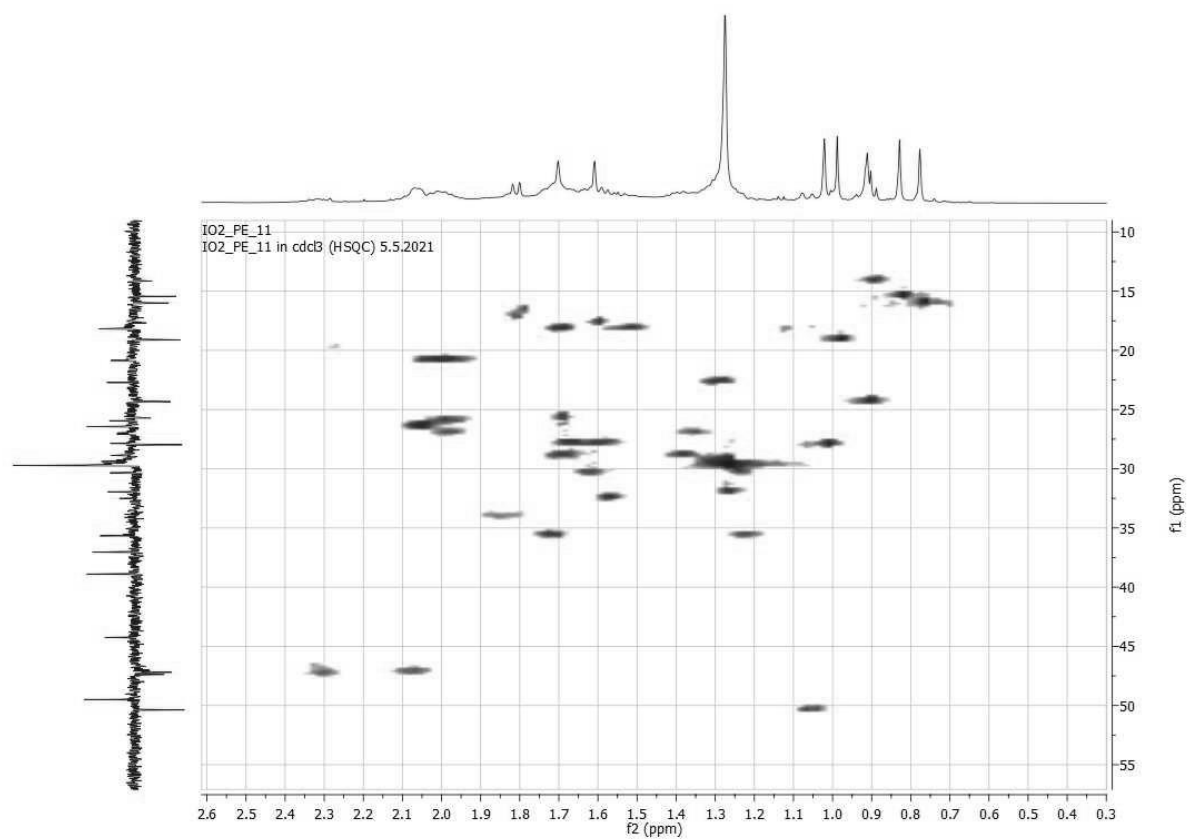


^{13}C

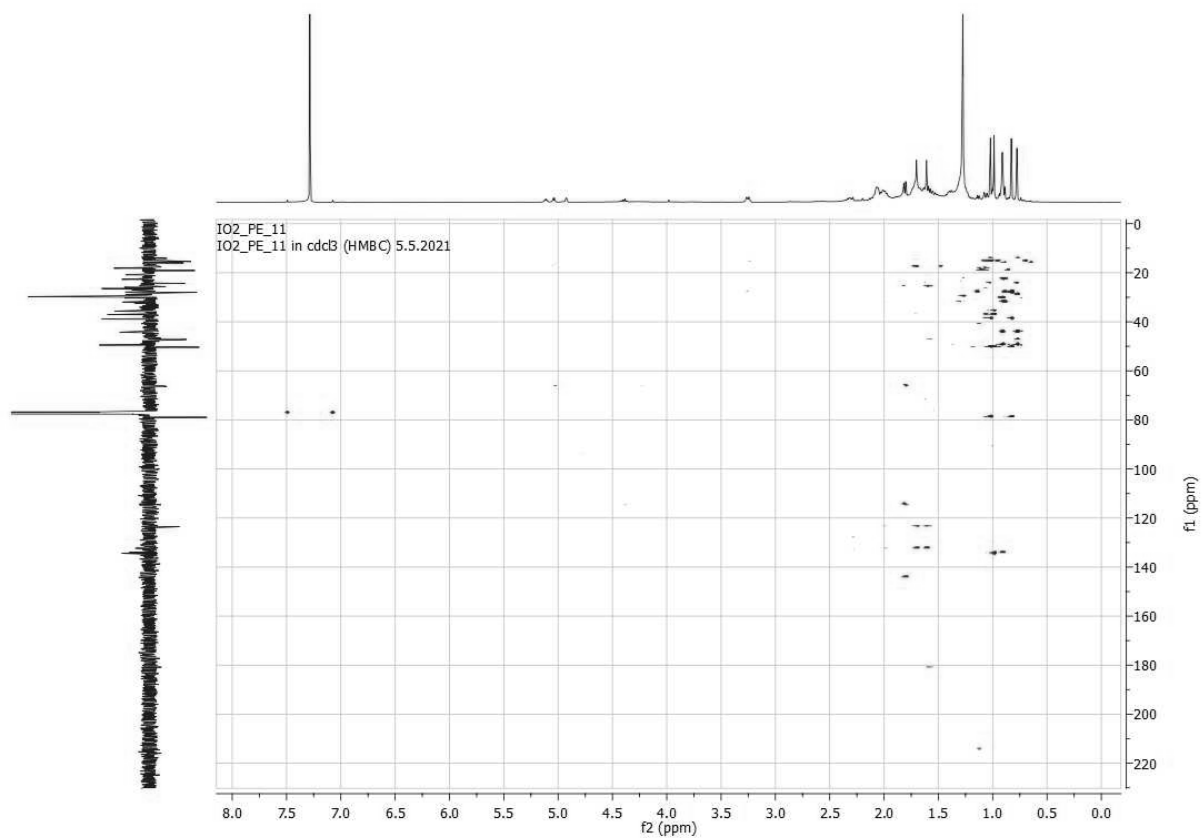


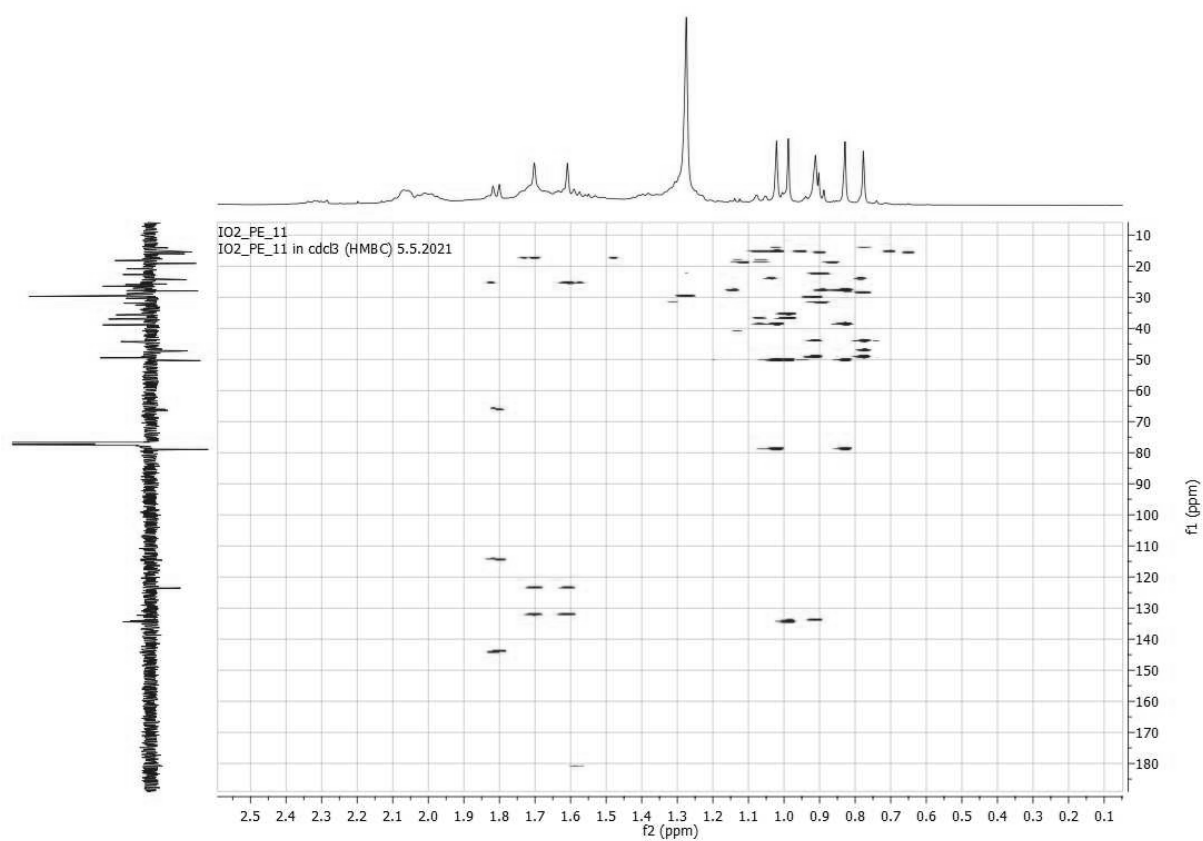
HSQC





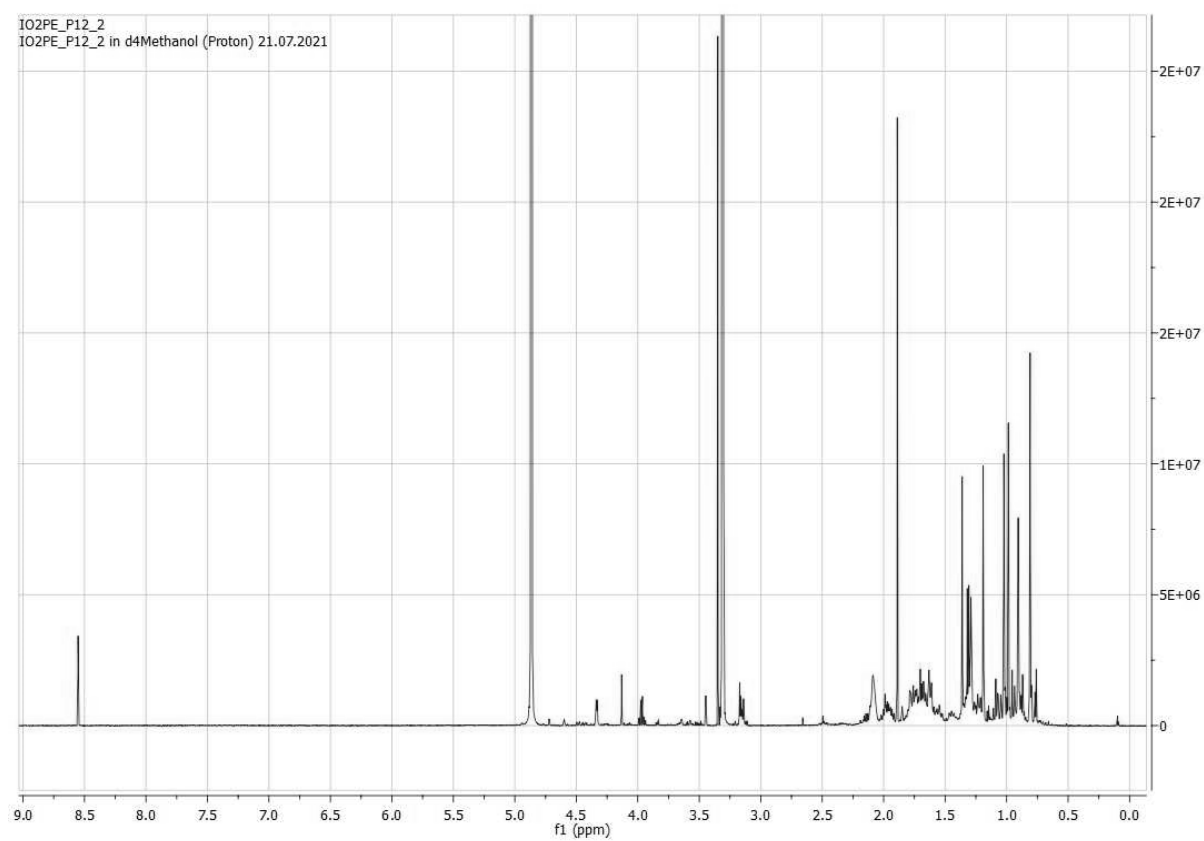
HMBC



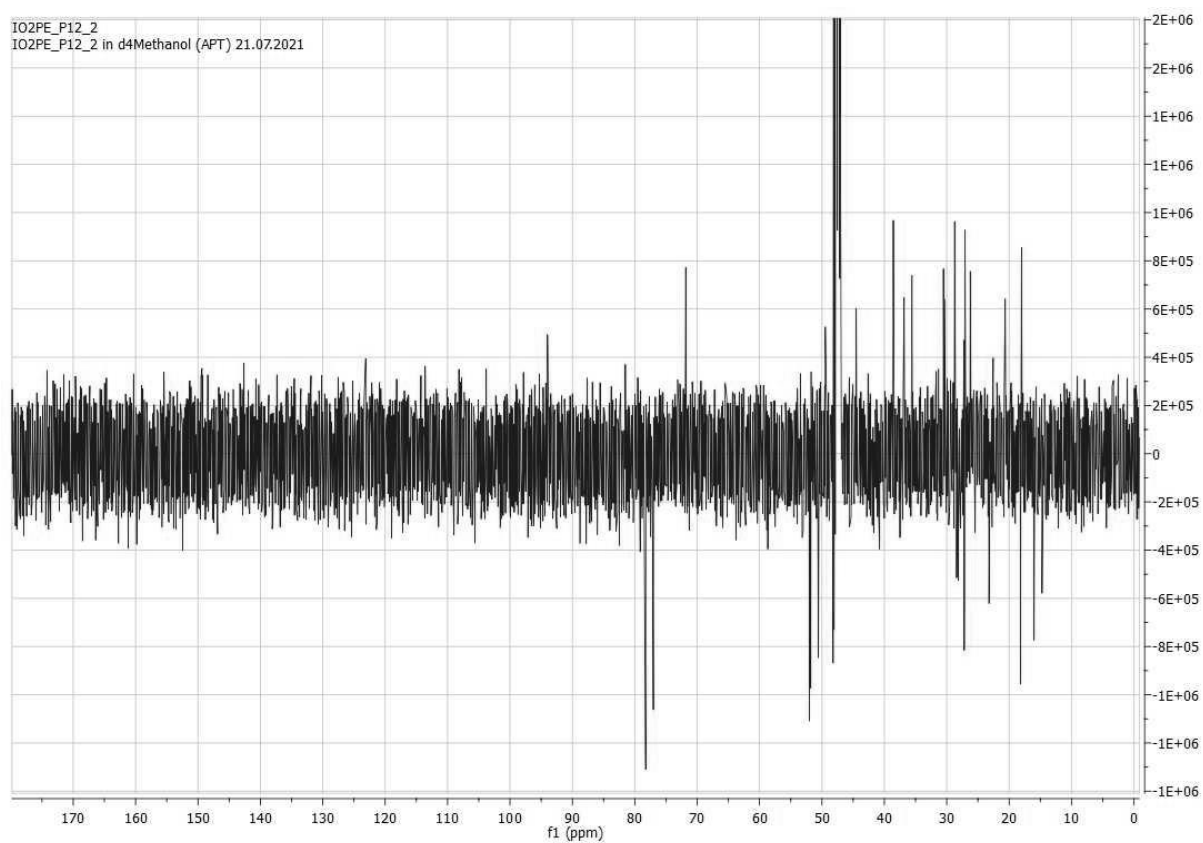


IO#2_PE_12_2

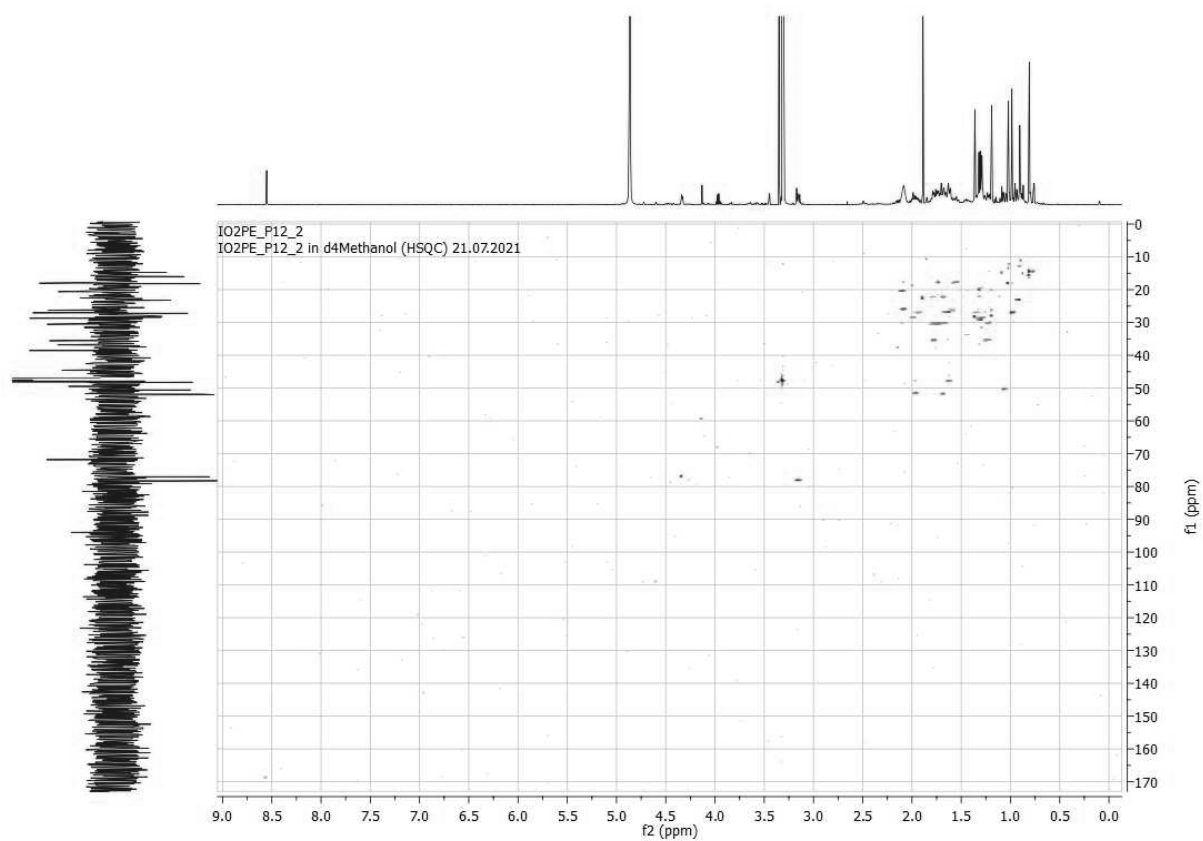
^1H

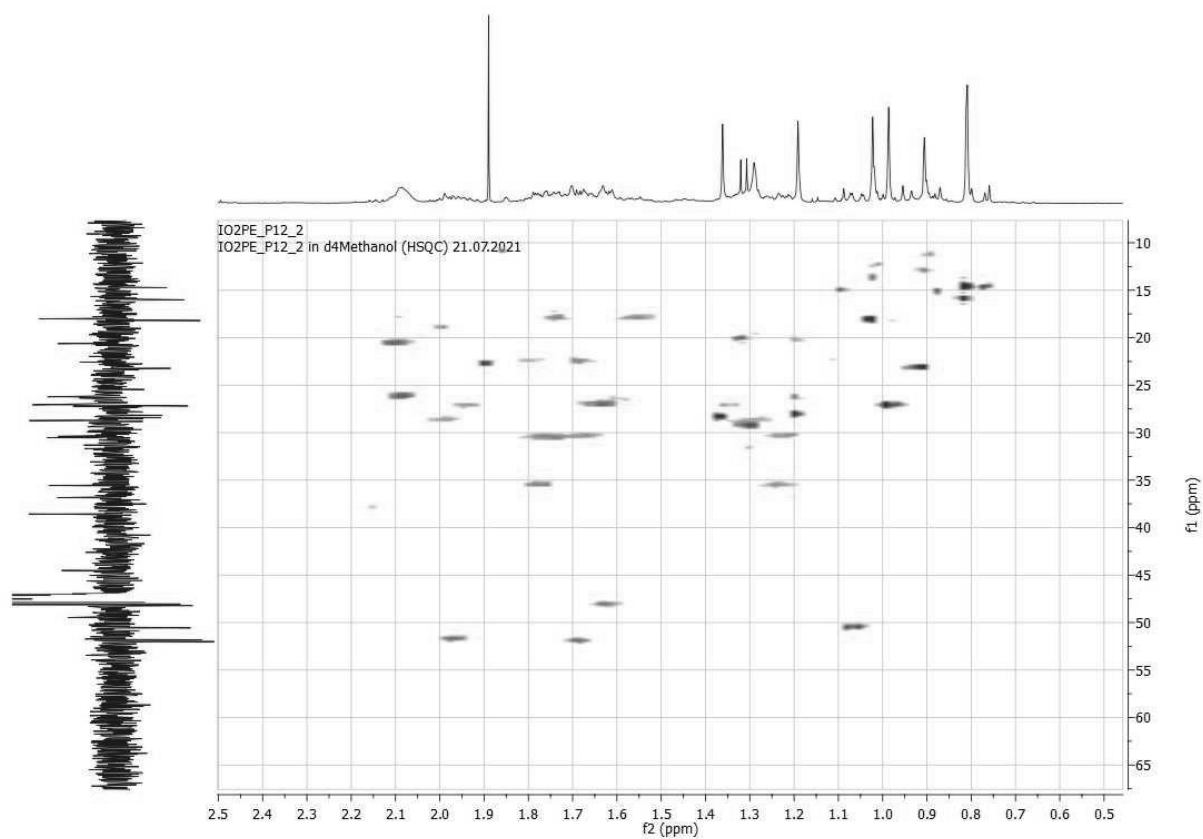


^{13}C

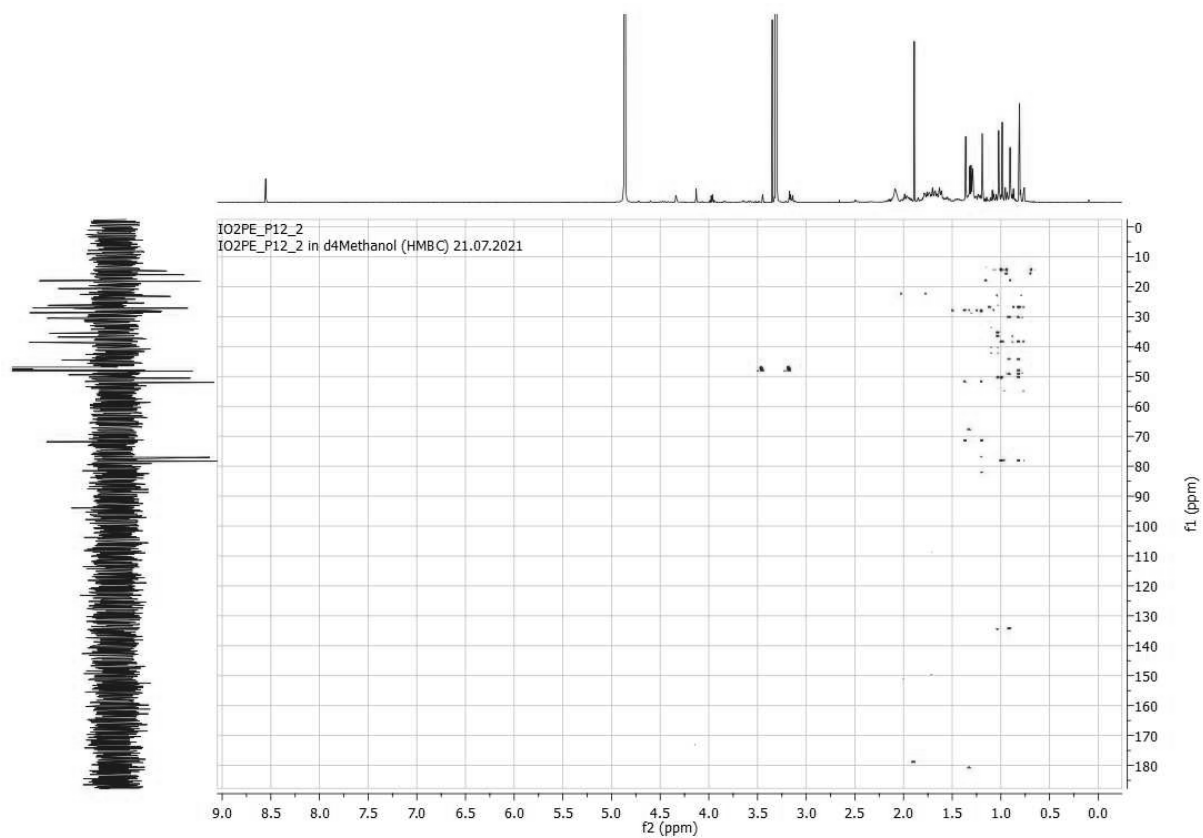


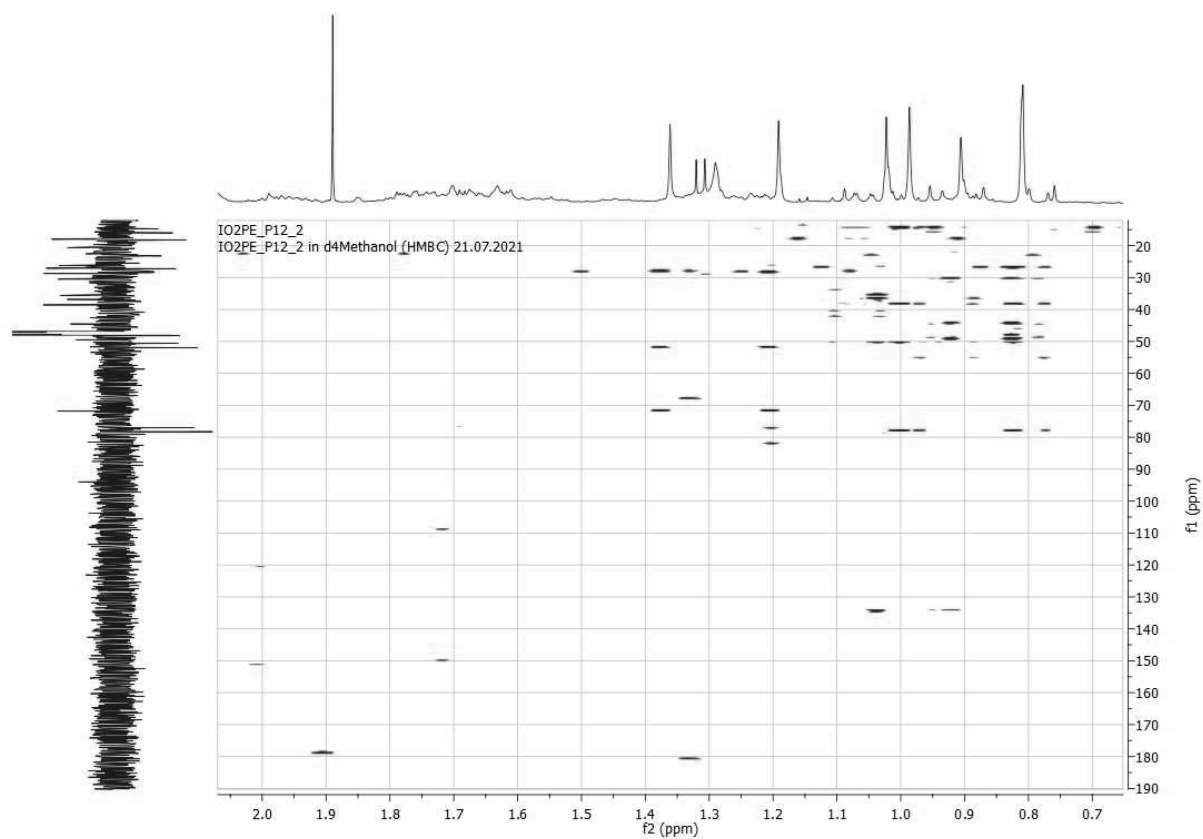
HSQC





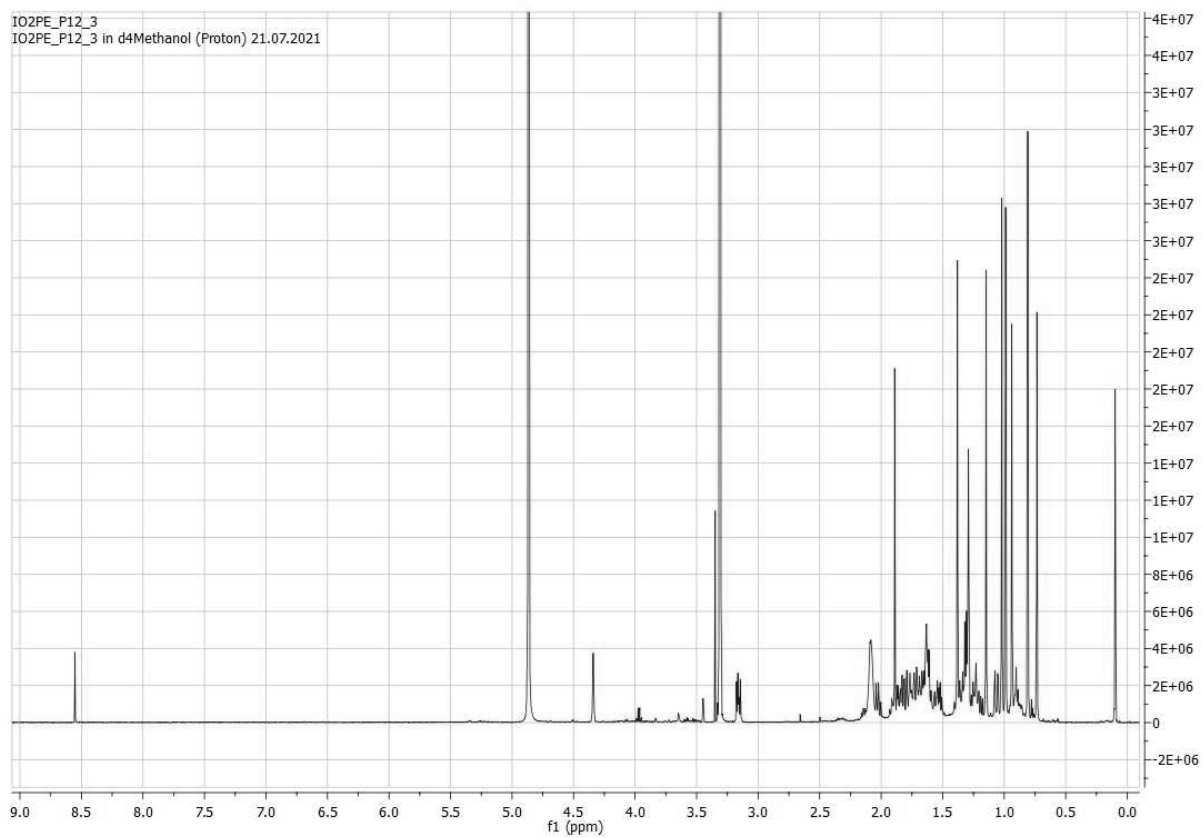
HMBC



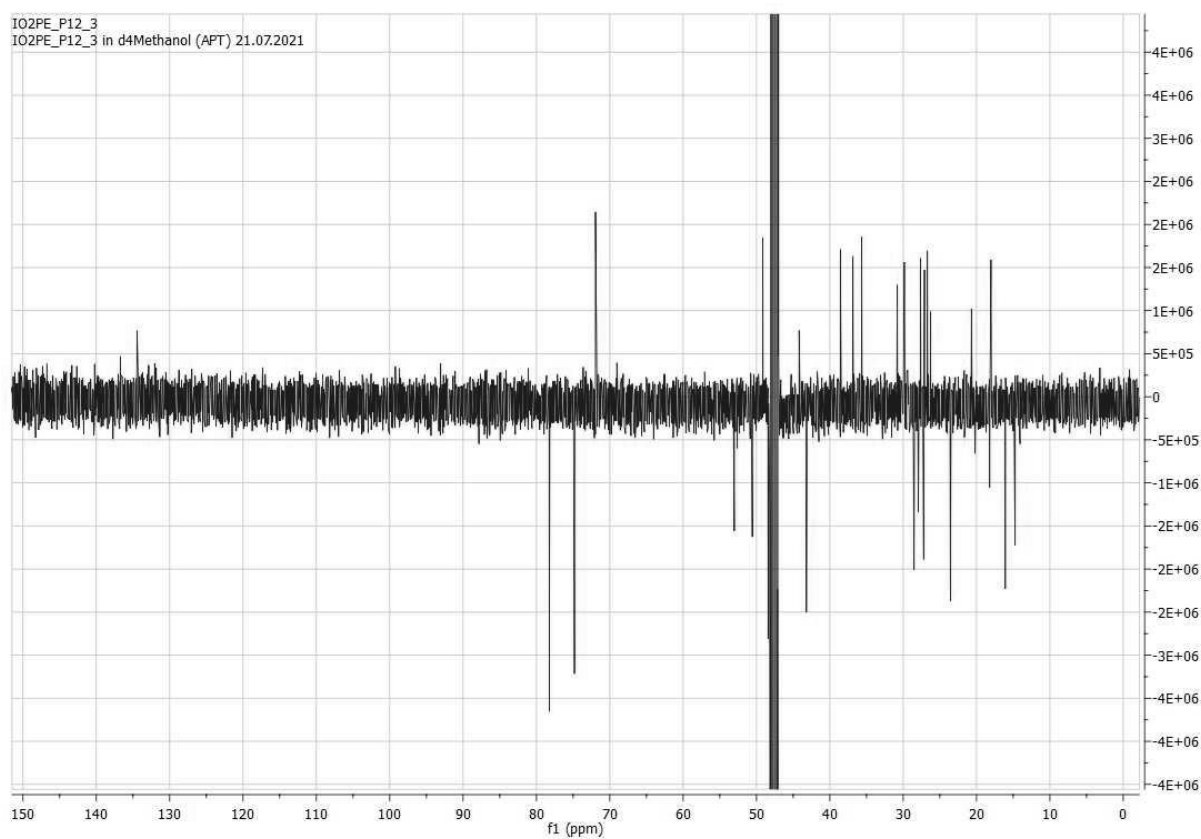


IO#2_PE_12_3

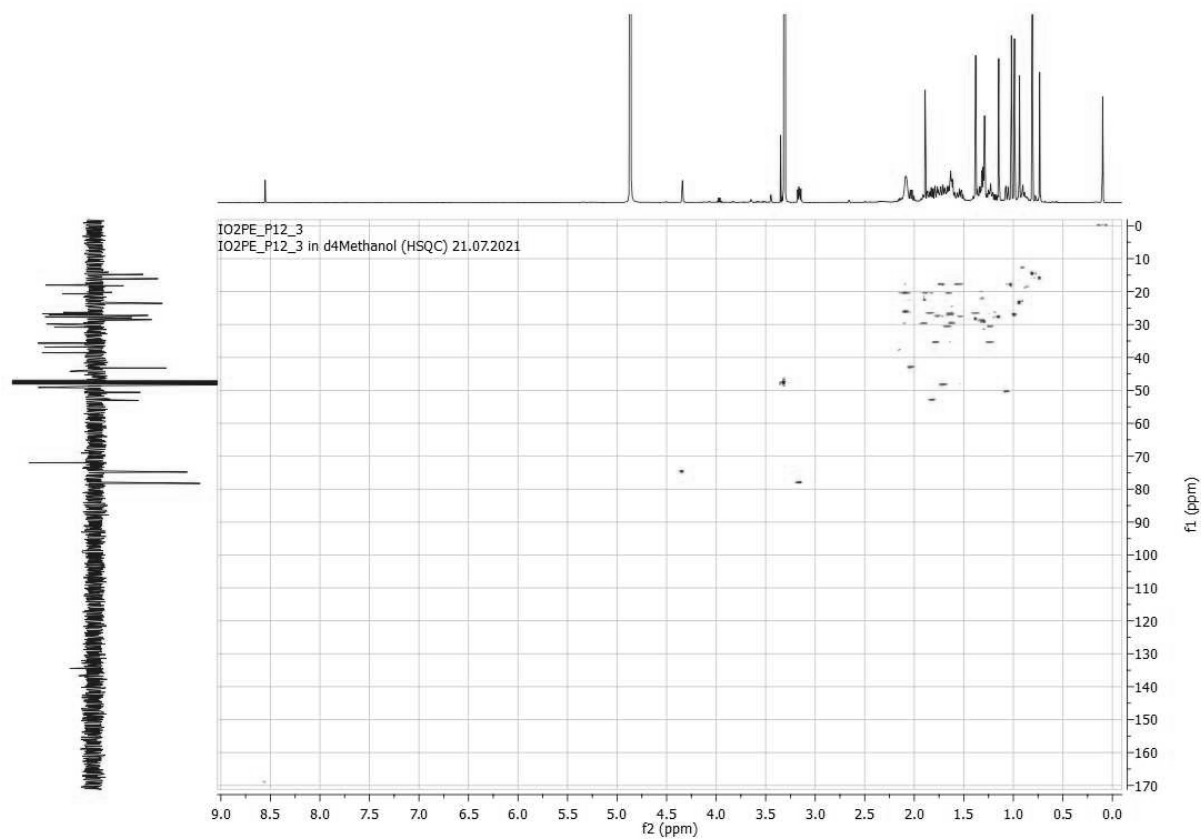
^1H

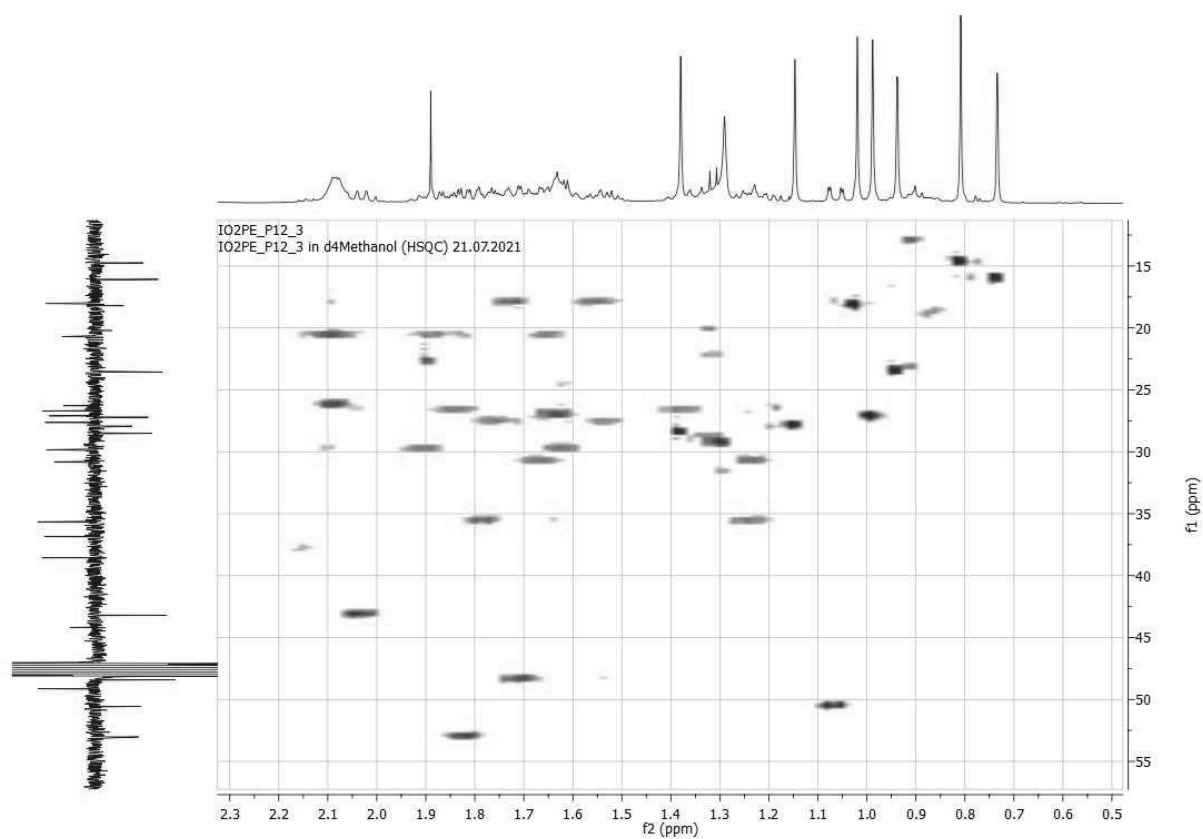


^{13}C

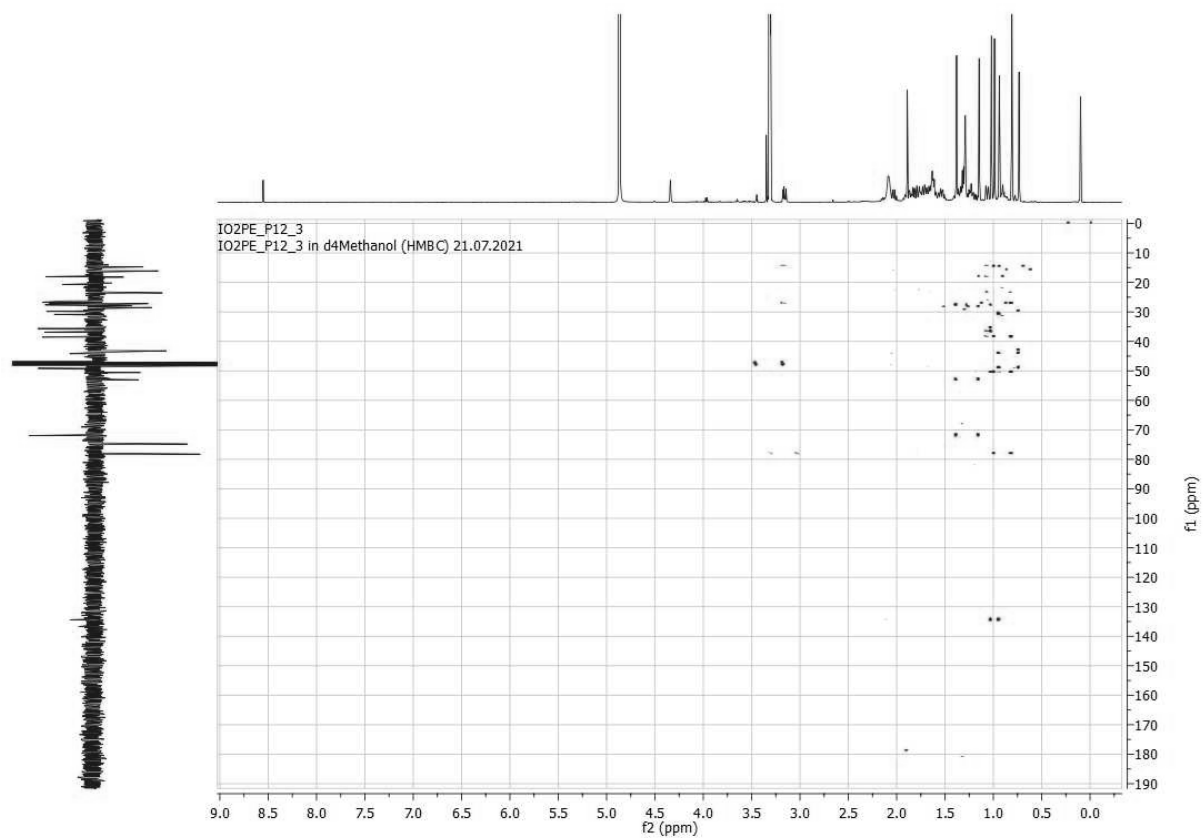


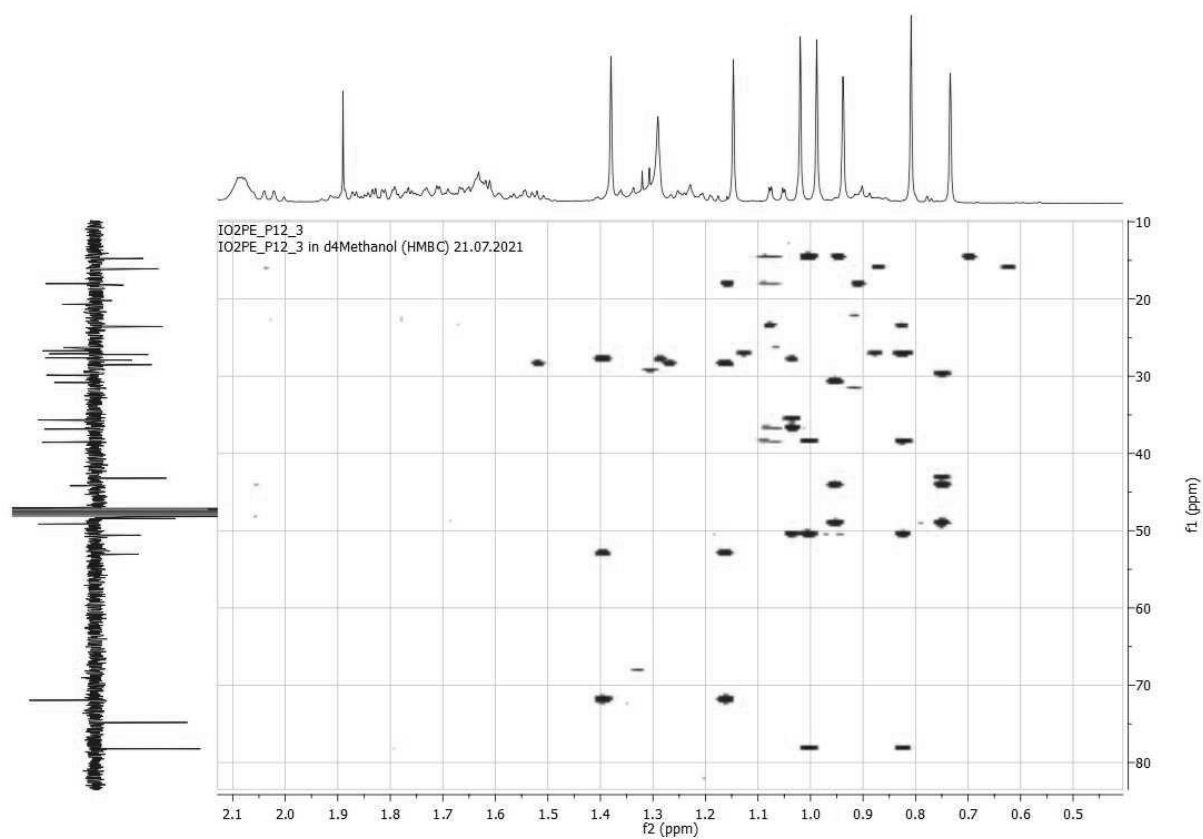
HSQC





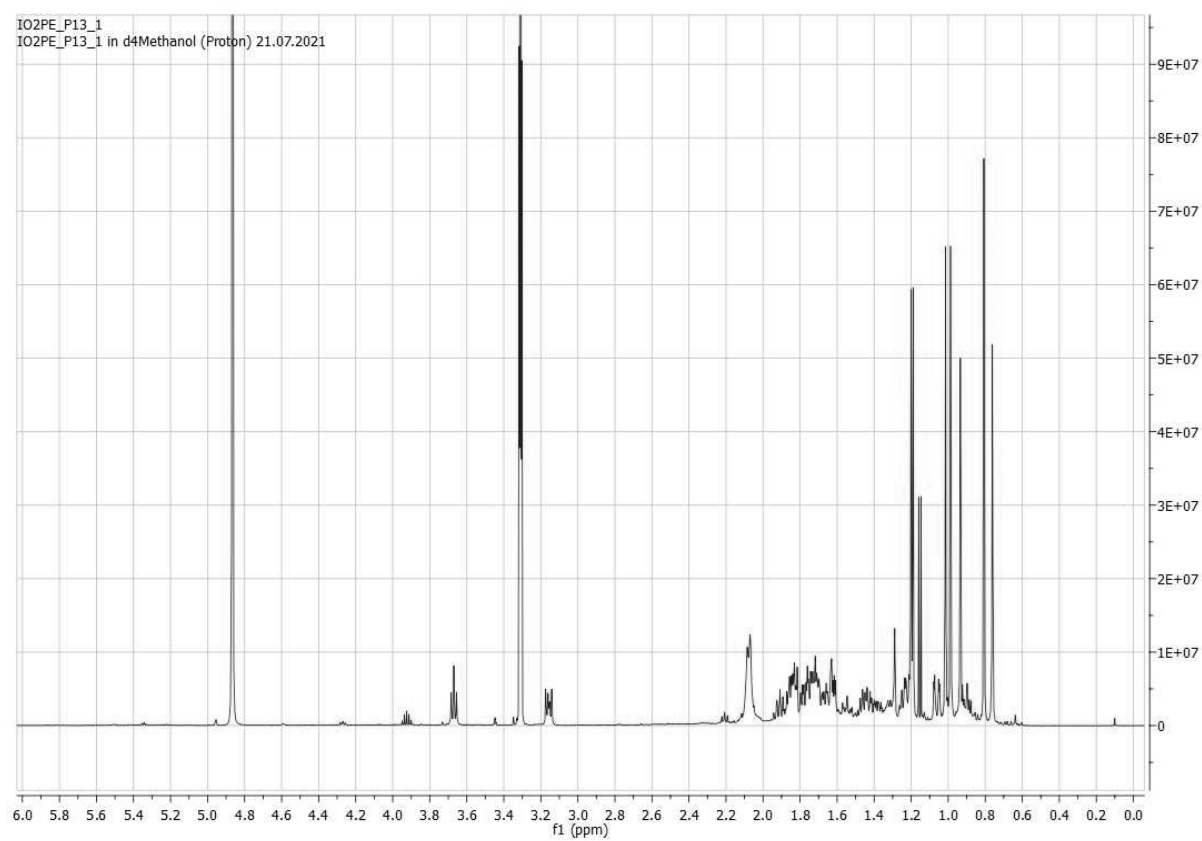
HMBC



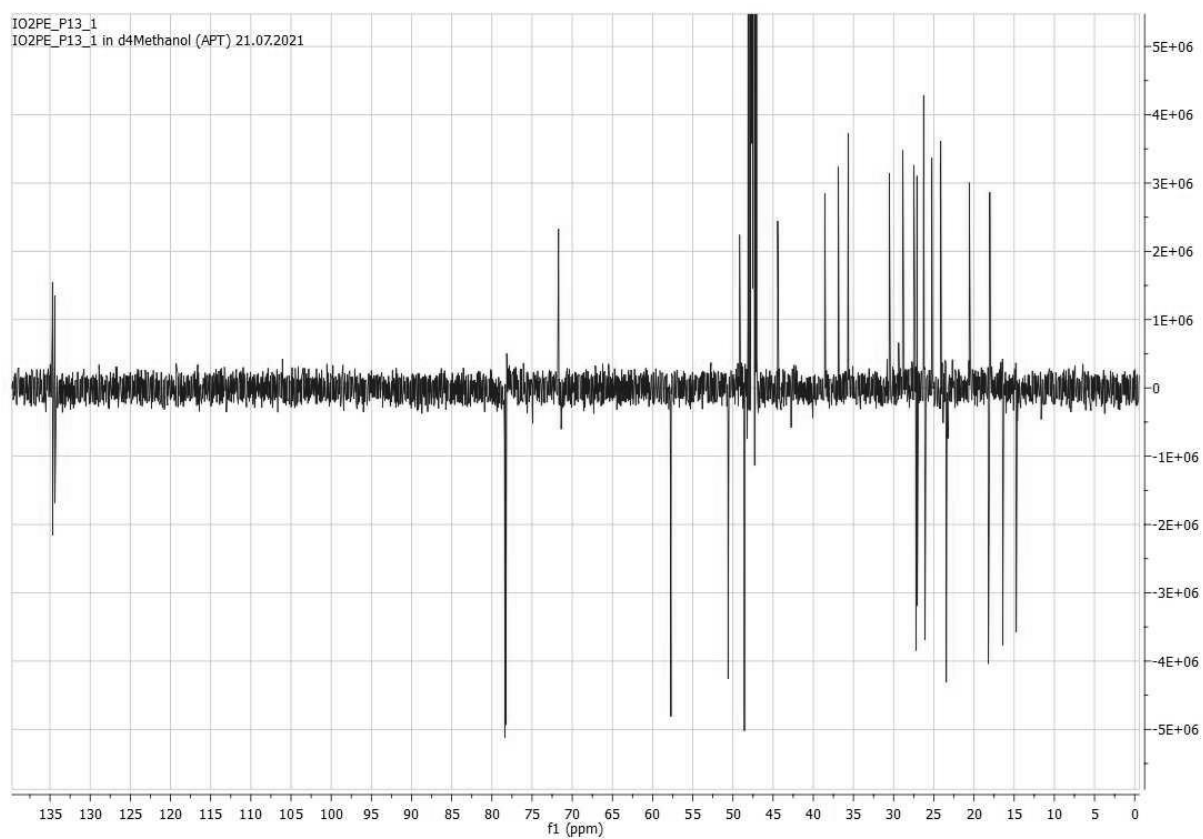


IO#2_PE_13_1

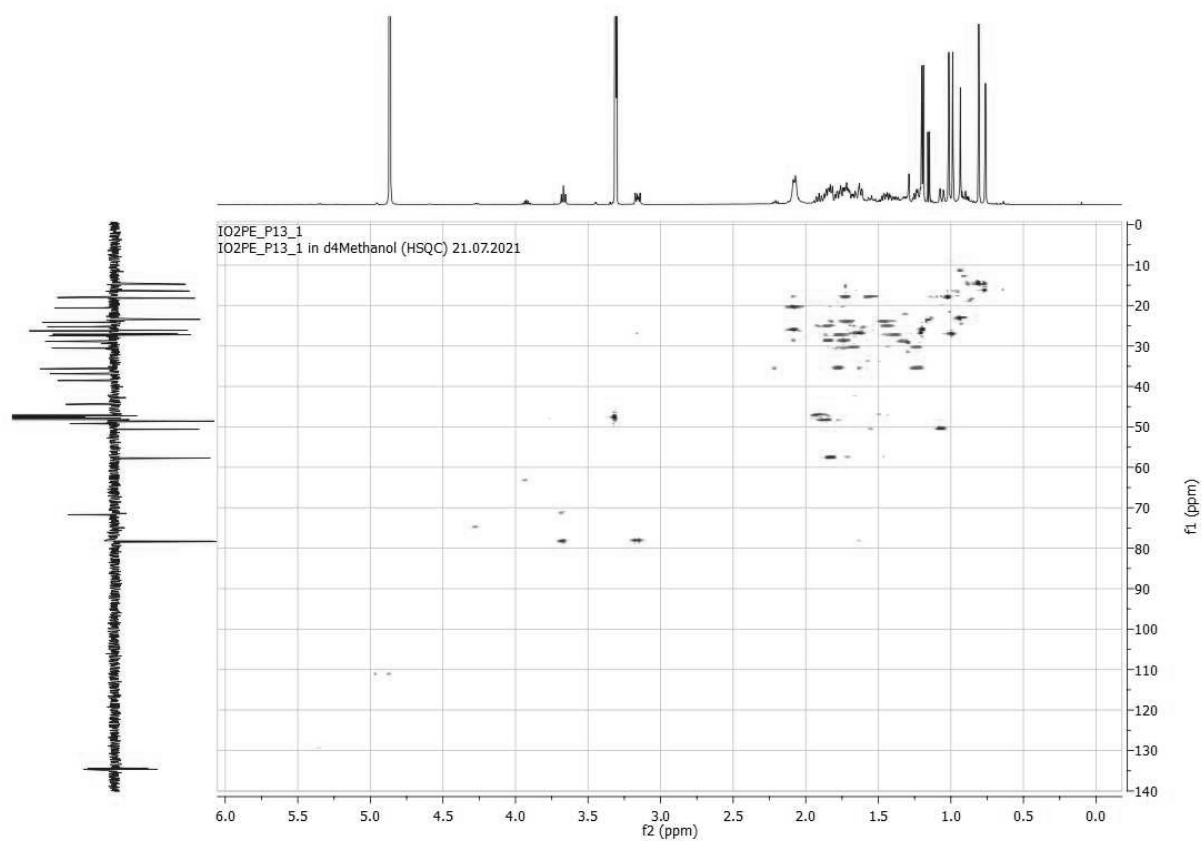
¹H

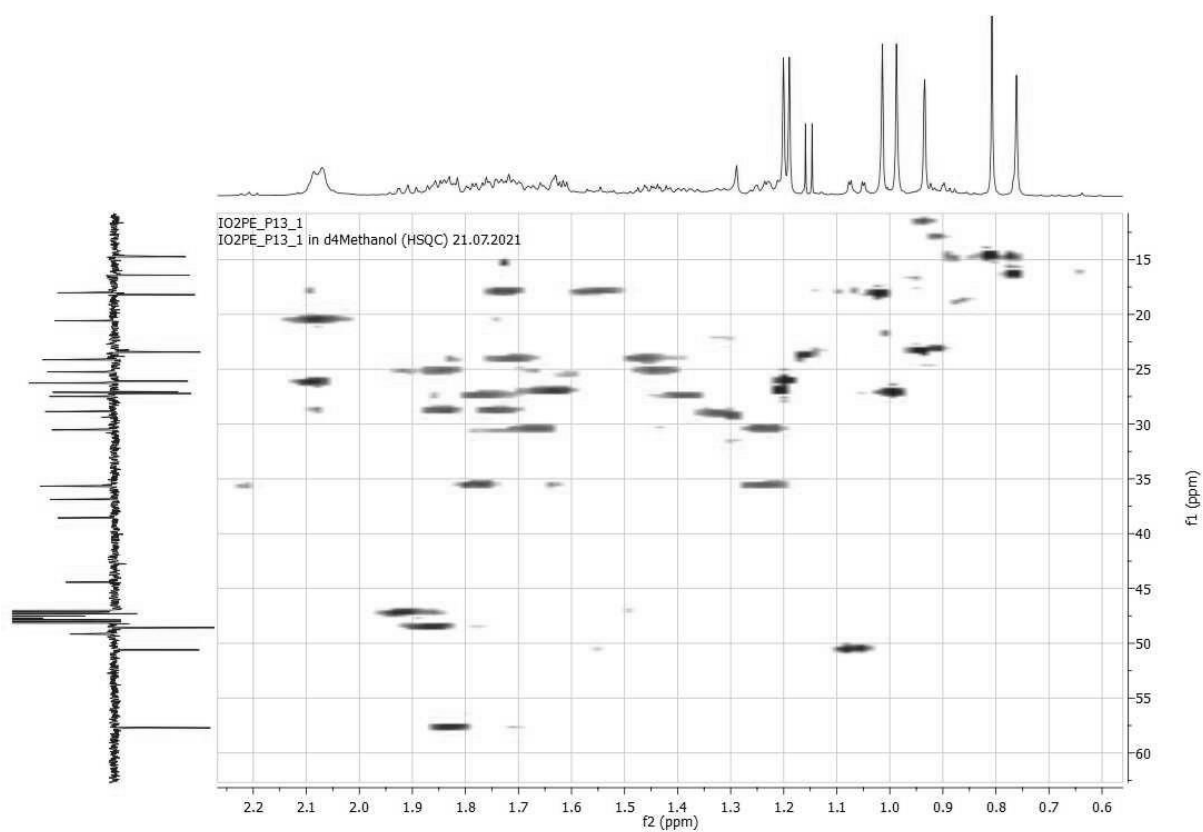


^{13}C

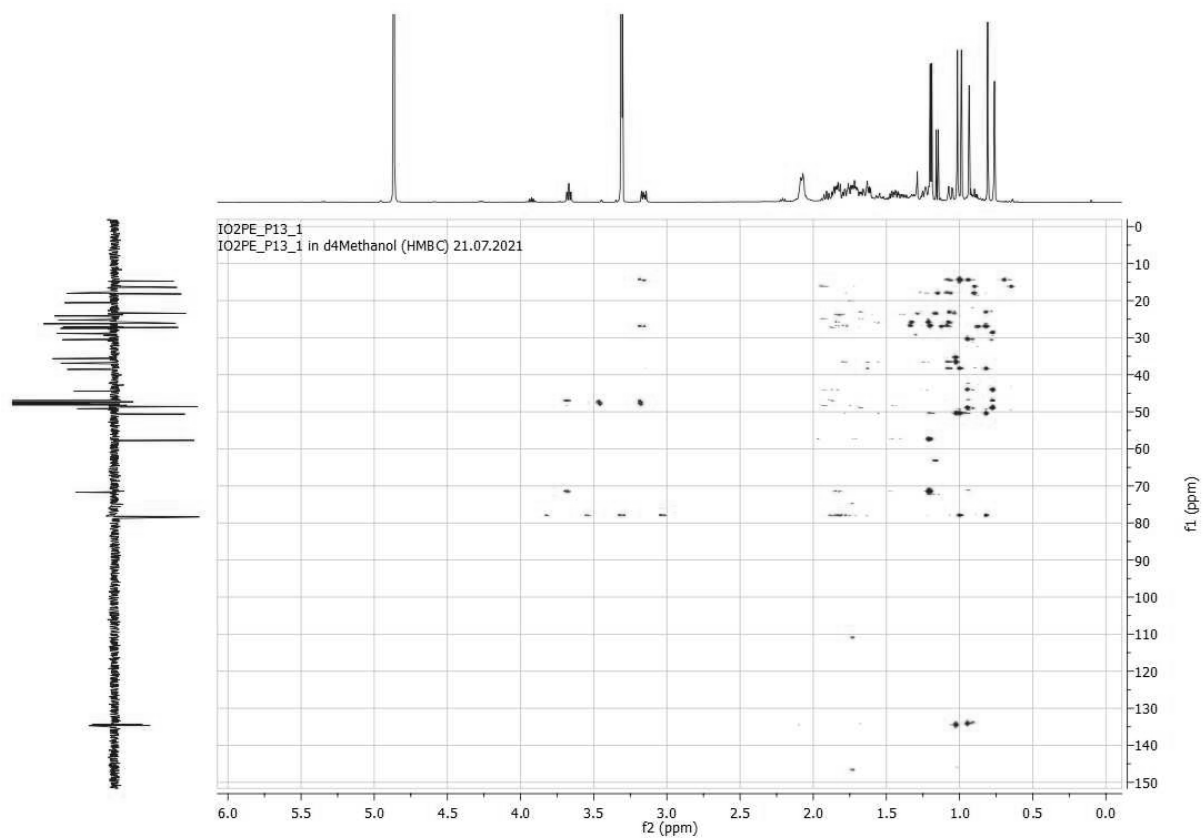


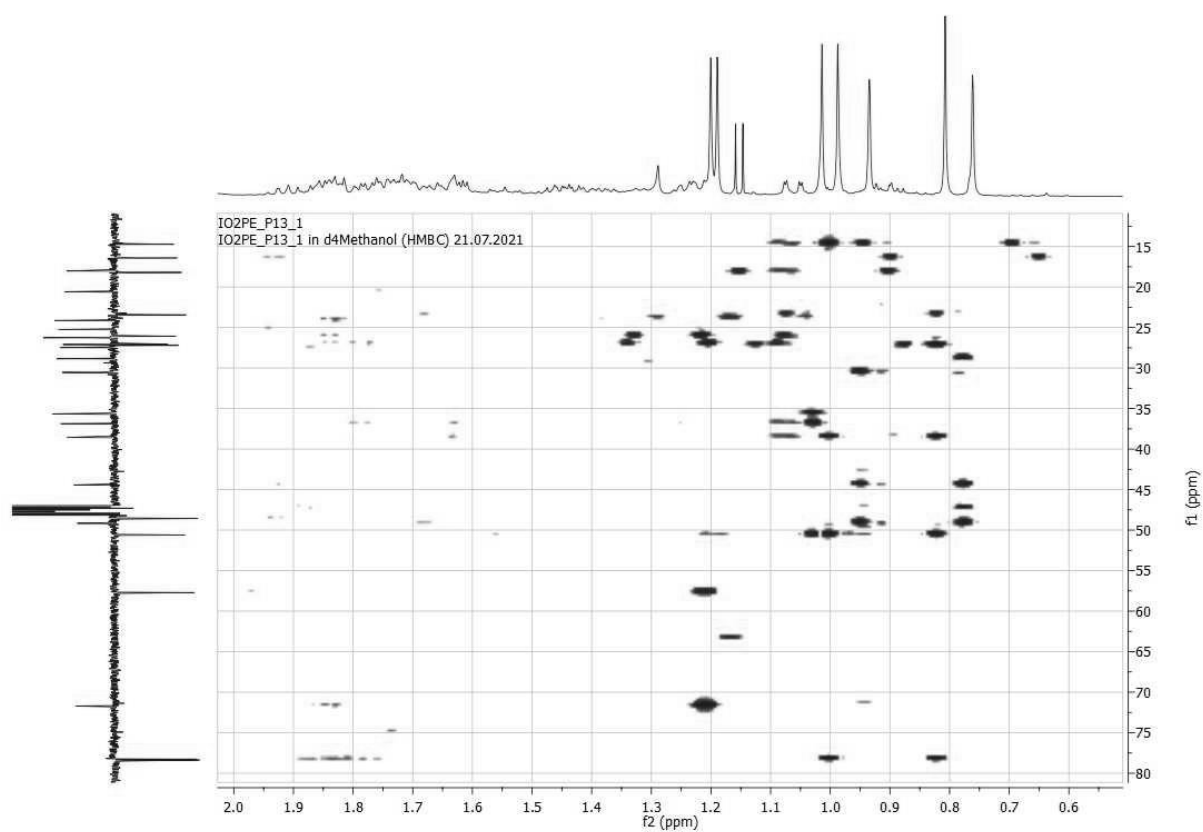
HSQC





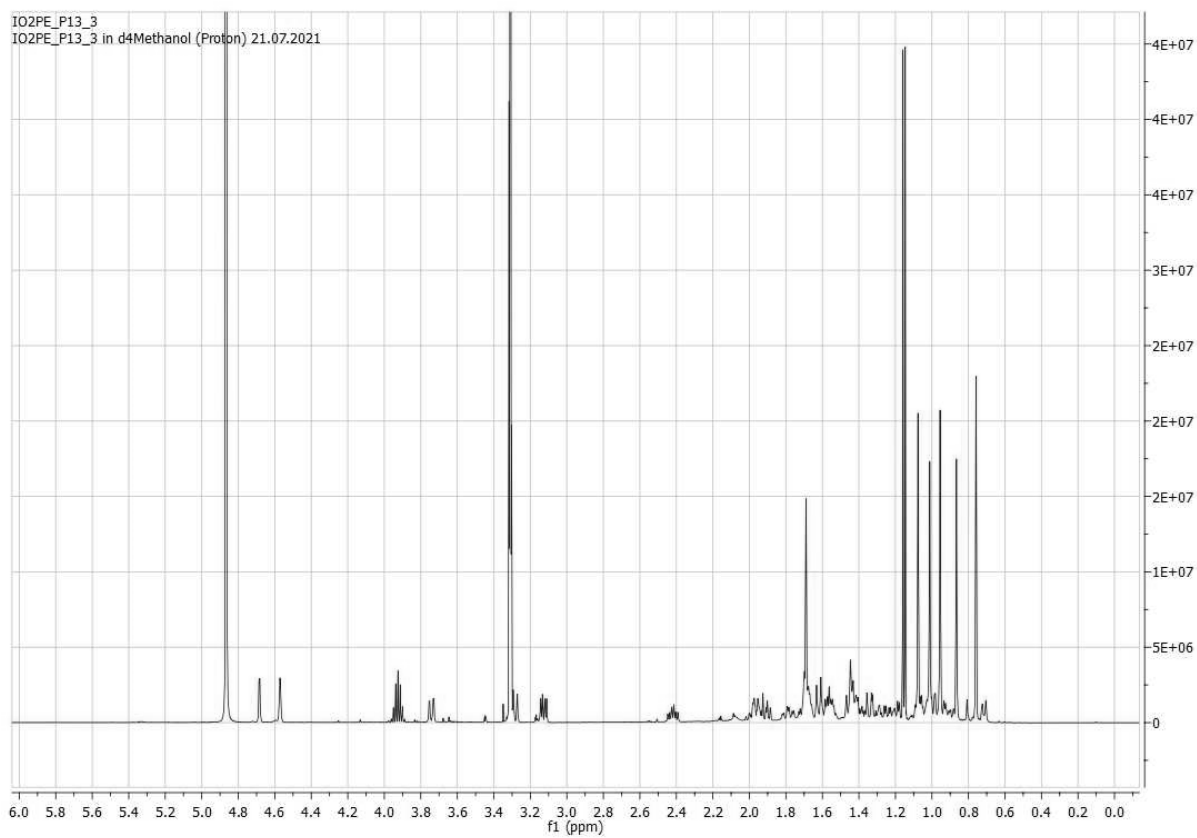
HMBC



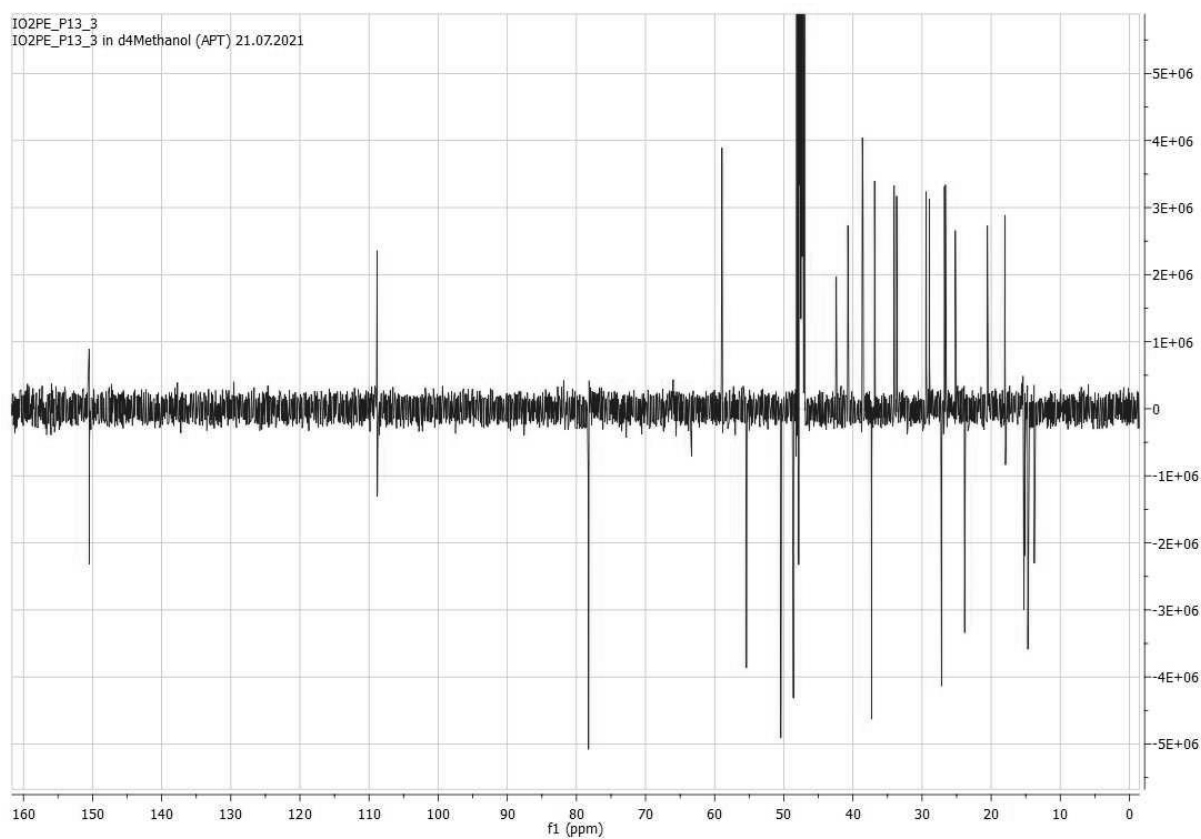


IO#2_PE_13_3

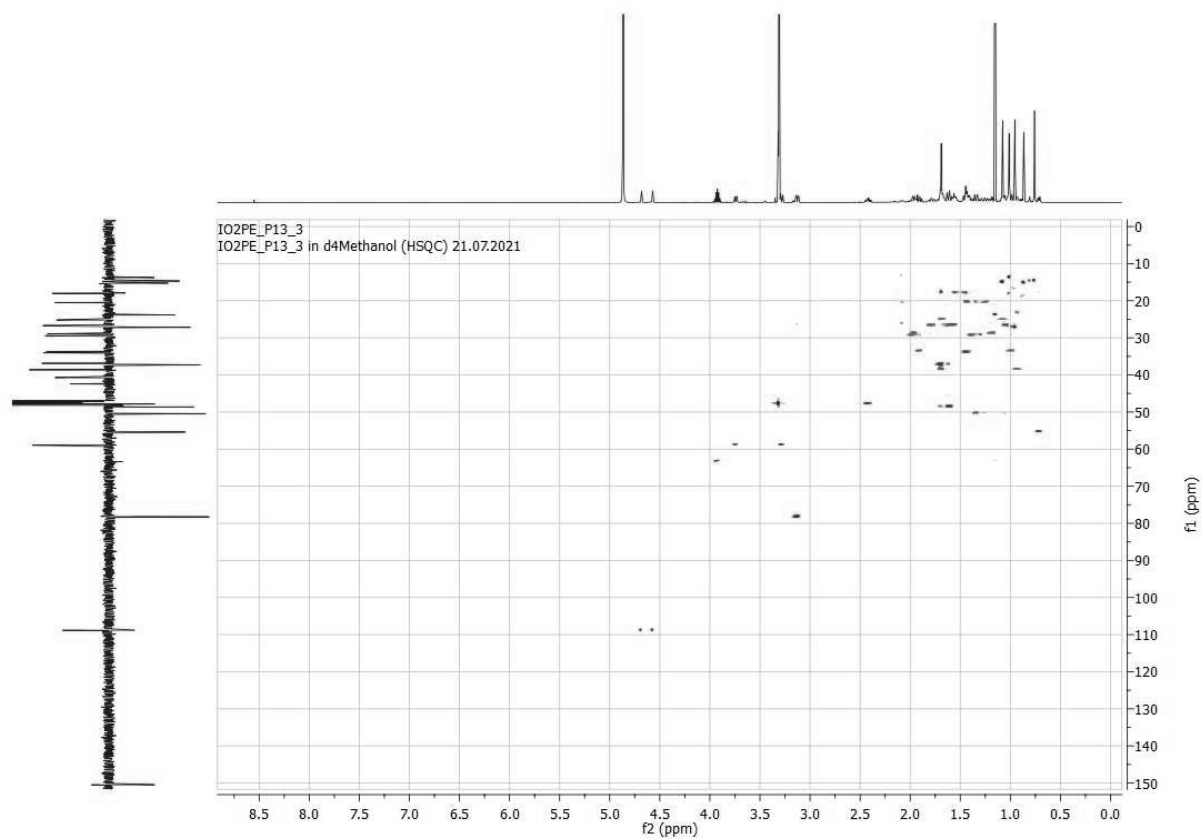
^1H

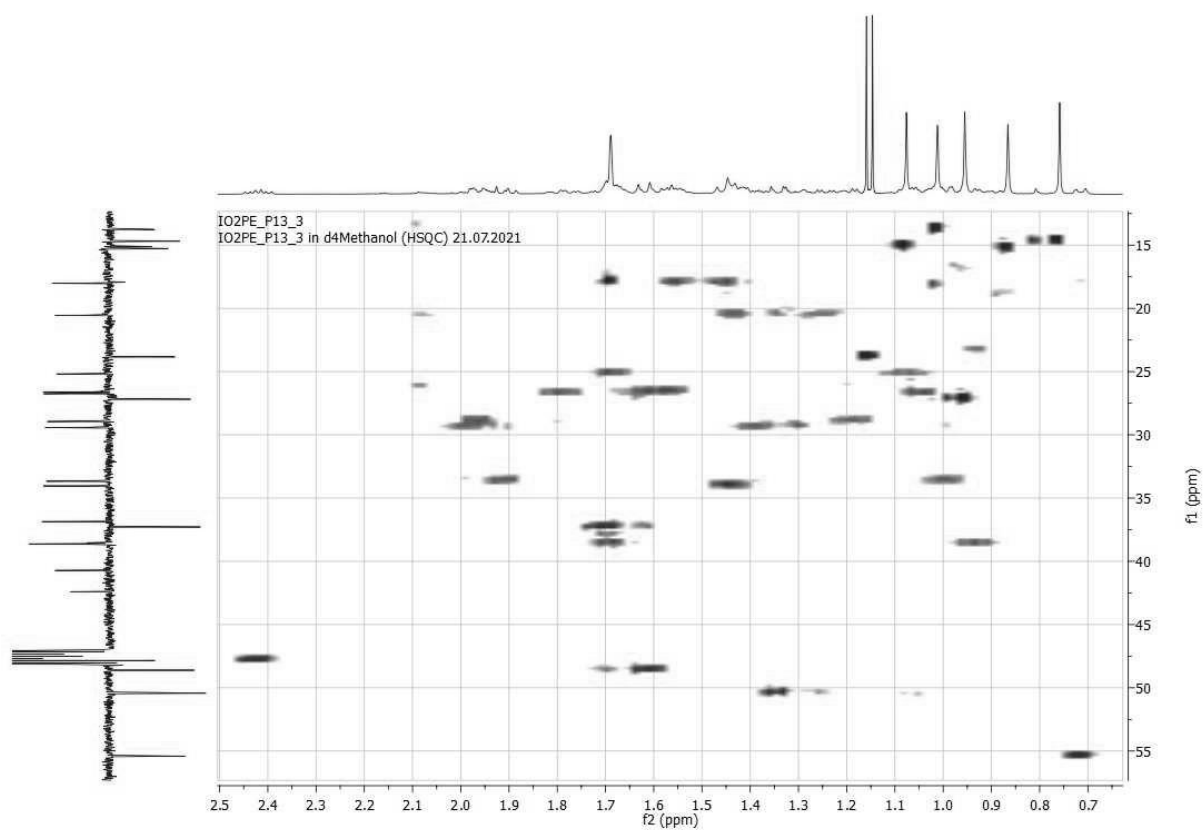


^{13}C

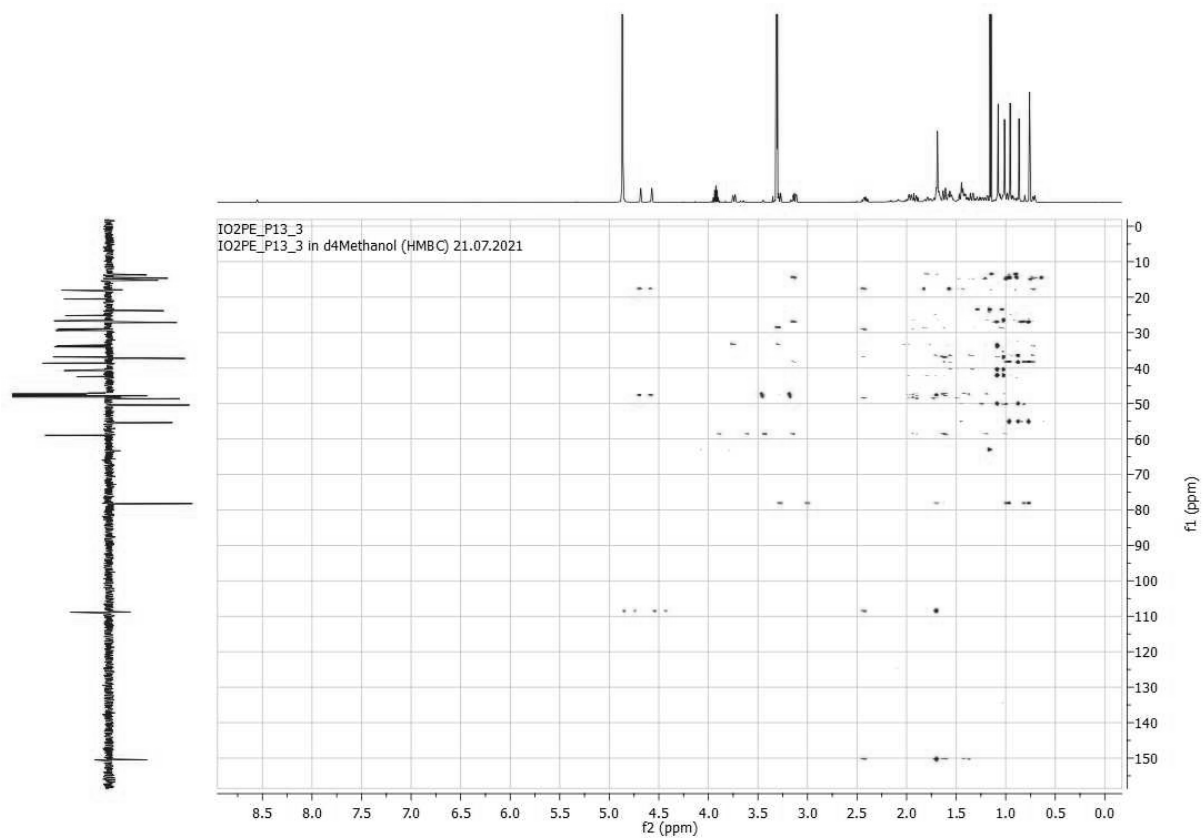


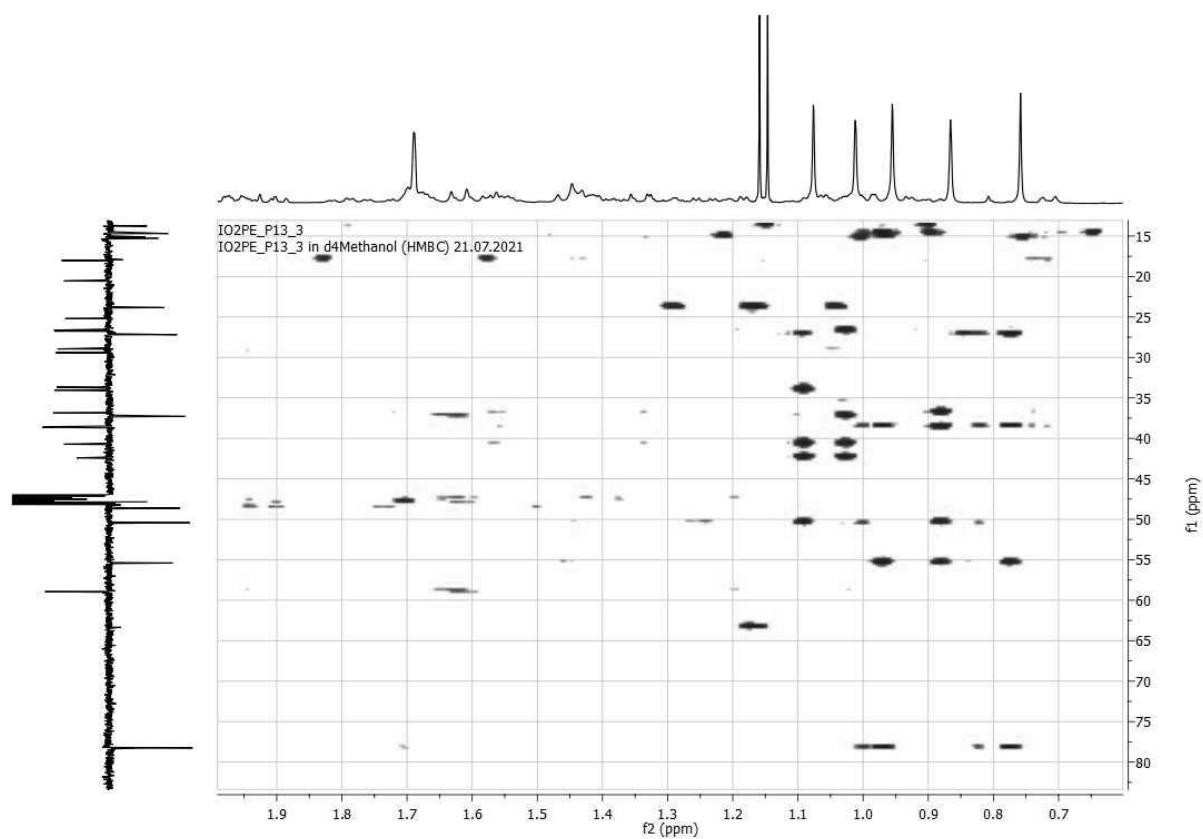
HSQC





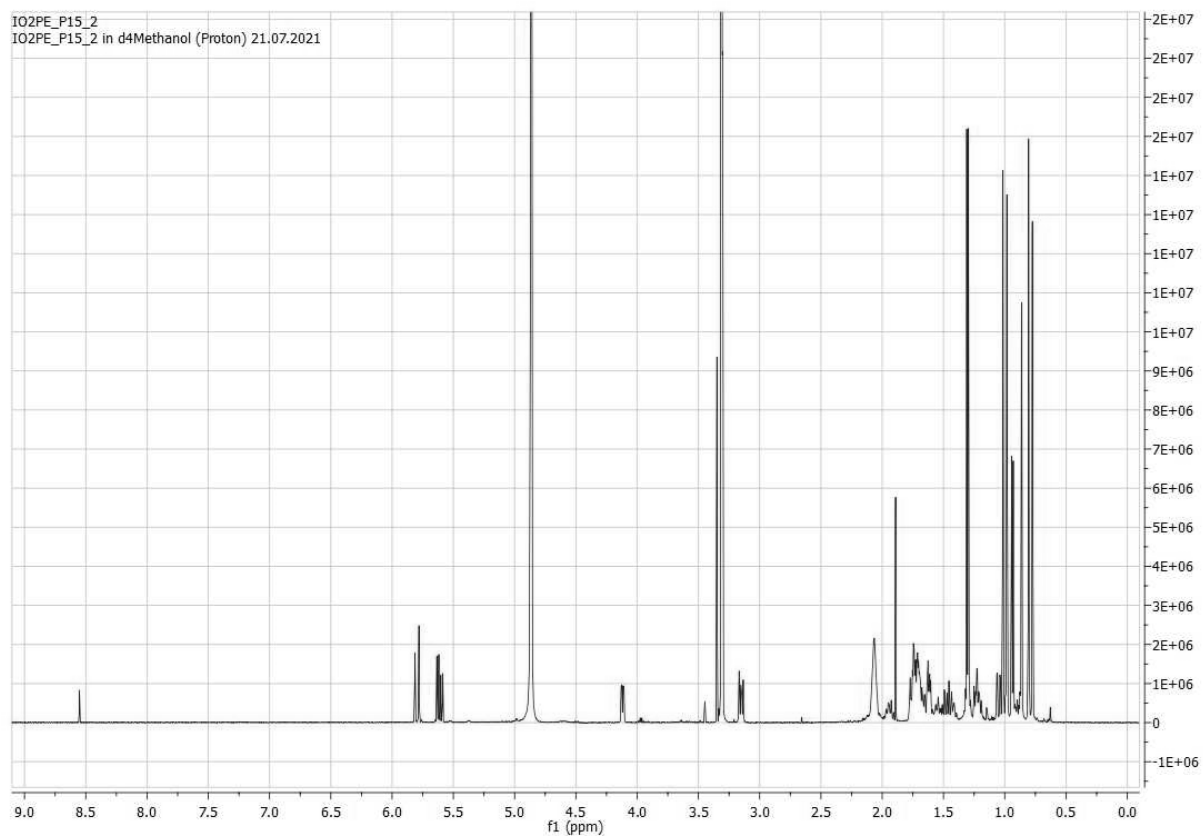
HMBC



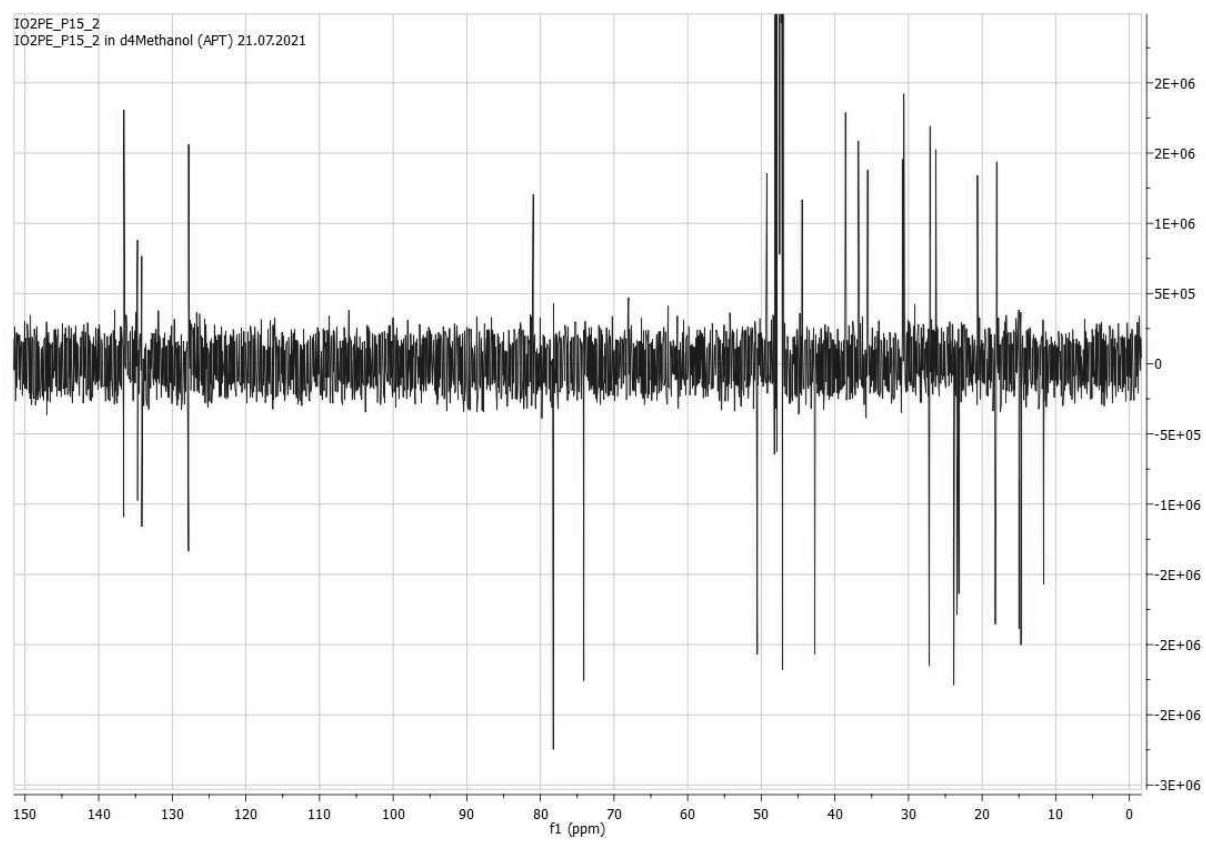


IO#2_PE_15_2

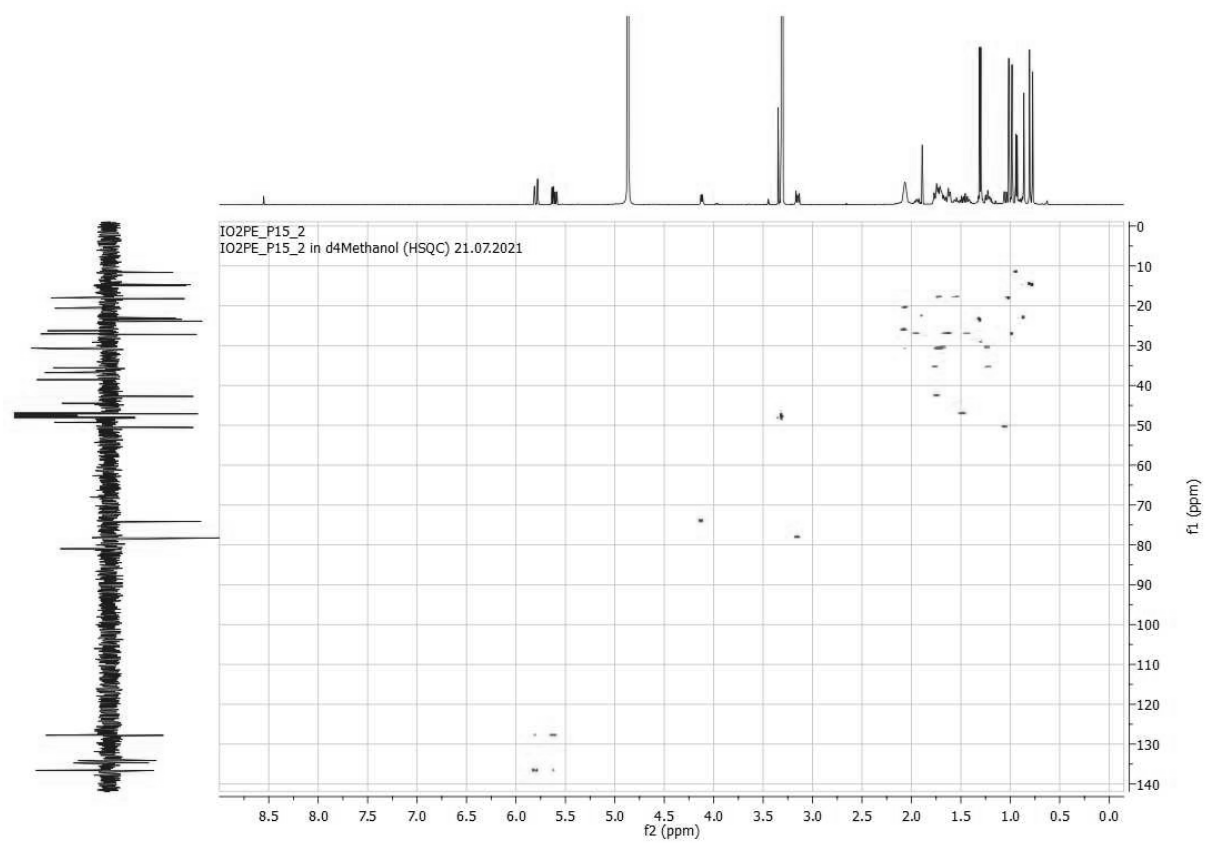
^1H

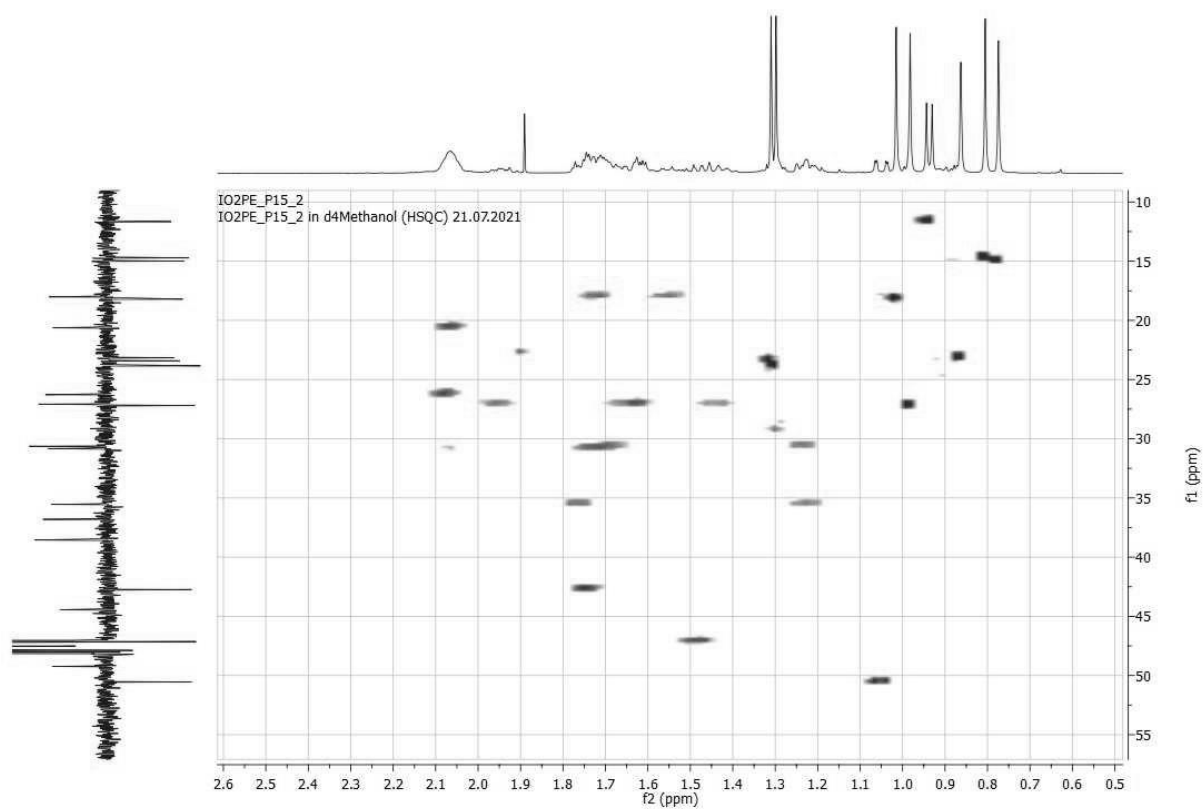


^{13}C

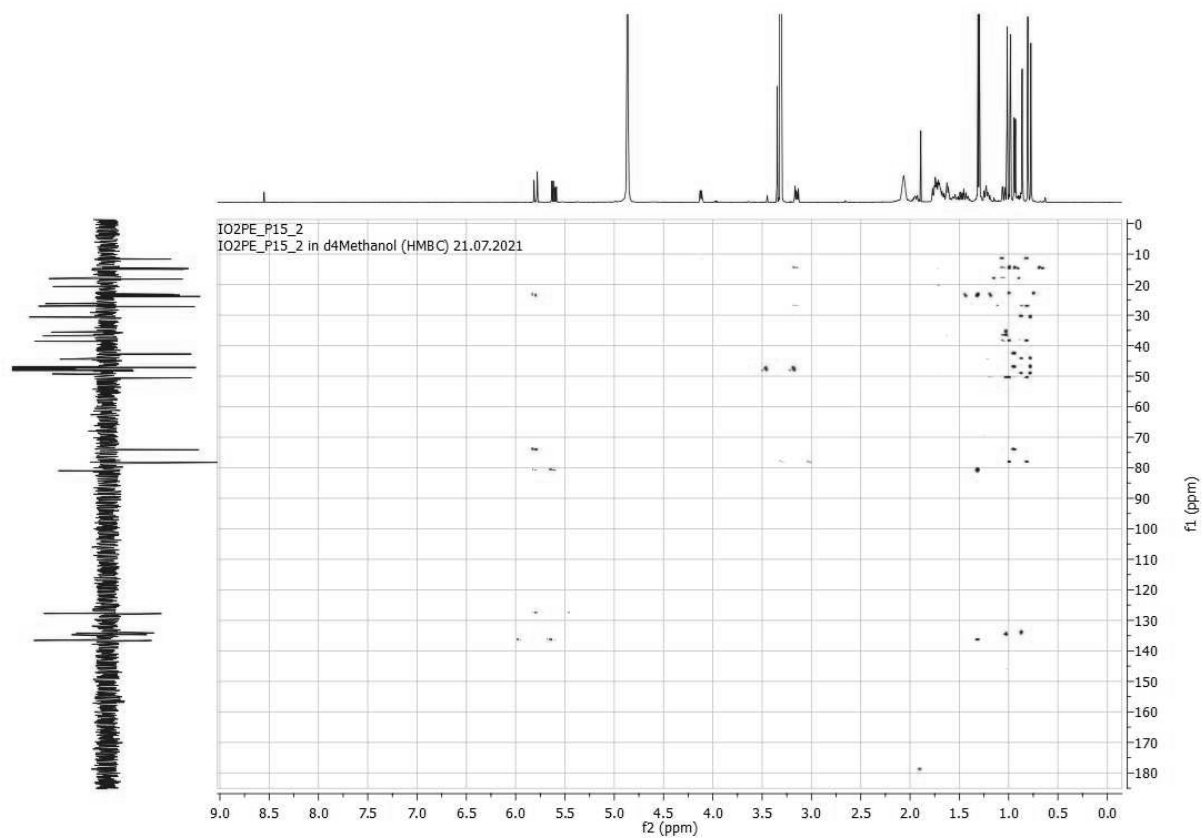


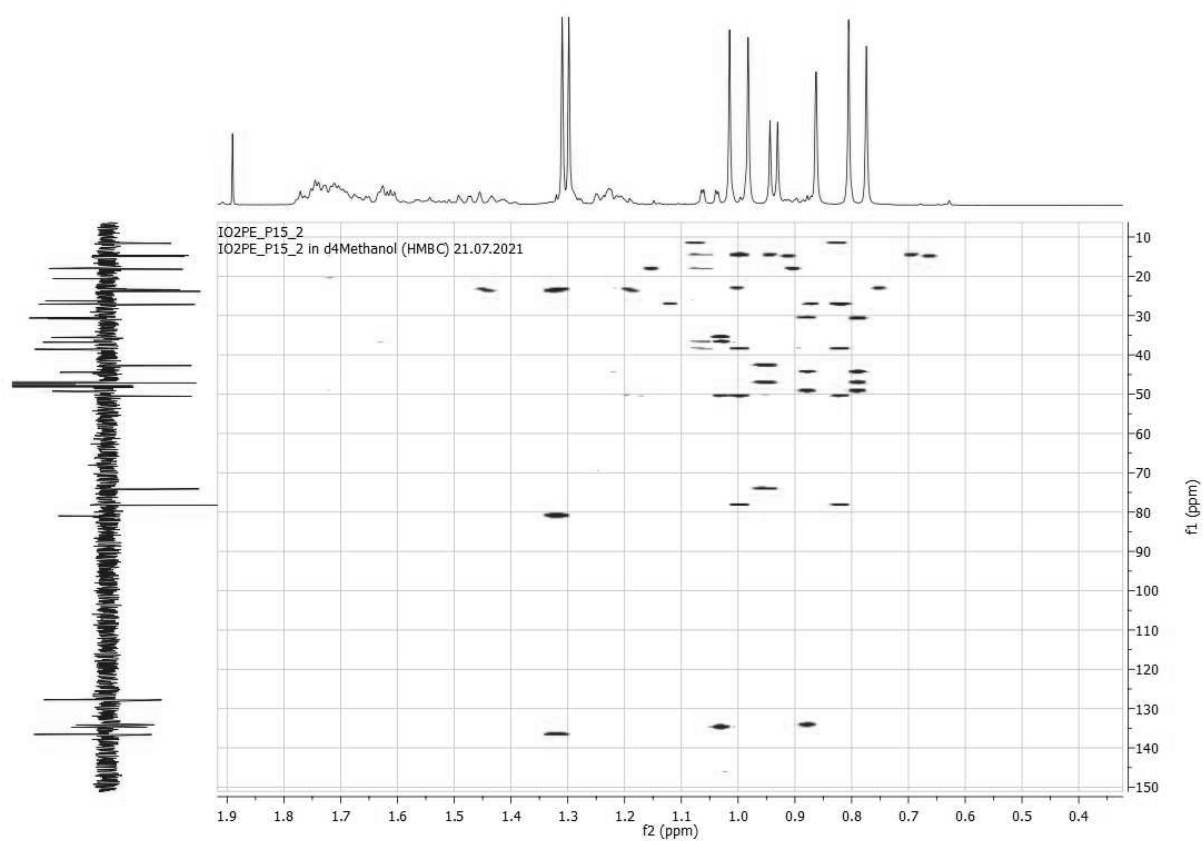
HSQC





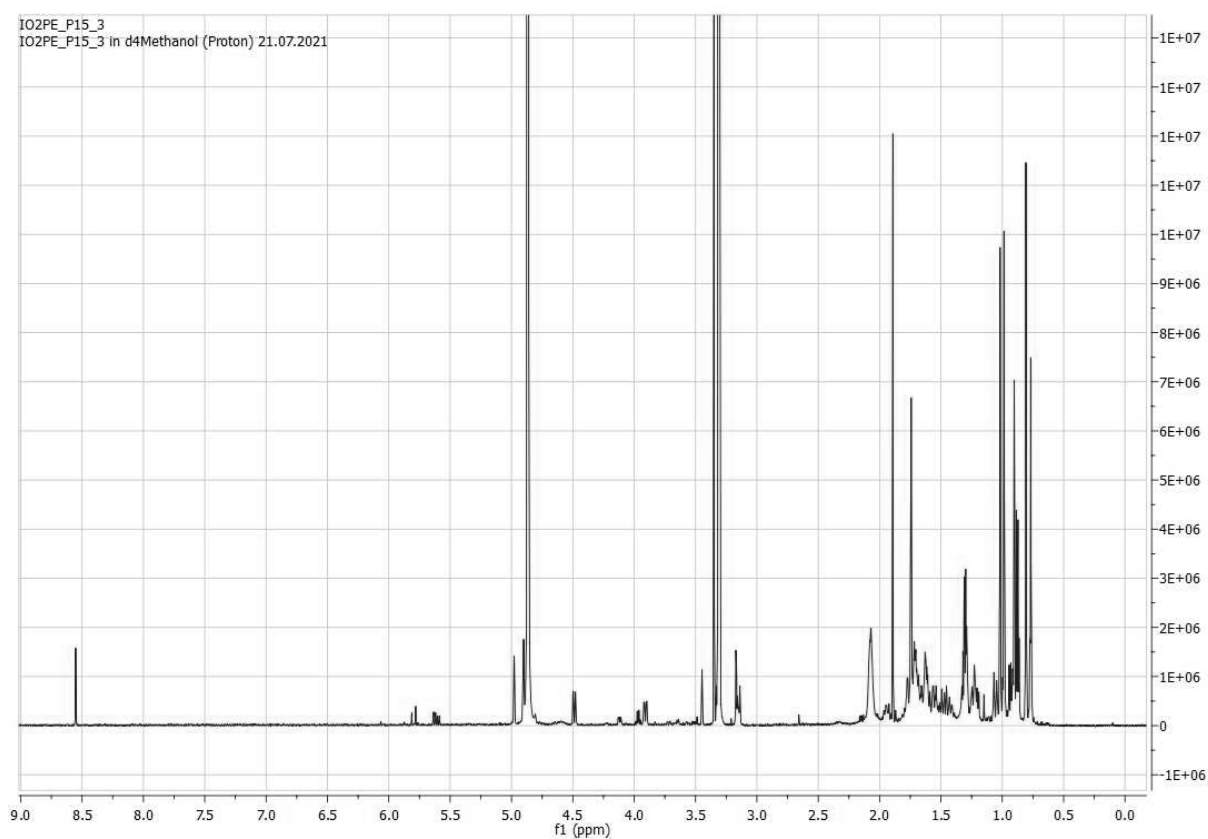
HMBC



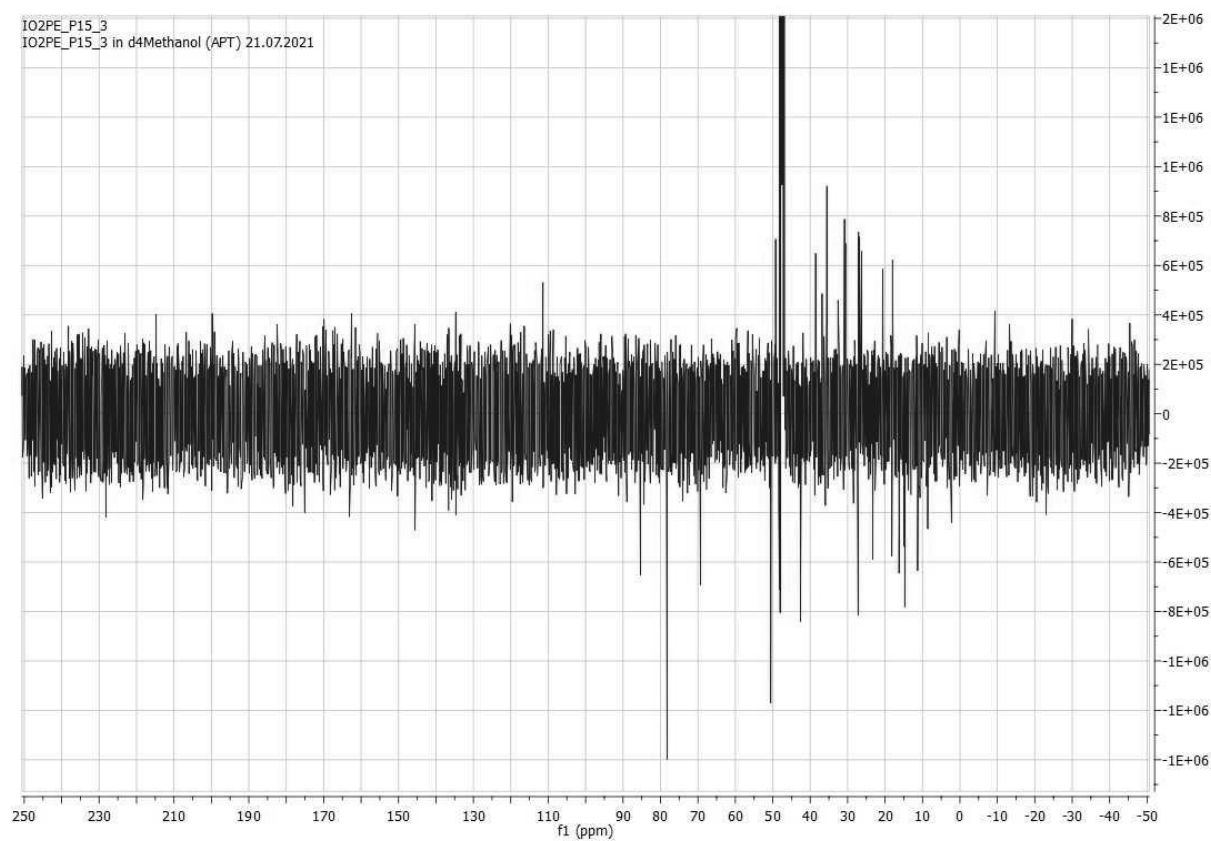


IO#2_PE_15_3

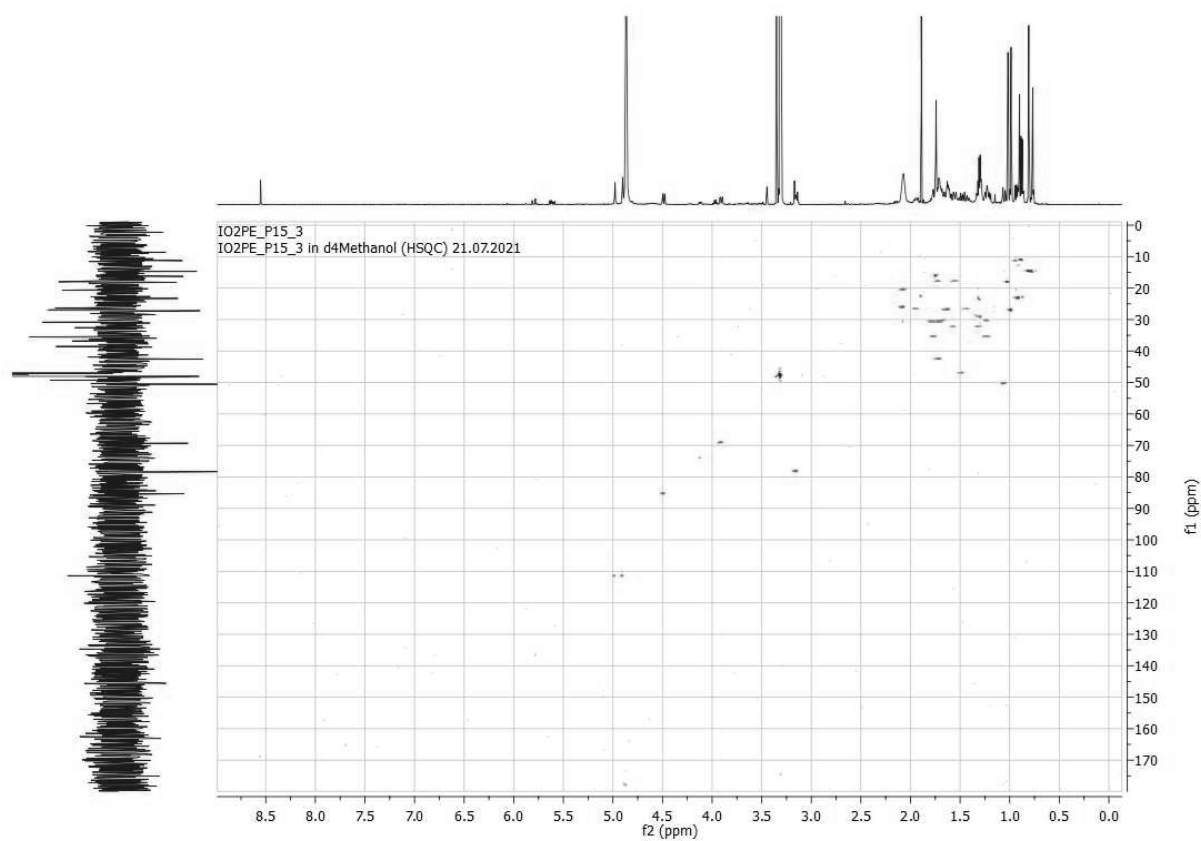
^1H

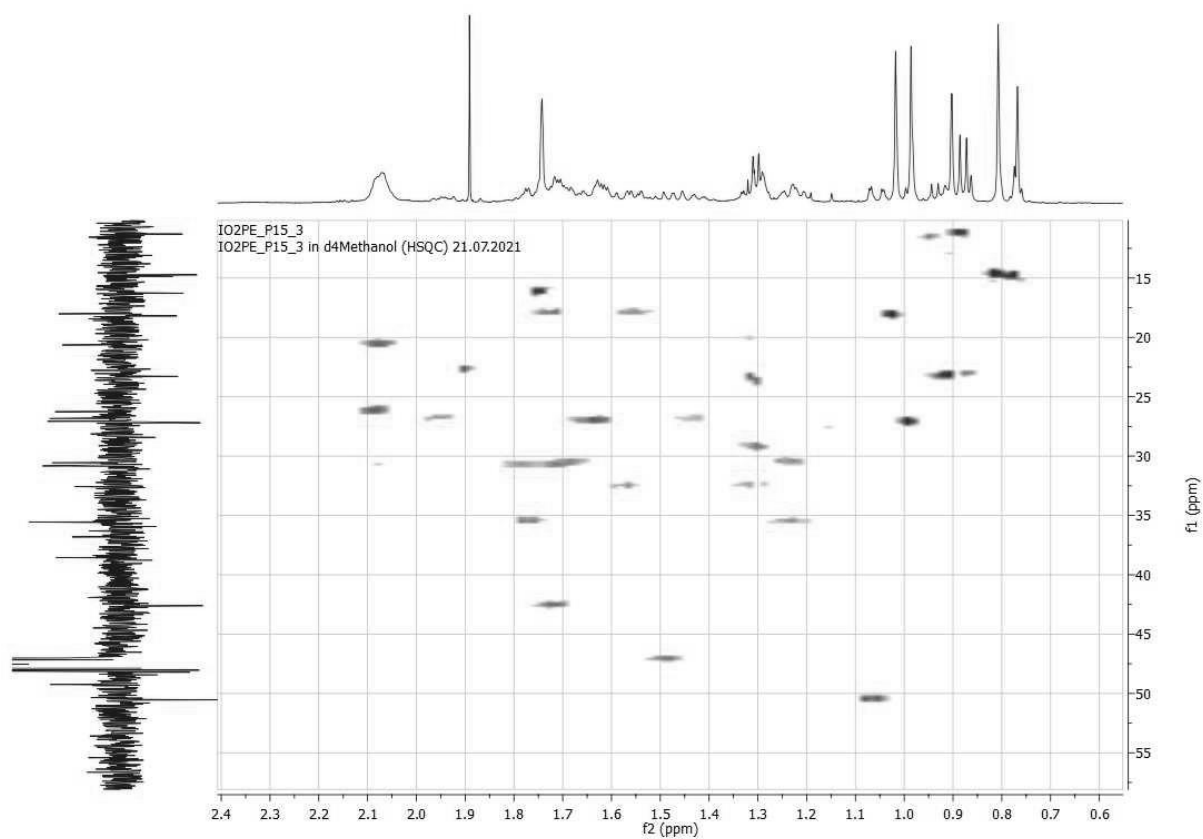


^{13}C

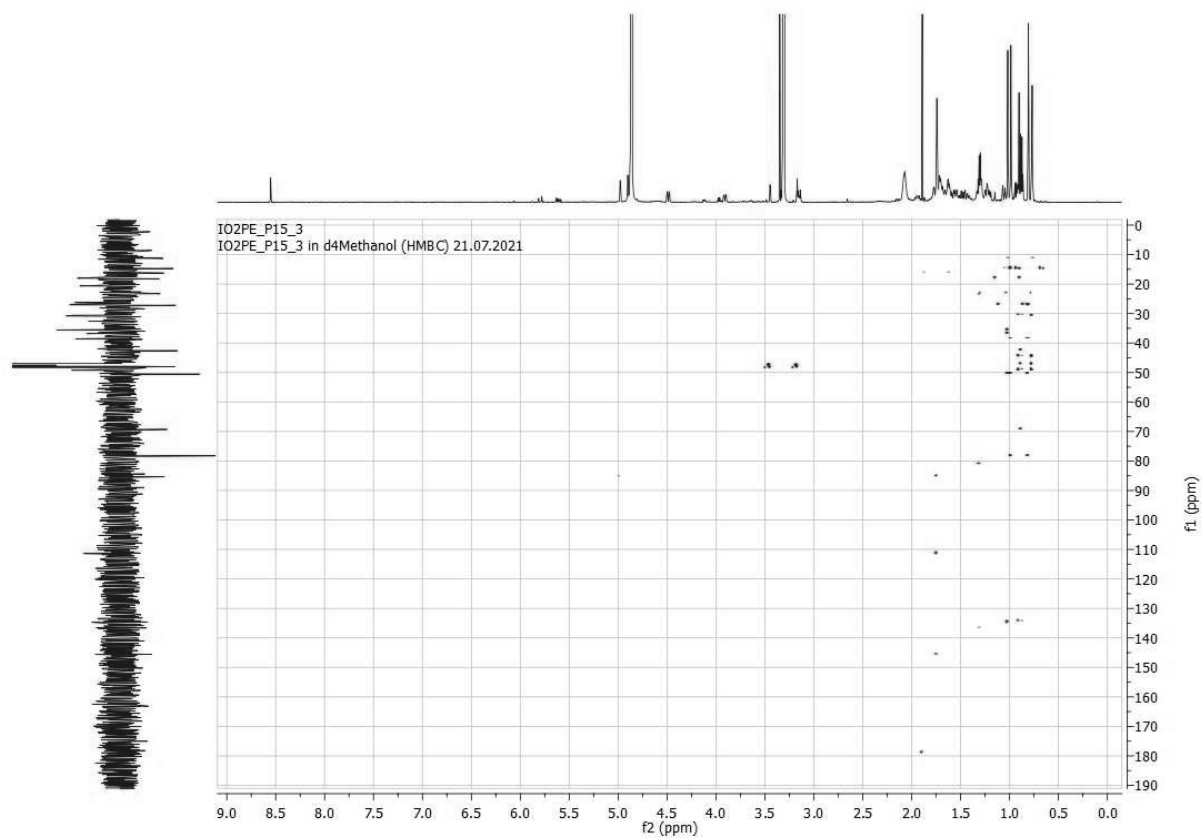


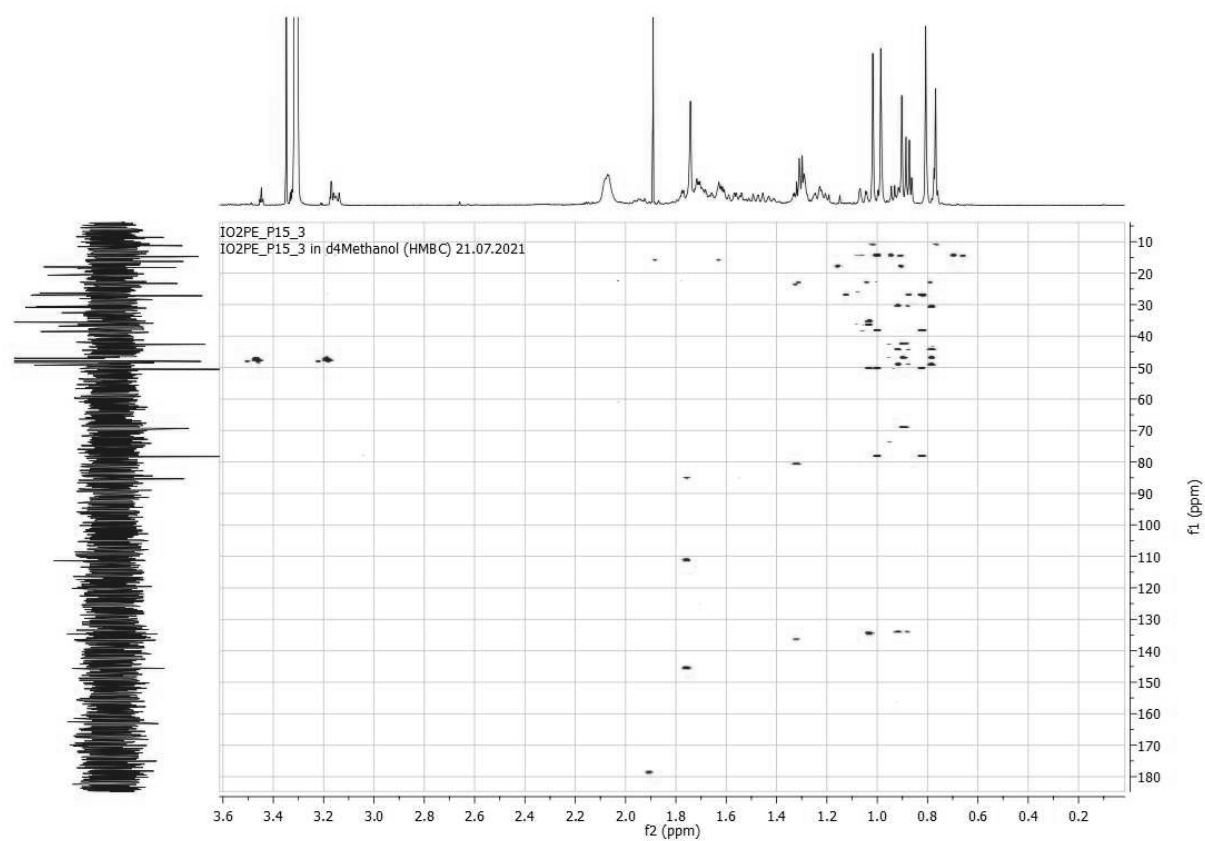
HSQC





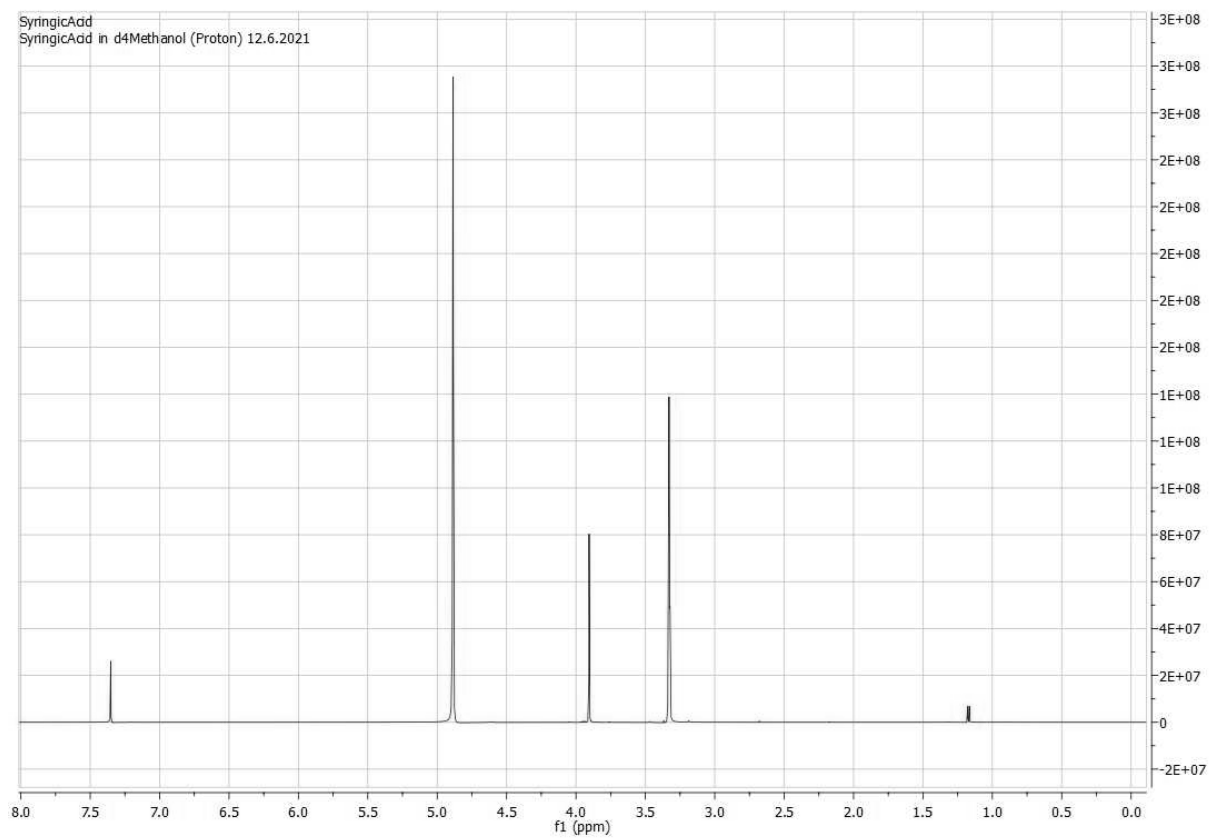
HMBC



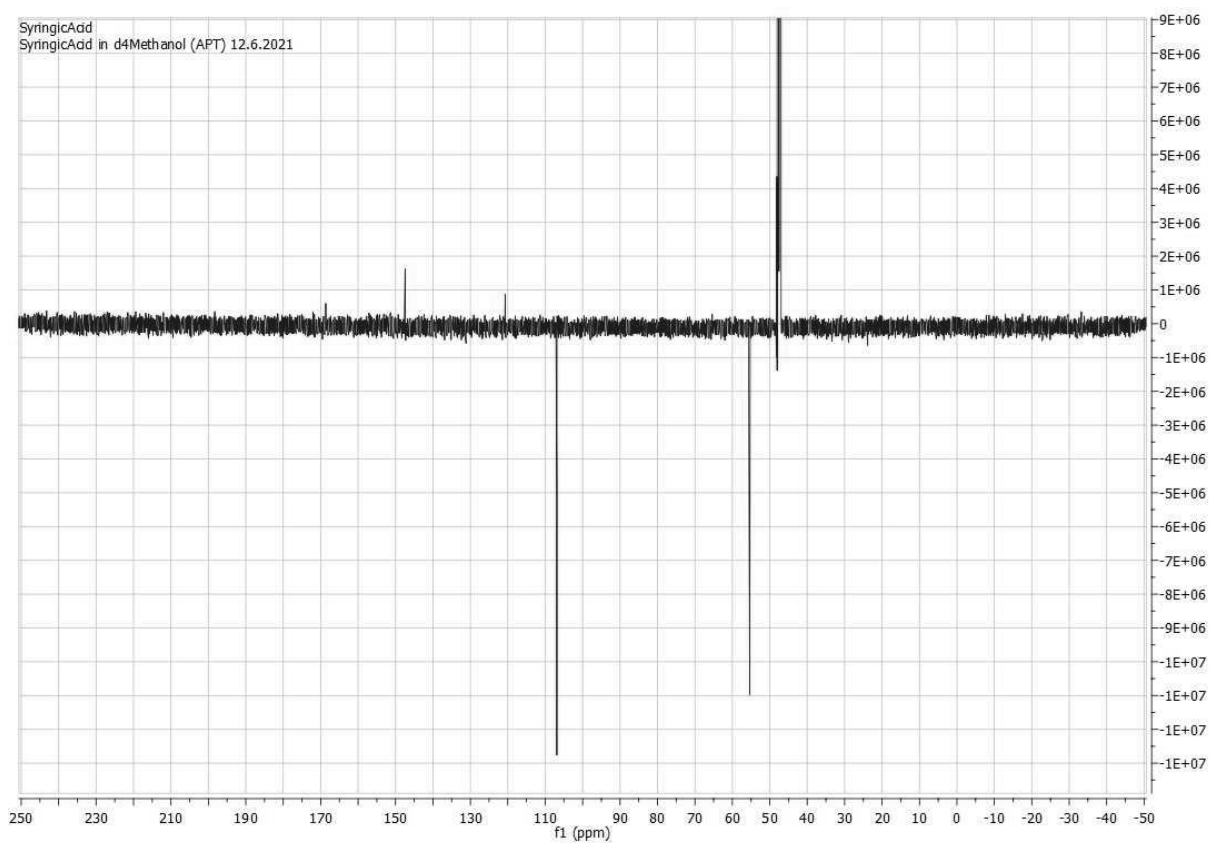


Syringic acid

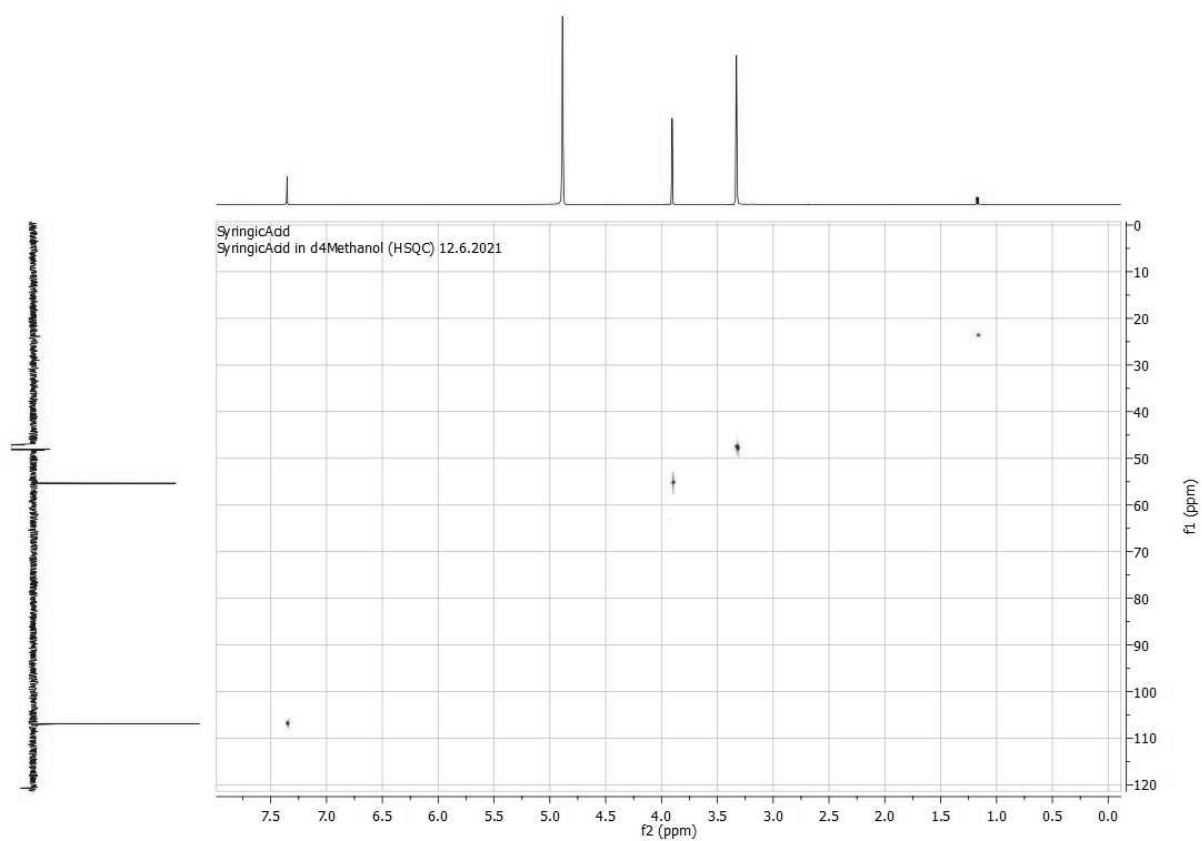
^1H



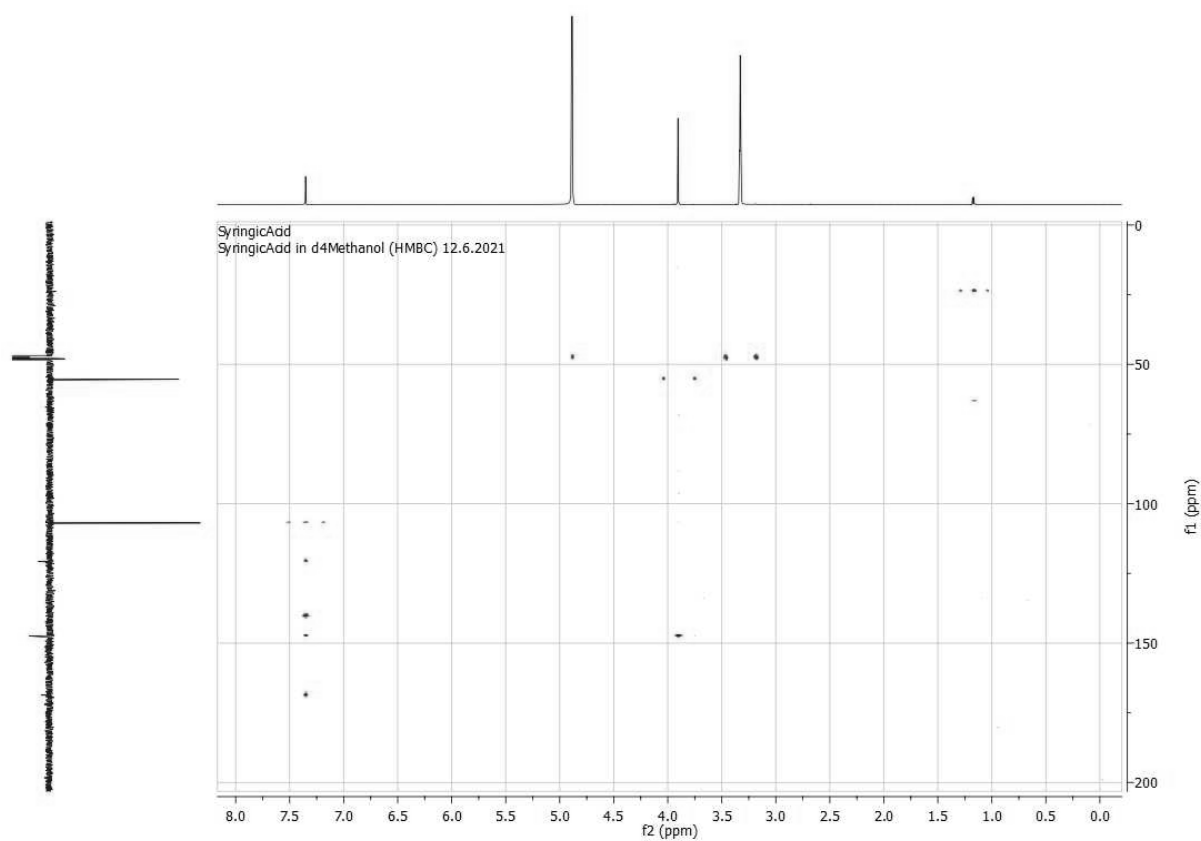
^{13}C



HSQC

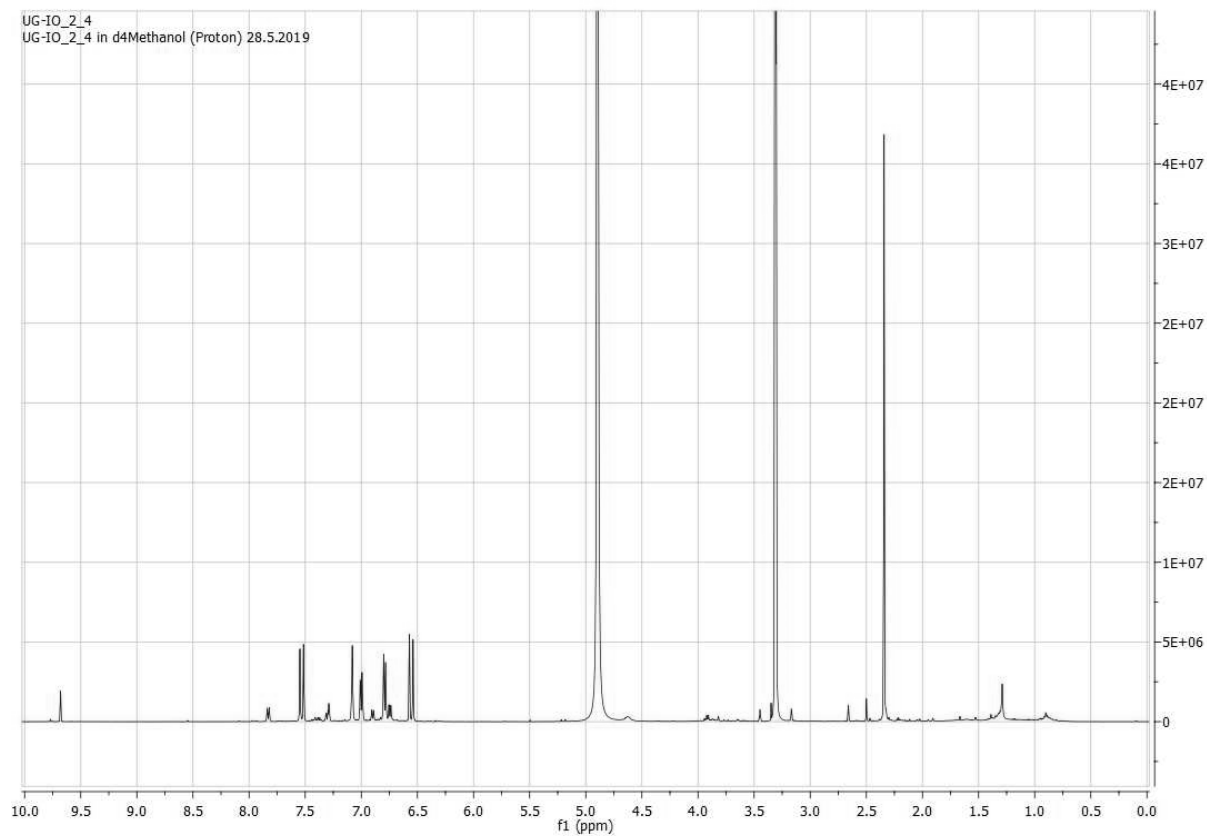


HMBC

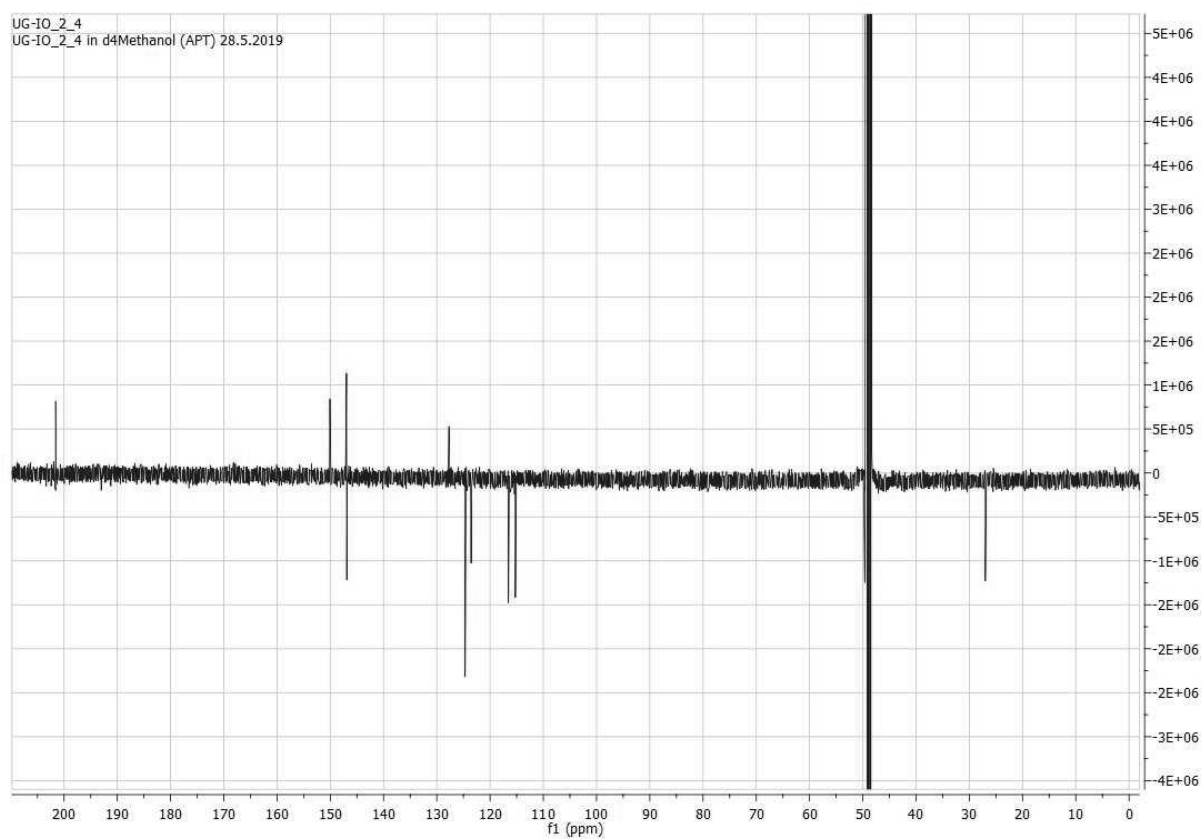


Osmundacetone

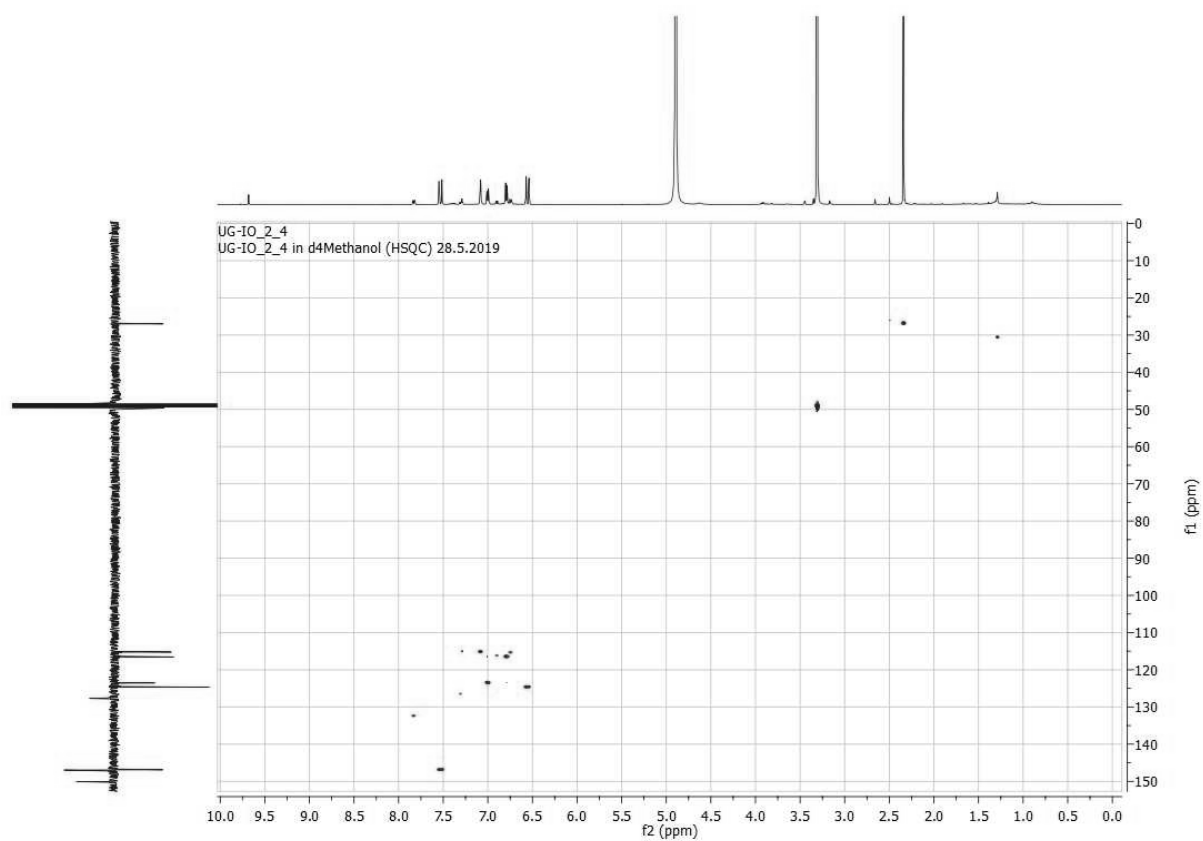
^1H



^{13}C



HSQC



HMBC

